

https://dspace.org/

Experimental investigation of erosion caused by gas-borne ash particles

Shandu, Richard Dumisani

2008-10-10T12:06:10Z
http://hdl.handle.net/10539/5741

Downloaded from a DSpace repository. https://dspace.org/

EXPERIMENTAL INVESTIGATION OF EROSION CAUSED BY GAS-BORNE ASH PARTICLES

Richard Dumisani Shandu

A dissertation submitted to the Faculty of Engineering, University of the Witwatersrand, in fulfillment of the requirements for the degree of Master of Science in Engineering.

Johannesburg 2007

Declaration

I declare that this dissertation is my own, unaided work. It is being submitted for the Degree of Master of Science in Engineering in the University of the Witwatersrand, Johannesburg. It has not been submitted before for any degree or examination in any other University.

_____

(Signature of candidate)

_____day of_____ (year) _____

Abstract

A test facility was constructed to conduct experimental investigation of erosion caused by gas-borne ash particles. The test facility was used to carry out the main objective of the study which was the determination of the critical angle of attack that gives maximum erosion on the target material, mild steel, and the effect of particle velocity and concentration on the erosion of the target material. The tests were carried out using ash samples from three different Eskom fossil-fuelled power stations, namely Matimba Power Station, Matla Power Station and Lethabo Power Station. The selection of the ash samples was based on the ash chemical composition that has the highest content of the chemical elements that have a significant influence in the material erosion of the target material. These chemical elements are quartz and other abrasive materials. These ash samples had a high content of these erosive materials.

The first test that was carried out in this study was the determination of the critical angle of attack that gives maximum erosion on the target material. It was decided to start by doing this test because the velocity and concentration tests needed a predefined critical angle of attack that gives maximum erosion on the target material. During the velocity and concentration tests the angle of attack was kept at the predefined critical angle of attack.

The results in this study indicate that the critical angle of attack that gives maximum erosion on the target material is at 27º ± 3º orientation of the target surface. The velocity test results indicate that the material erosion rate increases with increasing velocity. The results produced a power relationship between erosion rate and velocity. In this power relationship the velocity exponent for the three ash samples was found to be in the range between 2.42 and 3.64. The concentration test results also indicate that the material erosion rate increases with increasing particle concentration. These results produced a linear relationship between erosion rate and particle concentration.

Dedication

This is dedicated to my first born daughter, Simphiwe, and her brother, Nkosana, not forgetting her half brother, my son Mpiyezintombi aka Ofentse. When I think about you I get motivated to do more things in life. My family; my dad Siyagqoma Siyagqakaza aka Mbheduyajika, my sisters Samukelisiwe and Hlengiwe and my brothers Thulani and Sifiso aka Tito, I value your continued support. In the memory of my mom Alexinah, the words you breathed to me while you were still on this side of the earth are still keeping me going and motivated.

This is also dedicated to Msimang family, Rev. B. A. Msimang, his wife Jolinkomo and my big brother from another mother, Coco. This family looked after me from an early age after my mom passed away. They made sure that I grew up fine, went to school and enjoyed being part of their family. Lastly to my mom's younger sister, Mrs. Ntombinkulu Ester Zulu, I call her Mahlobo, and Makoti MaNgobese, I want to thank you for your continued support and the love you have shown to me and my family. Thank you for looking after my younger brother, Tito.

Acknowledgements

I would like to thank my supervisor Prof. T. J. Sheer for granting me the opportunity to carry out this study under his supervision. I would also like to thank him for guiding me through the process of making a submission of the work done in this study. I would also like to thank Mrs. Isaacs for arranging finances when there was a need.

I would like to thank people from Matimba, Matla and Lethabo Power Stations for helping me with ash samples that I used in this study. I would like to thank all Boiler Engineering Departments from these power stations for coordinating this project of collecting ash from the power stations. I would like to thank Pinky the chemical analyst from Matimba Power Station for helping me with information on daily coal analysis. From Lethabo Power Station I would like to thank Thando Ndiki for helping me with ash samples collection from the power station, and from Matla Power Station I would like to thank their Ash Plant staff for organizing the ash samples for me that I used in this study. I would also like to thank Mike Lander from Eskom Research Institute for the vital role he played at the inception of this study.

The laboratory staff at the School of Mechanical, Industrial and Aeronautical Engineering, University of the Witwatersrand, Johannesburg, made me feel at home. I really appreciate their support and words of wisdom that they preached to my ears. I want to thank all of them for being available at all times to give a hand whenever there was a need. I would also like to thank them for their involvement in the manufacturing of the test facility assembly components.

To my friend Buti Mabena, I really appreciate your continued support and just being a friend. Pule Seane, the words of wisdom you said to me will never be forgotten. John Mbabazi, the great man, I call him J, this is the person that made a huge impact in my life. Working with him made me a better person. I value his advices, commitment to his work and being friendly to people around him.

CONTENTS

		Page
DECLARATION		2
ABSTRACT		3
DEDICATION		4
ACKNOWLEDGEMENTS		5
CONTENTS		6
LIST OF FIGURES		9
LIST OF TABLES		11
LIST OF SYMBOLS		13
NOMENCLATURE		15
1	**INTRODUCTION**	**16**
1.1	**Statement of the Problem**	**16**
1.2	**Definition of Terms**	**19**
1.2.1	Erosion	19
1.2.2	Rotary Regenerative heat Exchanger	19
1.2.3	Heat Transfer Elements	22
1.3	**Objectives of the Present Study**	**25**
1.3.1	Construction of the Erosion Test Facility	25
1.3.2	Collection of Ash Samples	25
1.3.3	Determination of Erosion Rates	26
1.3.4	Comparison with Work of Others	26
1.4	**Structure and Outline of the Report**	**26**
2	**LITERATURE SURVEY**	**28**
2.1	**Factors Determining the Rate and Nature of Erosion**	**28**
2.1.1	Angle of Impingement of the Erodent	28
2.1.2	Particle Size	30
2.1.3	Particle Shape and Hardness	33
2.1.4	Particle Impact Velocity and the Velocity Exponent	36
2.1.5	Particle Velocity in the Fluid Stream	38
2.1.6	Temperature Effects of the Two Phase Flow	40

2.1.7 Nature of Material Removal 41
2.2 Summary of the Findings from the Literature Review 44
3 DESIGN OF THE TEST FACILITY 46
3.1 Test Facility Requirements 47
3.1.1 Blower 48
3.1.2 Orifice Meter 49
3.1.3 Ash Feeder 49
3.1.4 Test Specimen 50
3.1.5 Data Acquisition 50
3.1.6 Sizing of the Test Facility 51
3.1.6.1 Parameters Used in the Sizing of the Test Facility 52
3.1.6.2 Pressure Drop in the Test Section 53
3.1.6.3 Pressure Drop in the Acceleration Section 53
4 EXPERIMENTAL PROCEDURE 56
4.1 The Test Facility 60
4.1.1 The Test Specimen 60
4.1.2 The Test Section 60
4.1.3 The Filter 61
4.1.4 The Hopper 61
4.1.5 The Ash Feeder 62
4.1.6 The Orifice Meter 62
4.1.7 The Blower 62
4.2 Overall Experimental Procedure 63
4.3 Scanning Electron Microscope 64
4.4 Method of Analysis of the Eroded Plates 64
5 RESULTS AND DISCUSSION 65
5.1 Determination of the Critical Angle of Attack 65
5.2 Effect of Particle Velocity, Shape and Size 75
5.3 Effect of Particle Concentration 84
6 CONCLUSIONS AND RECOMMENDATIONS 85

6.1 Conclusions **85**

6.2 Recommendations **88**

REFERENCES **89**

APPENDIX A: ENGINEERING DRAWINGS OF THE TEST FACILITY **92**

APPENDIX B: ASH FEEDER TECHNICAL SPECIFICATION **93**

APPENDIX C: MASS BALANCE SCALE TECHINCAL SPECIFICATION **94**

APPENDIX D: ASH ANALYSIS FOR THE THREE POWER STATIONS **95**

APPENDIX E: MATIMBA DAILY COAL ANALYSIS **104**

APPENDIX F: TEST SPECIMEN ANALYSIS **114**

APPENDIX G: UNCERTAINTY ANALYSIS **116**

APPENDIX H: PUBLISHED TECHINCAL PAPER **122**

List of Figures

Figure		Page
1.1	Regenerative heat exchanger in operating environment	20
1.2	Ljungstrom regenerative heat exchanger	21
1.3	Rothemühle regenerative heat exchanger	21
1.4	Undulated and Corrugated plates	22
1.5	Heat transfer element profiles	23
1.6	Heat transfer elements packed in a Ljungstrom RAH	24
1.7	Heat transfer elements packed in three layers	24
2.1	Effect of angle of attack on erosion rate	29
2.2	Effect of particle size on erosion rate	31
2.3	Effect of particle size	32
2.4	Erosion rates of AISI 1020 steel	34
2.5	Erosion wear of steel alloys of different hardness	36
2.6	Effect of impact angle on velocity exponent	38
2.7	Effect of particle concentration on erosion	39
2.8	Effect of dust concentration on erosion	39
2.9	Effect of temperature on erosion	40
2.10	Differences in particle erosivity	41
2.11	Effect of angle of impingement on erosion	43
2.12	Platelet formation on metal surface	44
3.1	Layout of the test facility	46
5.1	Determination of critical angle of attack: Test results	67
5.2	Macroscopic erosion at 90º orientation of the target surface	68
5.3	Microscopic erosion at 90º orientation of the target surface	68
5.4	Macroscopic erosion at 70º orientation of the target surface	69
5.5	Microscopic erosion at 70º orientation of the target surface	69
5.6	Macroscopic erosion at 55º orientation of the target surface	70
5.7	Microscopic erosion at 55º orientation of the target surface	70
5.8	Macroscopic erosion at 45º orientation of the target surface	71
5.9	Microscopic erosion at 45º orientation of the target surface	71
5.10	Macroscopic erosion at 35º orientation of the target surface	72
5.11	Microscopic erosion at 35º orientation of the target surface	72

5.12	Macroscopic erosion at 25º orientation of the target surface	73
5.13	Microscopic erosion at 25º orientation of the target surface	73
5.14	Macroscopic erosion at 20º orientation of the target surface	74
5.15	Microscopic erosion at 20º orientation of the target surface	74
5.16	Matimba Power Station ash particles	76
5.17	Matla Power Station ash particles	76
5.18	Lethabo Power Station ash particle	77
5.19	Effect of particle velocity on erosion: Matimba test results	79
5.20	Effect of particle velocity on erosion: Lethabo test results	80
5.21	Effect of particle velocity on erosion: Matla test results	81
5.22	Combined velocity test results	82
5.23	Uncertainties in the test results	83
5.24	Effect of particle concentration on erosion: Test results	84
D.1	Matimba Power Station ash particle size	98
D.2	Lethabo Power Station ash particle size	101
D.3	Matla Power Station ash particle size	103
F.1	Test specimen analysis	115

List of Tables

Table		Page
2.1	Erodent particles and rates of erosion of AISI 1020 steel	34
2.2	Coal minerals and hardness numbers of ash products	35
4.1	Initial tests programme	57
4.2	Determination of critical angle of attack	58
4.3	Effect of particle velocity and concentration: Matimba ash	58
4.4	Effect of particle velocity and concentration: Lethabo ash	59
4.5	Effect of particle velocity and concentration: Matla ash	59
5.1	Chemical composition of the three ash samples	78
D.1	Matimba Power Station ash chemical analysis	96
D.2	Matimba Power Station ash particle size analysis	97
D.3	Lethabo and Matla Power Stations ash chemical analysis	99
D.4	Lethabo Power Station ash particle size analysis	100
D.5	Matla Power Station ash particle size analysis	102
E.1	Matimba Power Station Daily Coal Analysis Report: 4648	105
E.2	Matimba Power Station Daily Coal Analysis Report: 4649	106
E.3	Matimba Power Station Daily Coal Analysis Report: 4650	107
E.4	Matimba Power Station Daily Coal Analysis Report: 4651	108
E.5	Matimba Power Station Daily Coal Analysis Report: 4652	109
E.6	Matimba Power Station Daily Coal Analysis Report: 4653	110
E.7	Matimba Power Station Daily Coal Analysis Report: 4654	111
E.8	Matimba Power Station Daily Coal Analysis Report: 4655	112
G.1	Parameters used in the experimental test	117
G.2	Sensitivity coefficients for Matimba Power Station ash	117
G.3	Sensitivity coefficients for Lethabo Power Station ash	117
G.4	Sensitivity coefficients for Matla Power Station ash	118
G.5	Uncertainties in the measured values of temperature, pressure drop and diameters	118
G.6	Parameters used to calculate uncertainty in the air density	119
G.7	Sensitivity coefficients and uncertainty in the air density	119
G.8	Uncertainties in the Matimba Power Station velocity test results	119
G.9	Uncertainties in the Lethabo Power Station velocity test results	119

G.10 Uncertainties in the Matla Power Station velocity test results 120
G.11 Uncertainties in the measured values of mass 121
G.12 Sensitivity coefficients and uncertainties in the Matimba test results 121
G.13 Sensitivity coefficients and uncertainties in the Lethabo test results 121
G.14 Sensitivity coefficients and uncertainties in the Matla test results 121

List of Symbols

V	Velocity	m/s
V_n	Normal component of velocity	m/s
V_t	Tangential component of velocity	m/s
W	Wear of material	mg/g
W_d	Deformation wear of material	mg/g
W_c	Cutting wear of material	mg/g
M_p	Mass of particles	kg
B, K_1, K_2	Wear constants depending on material Properties of the particle wall, such as Density and Poisson's ratio	
ε_c, ε_d	Coefficients of erosion	J/m^3
C_v	Volumetric concentration	
H_v	Vickers Hardness	kg f mm^{-2}
ε	Erosion rate	mg/g
k	Material constant characterizing the relative erosivity	
α	Angle of attack	degrees(˚)
dp	Particle diameter	mm
b	Constant relative to particle size	
a	Velocity exponent	
ρ	Density	kg/m^3
g	Gravitational acceleration	m/s^2
μ_{air}	Viscosity of air	Ns/m^2
D	PVC pipe diameter	mm
d_m	Acceleration section pipe diameter	mm
L_m	Acceleration section pipe length	m
L	PVC pipe length	m
μ	Mass load ratio	
d_o	Orifice diameter	mm
Q	Volumetric flow rate	m^3/s
A	Area	m^2

La	Acceleration length in Marcus formula	m
Re	Reynolds number	
f_1	Friction factor of air	
λ_1	Friction factor of ash particles	

Nomenclature

CAER	Cold Accelerated Erosion Rig	
RAH	Regenerative Air Heater	
SS	Stainless steel	
SEM	Scanning electron microscope	
CFD	Computational Fluid Dynamics	
C.V.	Calorific value	MJ/kg
Vol	Volume	m^3
Tot moist	Total moisture	
Inh moist	Inherent moisture	
Surf moist	Surface moisture	
H.G.I.	Hardgrove index	
Mg/Fe abras	Amount of iron abrasives in coal per milligram	
Fix carb	Fixed carbon	

1 INTRODUCTION

1.1 Statement of the Problem

In all the thermal power stations for Eskom pulverized coal is burnt in the boiler furnace to produce process steam. The hot flue gases leaving the furnace are directed towards tube banks of the superheater and reheater. The hot flue gases then lose part of their heat to the process steam circulating within the tube banks. From the reheater the hot flue gases are directed to the tube banks of the economizer that is used to raise the temperature of the water being fed into the boiler. By the time the hot flue gases leave the economizer their temperature is in the region of 300 - 350ºC. More heat is extracted from the hot flue gases by directing the gases to the rotary regenerative heat exchanger that is used to preheat the air being supplied to the boiler.

The rotary regenerative heat exchanger is made up of a matrix of corrugated mild steel plates enclosed in a cylindrical structure. Rotary regenerative heat exchangers are commonly used in fossil-fuelled power stations. They improve thermal efficiency of the power stations by extracting heat from the flue gases leaving the boiler and use it to preheat air from the atmosphere that is drawn into the boiler as combustion air. The plates are packed in conveniently sized and robust packs, to facilitate easy handling and removal. The corrugated mild steel plates serve as the heat exchanger elements. They extract and store heat from the hot flue gases and later release the stored heat to the stream of cold air, passing over the heat exchanger elements. In the air preheater`, the hot flue gases flow through one side of the rotor, and the cold air being supplied to the furnace flows through the opposite side of the rotor. The heat exchanger elements pass alternately through the stream of hot flue gas and the stream of cold air. Part of the heat of the hot flue gases is transferred to the heat exchanger elements, which in turn are used to heat the stream of cold air being blown into the boiler furnace. The two streams of the hot flue gases and cold air are separated from each other by a small blanking section of sealing plates.

The coal supplied to the thermal power stations contains a certain amount of ash content that is dependant on the location where it is extracted. Part of this ash is removed from the bottom of the boiler. However, the hot flue gases leaving the boiler

furnace carry the smaller ash particles away. The hot fly ash particles, traveling at high velocities, impinge upon the surfaces of the tubes of the boiler heat exchangers and the surfaces of the plates of the regenerative heat exchangers. Over time, the bombarded surfaces get eroded. In the extreme cases of erosion, some holes are formed in parts of the elements of the heat exchangers. The air preheater elements are deemed to have failed once the extent of the erosion of the elements is such that the elements cannot maintain their structural integrity or heat transfer performance, or both. On average, each power station unit produces 600 Megawatts of power. If there is a shut down this production is lost and the cost of maintenance and returning the unit back to full operation is very expensive. The cost involved for maintenance of the air preheater alone is estimated at R6 million, but this depends on the size of the air preheater, the work that needs to be done, required resources, etc. It is desirable to predict the rate of erosion by fly ash of the preheater elements so as to be able to take measures to minimize the rate of erosion, and also to plan systematically for the replacement of the heat exchanger elements.

At the University of the Witwatersrand, the School of Mechanical, Industrial and Aeronautical Engineering has, for a number of years, been collaborating with Eskom. The area of research has been the performance of the regenerative air preheaters used in Eskom thermal power stations in South Africa. The research has been concerned with heat transfer, flow parameters and erosion by gas-borne ash particles. It has included experimental work as well as computational modelling. Crookes (2000) carried out experimental investigations using the Cold Accelerated Erosion Rig (CAER) at Eskom's Matimba Power Station. He carried out experiments to determine erosion rates of different element profiles. The most commonly used element profile in power station boilers is KH11, see Section 1.2.3. Wilson (1999) developed a numerical model to predict the erosion patterns, but not the erosion rate, of one of the designs of the air preheater element profiles, the KH11 profile. de Klerk (2001) investigated further the effect of alternating plate thickness of the air preheater elements. This was due to the recommendation made by Wilson (1999) of increasing the plate thickness of undulated elements, which he found to be eroding the fastest in his tests. de Klerk (2001) generated a simulation model to carry out thermal analysis in the air preheaters. In his simulation results on thermal analysis he found that thicker, colder undulated, plates were at risk of experiencing corrosion and fouling

because they could not attain the required temperature in the air preheater as compared to the thinner, warmer corrugated, plates. Mabena (2003), in a fouling investigation, listed the following problems associated with air preheater failures:

- Erosion
- Fouling or plugging
- Corrosion
- Fouling and erosion
- Fire damage

When running the CAER test rig at Matimba, tons of ash are required for the tests. An advantage with this test rig is that it is integrated into the Matimba Power Station plant. It is located in one of the power station units and it is integrated in the ash system in the plant. Because of the tons of ash required in order to perform the erosion tests, it would be cumbersome and expensive to transport ash samples from the different Eskom power stations to Matimba.

Many experimental investigations have been carried out elsewhere to determine or predict the rate of erosion by particles entrained in fluid flows on metal surfaces. For example, Tabakoff (1979) conducted experimental investigations to determine the effects of high temperature on the erosion rate of some selected metal surfaces. The test facility was meant to provide data in the range of operating temperatures experienced in compressors and turbines. Tabakoff *et al.* (1979) carried out experimental investigations to study the erosion of different materials, using quartz, alumina and coal ash particles. The method adopted and the information published is relevant in designing and operating a similar test rig. Raask (1985) conducted experimental investigations to determine the rate of erosion by fly ash of boiler tubes. The erosion tests were done using quartz grains and glass spheres in the range of 90 – 105 μm, with an average size of 100 μm. The test facility used by Tabakoff *et al.* (1979) involved small quantities of ash, leading to fractions of milligrams of the metal specimen being eroded. It may not be accurate to use the results from such low quantities of metal erosion to predict the erosion of equipment such as air preheater elements. Hence, there is a need to have a laboratory test facility that will achieve reasonable rates of erosion of metal surfaces without having to transport excessive quantities of ash.

1.2 Definition of Terms

1.2.1 Erosion

Erosion is the mechanical wear of the target metal surface by a stream of fluid carrying entrained solid particles. The type of target material influences the form of material removal. Material removal in ductile materials is by extrusion and pitting, while material removal in brittle materials is by plastic deformation, Levy (1985).

1.2.2 Rotary Regenerative Heat Exchanger

Rotary regenerative heat exchangers are commonly used in fossil-fuelled power stations. They improve thermal efficiency of the power stations by extracting heat from the flue gases leaving the boiler and use it to preheat air from the atmosphere that is drawn into the boiler as combustion air. Most power stations use two 50% duty rotary regenerative heat exchangers per boiler. The rotary regenerative heat exchangers are located in a power station as shown in Figure 1.1.

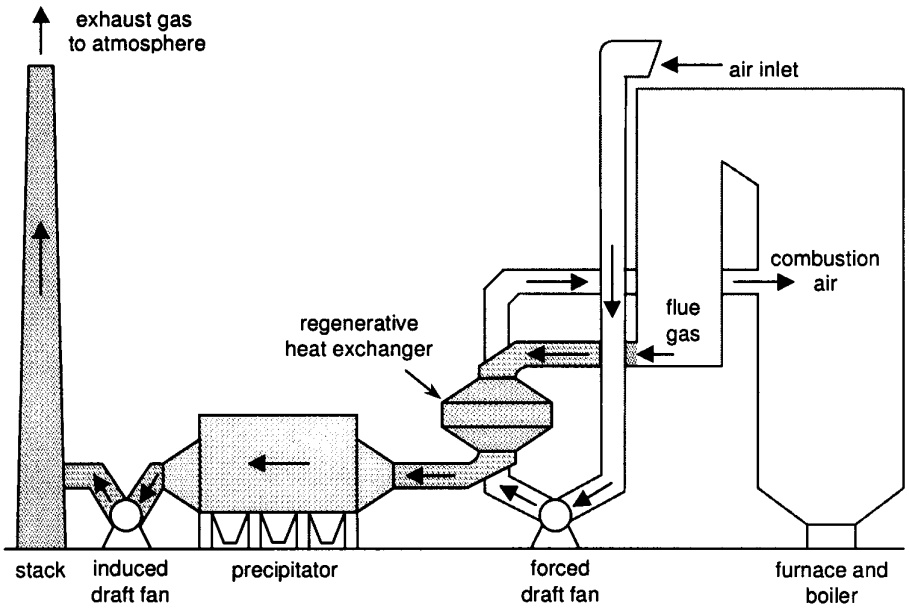


Figure 1.1: Regenerative heat exchanger position in operating environment
(Crookes, 2000)

The operation of the two main types of rotary regenerative heat exchanger designs is shown below. The Ljungstrom design, Figure 1.2, is also known as the rotating matrix regenerative heat exchanger. The rotating matrix is alternately exposed to the streams of cold air and hot flue gases. The heat extracted from the hot flue gases is transferred to the cold air, thereby increasing the temperature of the air entering the boiler burners.

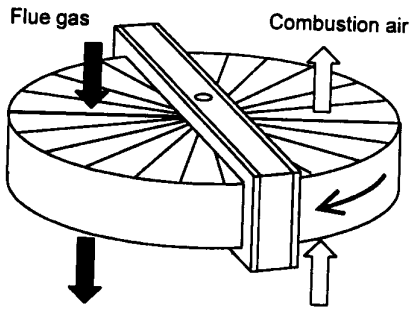


Figure 1.2: Ljungstrom regenerative heat exchanger, (Crookes, 2000).

The Rothemühle design operates with a static matrix and a rotating hood that directs the air flow. Combustion air flows through the rotating hood while flue gas flows through the fixed matrix as shown in Figure 1.3. During the rotation of the hood in the air preheater the process of heat transfer takes place where heat is extracted from the flue gas and transferred to the combustion air.

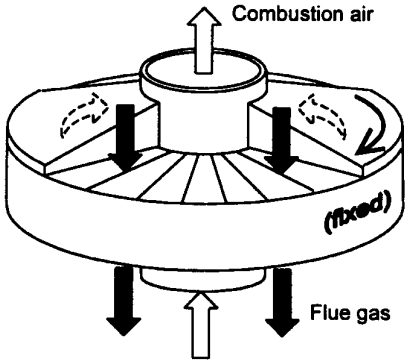


Figure 1.3: Rothemühle regenerative heat exchanger (Crookes, 2000).

1.2.3 Heat Transfer Elements

The regenerative heat exchangers are filled with heat transfer elements that extract heat from the flue gases and transfer it to the combustion air. Different element profiles are used in regenerative air heaters (RAH). Figure 1.4 shows the undulated and corrugated plates. These are the most commonly used plate elements in air preheaters. Some profiles that are also used in Eskom power stations are shown in Figure 1.5. Figure 1.6 shows a sectional view of a Ljungstrom regenerative heat exchanger showing packed heat transfer elements. The heat transfer elements are usually packed in more than one layer. Typically there is a hot layer, an intermediate layer and a cold layer with different element profiles. The hot end layer is the top layer of the pack elements. It is the layer that is exposed to the hot flue gases coming from the boiler. The hot end and intermediate layers are made out of low carbon steel material. The cold layer is the bottom layer that is exposed to the cold air from atmosphere. It is the first layer that comes into contact with the air from atmosphere which is drawn in for combustion purposes in the boiler. The cold layer is often made out of low alloy steel (Corten) to protect it against corrosion. These layers are shown in Figure 1.7.

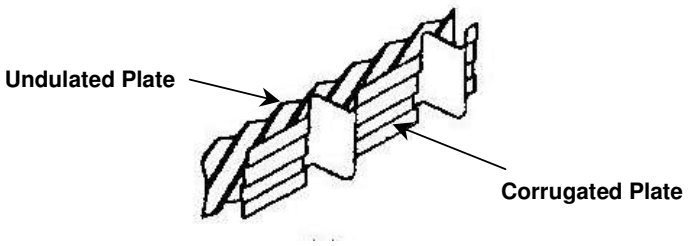


Figure 1.4: Undulated and Corrugated plates (de Klerk, 2001).

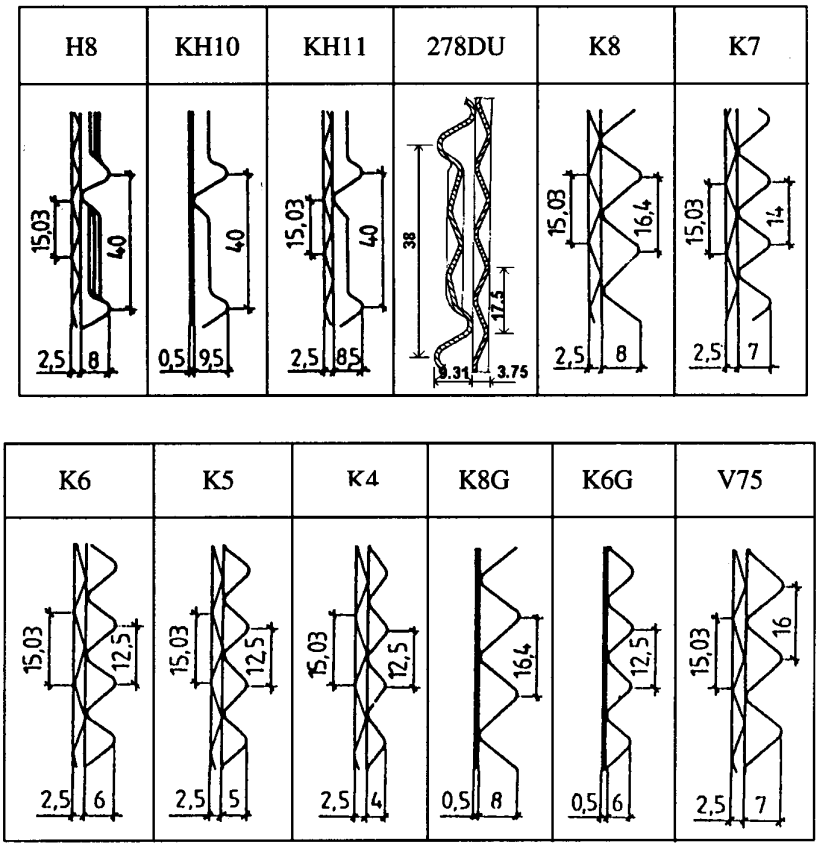


Figure 1.5: Heat transfer element profiles (Crookes, 2000).

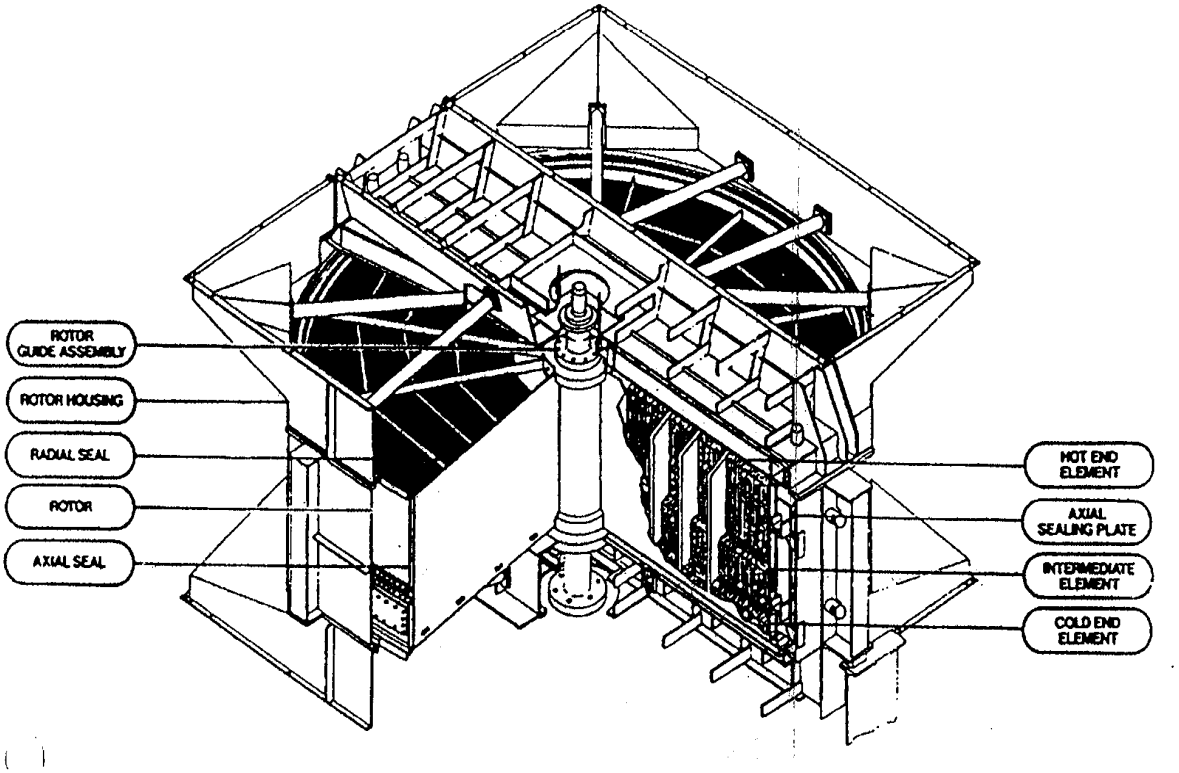


Figure 1.6: Heat transfer elements packed in a Ljungstrom RAH (Blackburn, 1996).

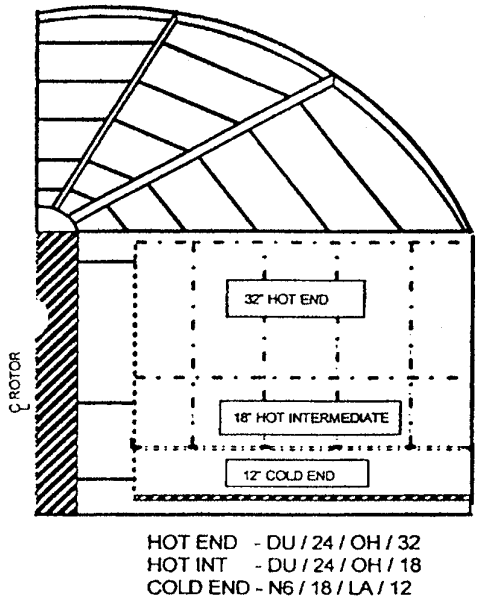


Figure 1.7: Heat transfer elements packed in three layers (Blackburn, 1996).

1.3 Objectives of the Present Study

The present study was undertaken to determine erosion rates of the air pre-heater elements' mild steel material by using ash samples from various Eskom fossil-fuelled power stations. This was to be done by using a test facility to be established in the laboratory of the School of Mechanical, Industrial and Aeronautical Engineering to determine the erosion potential of the ash samples from the various power stations.

1.3.1 Construction of the Erosion Test Facility

The construction of the test facility was considered as the most important objective since there was no other available facility that could be used to carry out the investigations that led to the conception of this study. The following had to be borne in mind when constructing the test facility:

- The test facility had to give erosion data that would be measurable and compared with data received from system engineers at various Eskom fossil-fuelled power stations.
- It had to be an accelerated erosion test facility that could give measurable results.
- It had to be used for similar work in future.
- It had to able to test different angular positions of the test specimen.
- It should be able to test erosion rates of mild steel.
- The test facility had to be constructed completely within budget.
- It had to fit the space available in the laboratory and still leave space for other apparatus, ash storage and other activities.

The test facility was then designed, built and commissioned at the University of the Witwatersrand in the School of Mechanical, Industrial and Aeronautical Engineering, for the reasons already mentioned above.

1.3.2 Collection of Ash Samples

Looking at the number of fossil-fuelled power stations that Eskom has, it would not be possible to collect ash samples from all power stations and test them. This is due to

the time allocated for the study and budget. So, a strategy had to be devised on how the tests could be done such that they are representative of the ash that is generally available at power stations. Ash analysis information was available at Eskom Technology Research and Investigations located in Rosherville, Johannesburg, and this indicated that not all power stations experience severe erosion. This came out of an analysis done by Bosch (1993). It was decided that by testing three or four ash types, a fair reflection of erosion that is experienced at power stations could be obtained. A few parameters were considered in the ash composition to be the most significant in the selection of the ash samples that would be broadly representative of the wide range of ash from different power stations. These parameters are the silica content (SiO_2), particle size, abrasiveness and ash content in coal.

1.3.3 Determination of Erosion Rates

This objective was broken down into three main series of tests to be conducted. These were the determination of the critical angle of attack that gives maximum erosion on the target material, and determination of the effect of particle velocity and concentration on the erosion rate of the target material. The first tests to be conducted were the determination of the critical angle of attack that gives maximum erosion on the target material. This test was the most important one to start with because the critical angle of attack that gives maximum erosion was to be used in the velocity and concentration tests with the target material in a fixed position throughout these tests.

1.3.4 Comparison with Work of Others

At the end of the first three objectives there were test results that came from the series of tests carried out in the determination of the erosion rates. These results were compared with the work of others from their investigations. This had to be done to measure the findings from this study against the findings from other investigations.

1.4 Structure and Outline of the Report

Chapter 2, the literature survey, describes some of the investigations that have been carried out on erosion as a material removal process. In most of the investigations

done the focus was on erosion experienced in gas turbines and boiler tubes. These investigations are also relevant to the present study because fly ash is the main erodent considered.

Chapter 3 deals with the test facility that was used to carry out the experimental investigations. The test facility was constructed and commissioned in the laboratory of the School of Mechanical, Industrial and Aeronautical Engineering. The design of the test facility is described in detail in this chapter.

Chapter 4 gives a detailed experimental procedure that was used in this study. This procedure also serves as a guideline to anyone operating the test facility.

Chapter 5 presents the test results from the tests carried out in this investigation. In this chapter the results are discussed in detail.

Chapter 6 gives conclusions and recommendations that were drawn from the results presented in Chapter 5.

2 LITERATURE SURVEY

Lee *at al.* (1999) have given a comprehensive summary of the factors that determine erosion. The factors that determine erosion are outlined below and discussed in this order in the text that follows.

2.1 Factors Determining the Rate and Nature of Erosion

1. Angle of impingement of the erodent.
2. Particle size.
3. Particle shape and hardness.
4. Particle impact velocity and the velocity exponent.
5. Particle concentration in the fluid stream.
6. Temperature effects.
7. Nature of material removal.

2.1.1 Angle of Impingement of the Erodent

In the investigations carried out by most researchers it has been found that the erosion rate is greatly affected by the angle of impingement of the erodent. Tabakoff and Wakerman (1979) observed that the erosion mass parameter (expressed as milligrams of material eroded per gram of abrasive impacting on the specimen surface) has a maximum value at an angle of attack of approximately 25°. They found that the effect of the angle of attack is independent of the particle velocities; however, the definition of the point of maximum erosion becomes much more explicit with increasing velocity, as shown in Figure 2.1. The tests were done using Kingston coal ash (a British power station). The tests were run with the target temperature varied from ambient to 649°C.

Raask (1985) observed that the maximum erosion occurs at impaction angle between 30° and 45°. Experiments were carried out using quartz grains and glass spheres as erodents on mild steel material. These erodents were chosen as they are major

abrasives found in coal. Zhong and Minemura (1996) found that the erosion mass parameter has a maximum value at an angle of attack of approximately 50°.

Oka *et al.* (1997), Tilly and Sage (1970), Grant and Tabakoff (1980), all found that the maximum value of the erosion mass parameter occurs at an impaction angle of approximately 20°. From these and other investigations about the effect of the angle of impingement on the eroded material it has generally been found that maximum erosion occurs at angles between 20° and 25°.

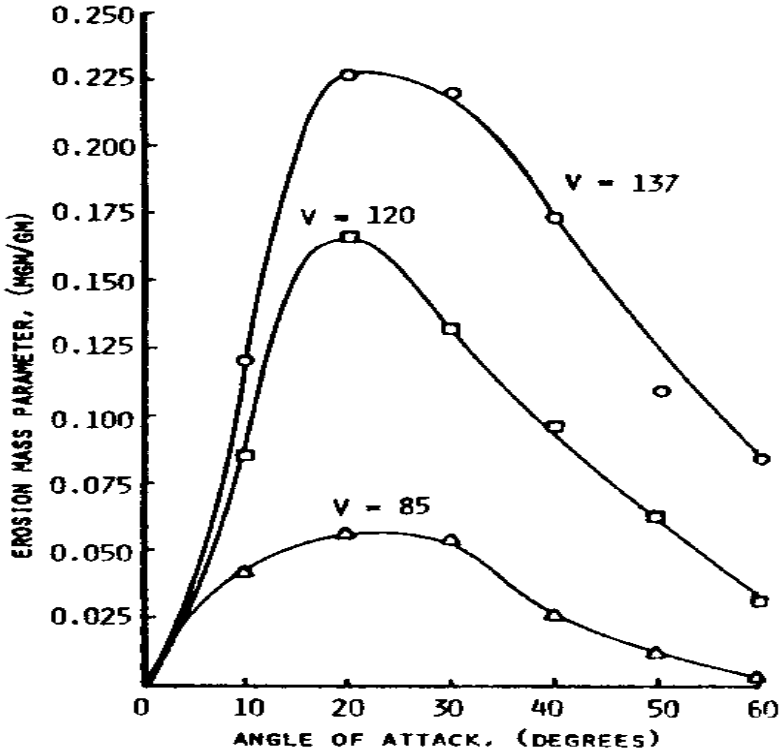


Figure 2.1: Effect of angle of attack on erosion rate (Tabakoff and Wakerman, 1979).

2.1.2 Particle Size

The particle size has also been found to be a very important contributing factor in accelerating erosion. Big particles traveling at high velocity can cause significant erosion at the point of impact because of their inertia. If these particles have high silica content the target surface will experience even more severe erosion at the point of impact, see section 2.1.3.

Zhong and Minemura (1996) carried out an investigation for the measurement of erosion due to particle impingement and numerical prediction of wear in a pump casing. They found that wear (W) on a target material is the sum of deformation wear (W_d) and cutting wear (W_c). They related this finding by the following equations:

$$W = W_d + W_c \tag{2.1}$$

where

$$W_d = (1/2)M_p(V_{ni} - K_1)^2/\varepsilon_d \tag{2.2}$$

$$W_c = \frac{1}{2} M_p \frac{\{V_{ti}^2 - K_2(V_{ni} - K_1)^{3/2}\}}{\varepsilon_c} \tag{2.3}$$

The terms ε_c and ε_d are coefficients of erosion, V_n and V_t are normal and tangential velocity components, respectively; M_p is the mass of the particles, B, K_1 and K_2 are constants depending on the material properties of the particle and wall, such as density and Poisson's ratio. The results of their investigation are shown in Figure 2.2. From these equations and Figure 2.2, it is apparent that an increase in particle size causes a decrease in cutting wear, while the deformation wear will not change.

Tilly and Sage (1970) observed erosion caused by quartz particles of sizes ranging from 0 to 150 μm. The results of their investigation are shown in Figure 2.3. It can be seen that erosion is very small for particles smaller than a threshold size of about 20μm, which is dependent upon the target material. For nylon and steel there is also a saturation level where erosion is independent of particle size.

Finnie *et al.* (1967) eroded annealed commercially pure aluminum (1100-0), at impaction angle of 20° and velocity of 152.4 m/s, with different sizes of silicon carbide (SiC) particles. It was found that the particles with sharp edges produced high erosion rates compared to spherical particles. This was due to the sharp edges cutting deeper into the target surface resulting in more material eroded from the surface.

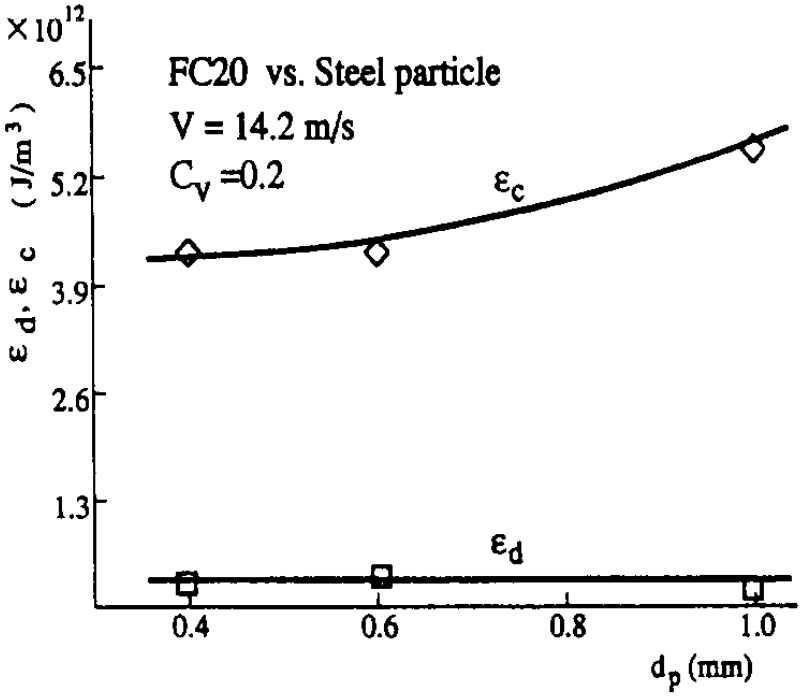


Figure 2.2: Effect of particle size on erosion rate (Zhong and Minemura, 1996).

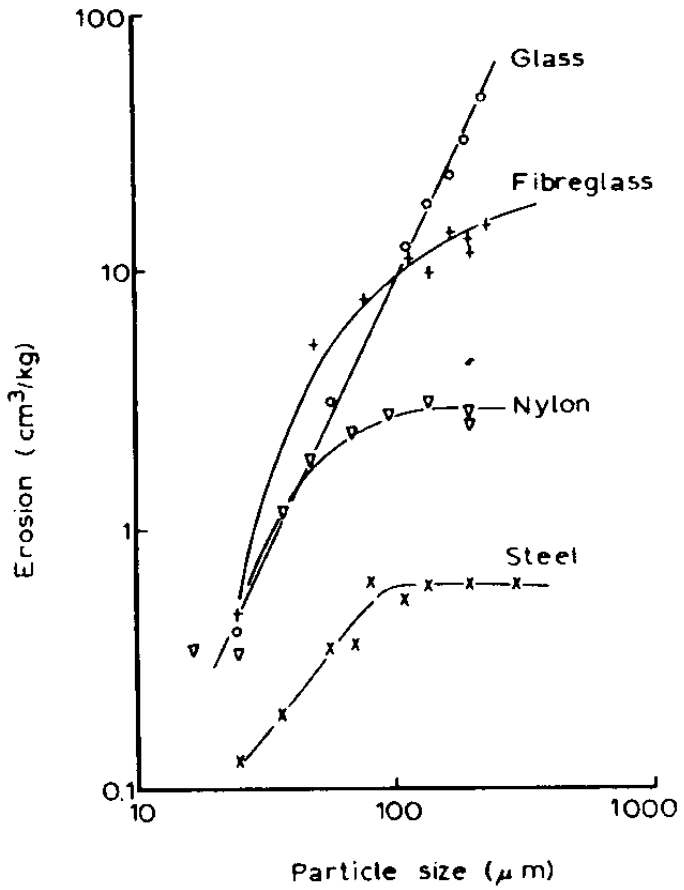


Figure 2.3: Effect of particle size (Tilly and Sage, 1970).

2.1.3 Particle Shape and Hardness

It has been found that angular particles are more erosive than spherical particles. Angular particles erode materials by cutting. When a material is struck by spherical particles, some of the particles bounce off the material without eroding it.

Levy and Chik (1982) carried out investigations on the effects of erodent composition and shape on the erosion of steel. They used particles of five different erodents, all angular in shape, and in the size range 180 – 250 μm. Also, two different shapes of the same particle composition were used to study the effect of shape on erosion rate. The particles used were steel shot (spherical) and grit (angular) with an average size of 100 μm. The steady state erosion rates of the AISI 1020 steel with a Vickers hardness number, H_v = 150 kg f mm^{-2}, eroded by each type of particle are listed in Table 2.1. The rates for the brittle erodents are plotted in Figure 2.4. It can be seen that the erosion rates are very low for the softest materials, such as calcite and apatite. Once the Vickers hardness number of the particles reaches approximately 700 kg f mm^{-2}, the erosion rates remain essentially constant as the hardness of the particles increases further. Thus silica (SiO_2) at H_v = 700 $kgfmm^{-2}$ has nearly the same erosivity as silicon carbide (SiC) at H_v = 3000 kg f mm^{-2} although silicon carbide has over four times the hardness of the silica.

When coal is burnt in a boiler flame, the coal's abrasive characteristics are markedly changed, Raask (1985). The mineral in coal consists of a mixture of different species, which have widely different hardness numbers, as shown in Table 2.2. The ash particles have less variable hardness characteristics. Shown in Figure 2.5, the glassy particles, which make up the bulk of pulverized fuel ash, have a comparatively high Vickers hardness number of about 600 kg f mm^{-2}. Raask (1985) observed that the erosion damage caused by these particles is limited because of their spherical shape. The gritty fraction of the pulverized fuel ash consists largely of unfused quartz particles and irregularly shaped agglomerates of sintered ash. Raask (1985) determined the relationship between erosion and Vickers hardness for a number of steels, as shown in Figure 2.5.

Table 2.1: Erodent particles and rates of erosion of AISI 1020 steel (Levy and Chik, 1982).

Erodent particles and rates of erosion of AISI 1020 steel

Particle composition	*Density* (g cm^{-3})	*Mohs' hardness*	*Vickers' hardness* H_V (kgf mm^{-2})	*Erosion rates* ($\times 10^{-4}$ g g^{-1})	
				$\alpha = 30°$	$\alpha = 90°$
$CaCO_3$ (calcite)		3	115	0.03	Not measurable
$Ca_5(PO_4)_3$ (apatite)		5	300	0.5	0.3
SiO_2 (sand)	2.7	7	700	3.0	1.6
Al_2O_3 (alumina)	4.0	9	1900	2.6	1.4
SiC (silicon carbide)	3.2	> 9	3000	3.3	1.9
Steel grit	7.9			5.3	
Steel shot	7.9			1.4	

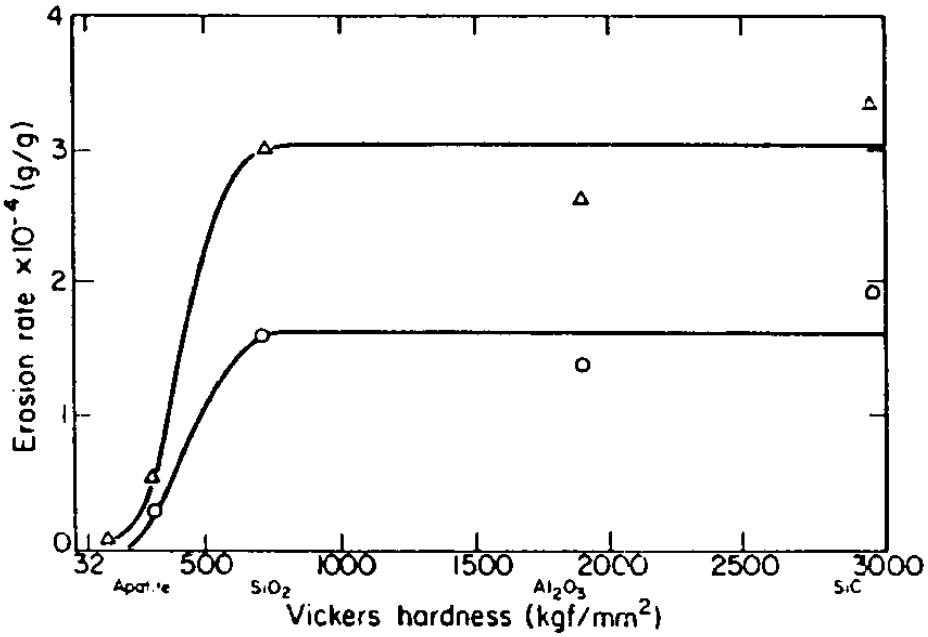


Figure 2.4: Erosion rates of AISI 1020 steel by five erodents: Δ, α = 30°, o, α = 90°, (Levy and Chik, 1996).

Mineral	Ash Products	Vickers Hardness, kg mm^{-2}
Silicates	Glassy spheres with some mullite needles in glassy matrix	550 to 600
Quartz	Glassy spheres and rounded quartz particles	600 to 1200
Pyrites	Spherical particles of magnetite and haematite	500 to 1100

Table 2.2: Coal minerals and hardness numbers of ash products (Raask, 1985).

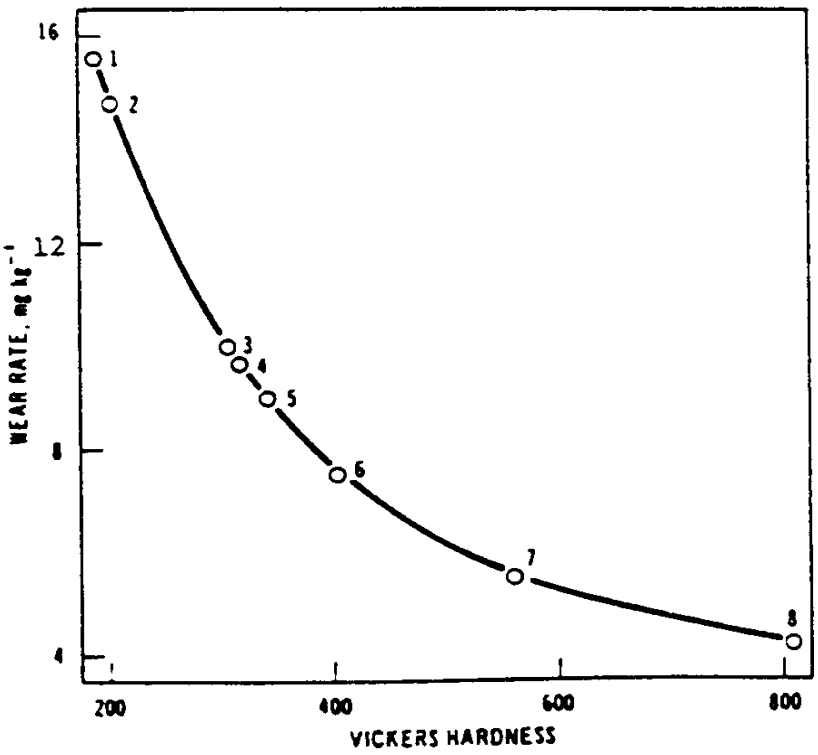


Figure 2.5: Erosion wear of steel alloys of different hardness (Raask, 1985).

Quartz impaction; velocity 27.5 m/s

1-Mild steel

2-Austenitic

3, 4, 5, 6-Hardened steels

7-CrB-steel

8-Ni-hard.

2.1.4 Particle Impact Velocity and the Velocity Exponent

Tabakoff and Wakerman (1979) carried out experiments at high velocities of 85, 120 and 137 m/s, as shown in Figure 2.1. They found the occurrence of maximum erosion to be independent of velocity, but the definition of maximum erosion becomes much more defined at high velocities.

Tilly and Sage (1970) developed a relationship between erosion rate, ε, and velocity, V, by the power law:

$$\varepsilon = a V^{\alpha} \quad (2.4)$$

where a and α are material constants characterizing the relative erosivity and velocity exponent, respectively. For 125 – 150 μm quartz, the velocity exponent was found to be 2.3 for materials as diverse as metals and plastics. For particles of 125 μm down to 25 μm in size, the velocity exponent was found to decrease from 2.3 to 2.0.

Grant and Tabakoff (1980) investigated the effect of velocity at angles of impaction of 20° to 90°. At the angle of impaction of 20° they observed that the velocity exponent was approximately 2.8. At normal impaction or 90° impact, they found the velocity exponent to be of the order of 4.

Sheldon and Kanhere (1972) observed that the amount of material eroded, w, is a function of the particle impacting velocity, V, as well as the particle diameter, d_p. It is represented by power law equation:

$$w = kV^{a}d_p^{b} \quad (2.5)$$

where;

k = material constant characterizing the relative erosiveness

a = velocity exponent

b = constant relative to particle size

The material tested was 6061-TO aluminum alloy. They found that the velocity exponent is higher (2.83 for glass shot and 2.80 for steel shot) when either steel or glass shot impacts work hardened surfaces than annealed surfaces (2.52 for glass shot and 2.34 for steel shot) at a 20° angle. At 90° impaction, the results for the work hardened and annealed surfaces are equal, the velocity exponent being 2.41 when glass shot was used and 2.19 when steel shot was used.

Singh *et al.* (1990) studied room temperature erosion behavior of 304, 316 and 410 stainless steels. They related the erosion rate, ε, to particle velocity, V, by the power law:

$$\varepsilon = a V^{\alpha} \quad (2.6)$$

where α and a are velocity exponent and material constant, respectively.

From the results shown in Figure 2.6 it can be seen that the maximum velocity exponent for 304 and 316 stainless steels occurs at 30° impact angle, and that for 410 stainless steel occurs at 60° impact angle.

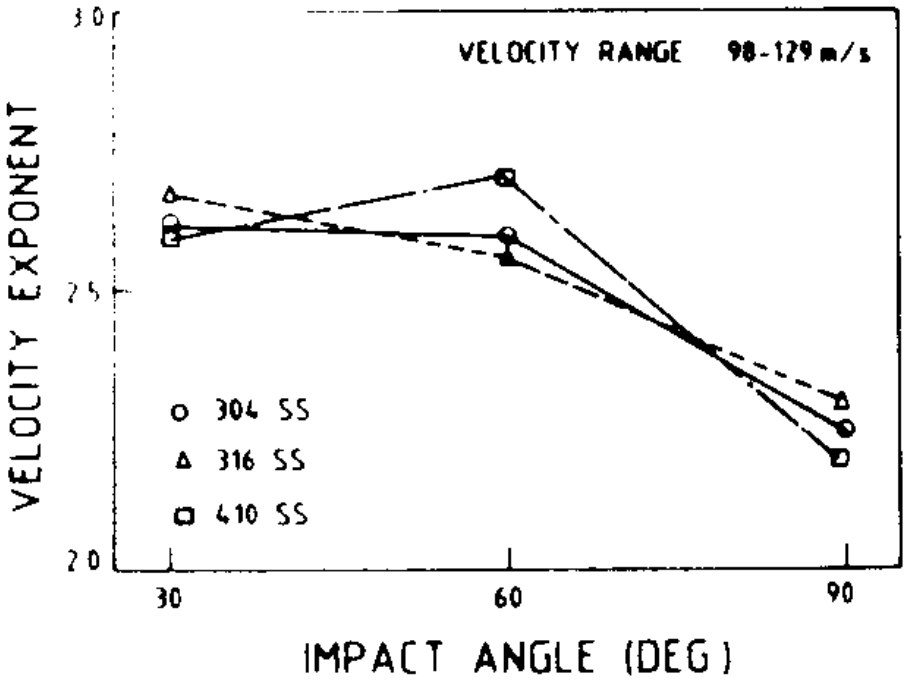


Figure 2.6: Effect of impact angle on velocity exponent (Singh *et. al.,* 1990).

2.1.5 Particle Concentration in the Fluid Stream

Zhongi and Minemura (1996) investigated the relationship between erosion coefficients, $\varepsilon_{c,}$ and ε_d, and particle concentration, C_v. The results are shown in Figure 2.7. Both ε_c and ε_d are seen to increase as C_v increases.

Tilly and Sage (1970) carried out experiments on a titanium alloy and steel to determine the effect of particle concentration on erosion under vacuum. They observed that the change in erosion was small. Two sizes of quartz dust, shown in

Figure 2.8 shows effect of particle concentration using dust particles as erodent to attack target material, Titanium alloy and 11% Chromium steel. This figure shows that small particles cause less erosion when compared to big particles. The highlight in this figure is the relationship between erosion rate and concentration. It shows erosion as decreasing with increasing concentration. This is totally opposite to the relationship shown in Figure 2.7. This is one finding that came up with a trend that did not follow any of the work done by others. This was not explained as to why it is so.

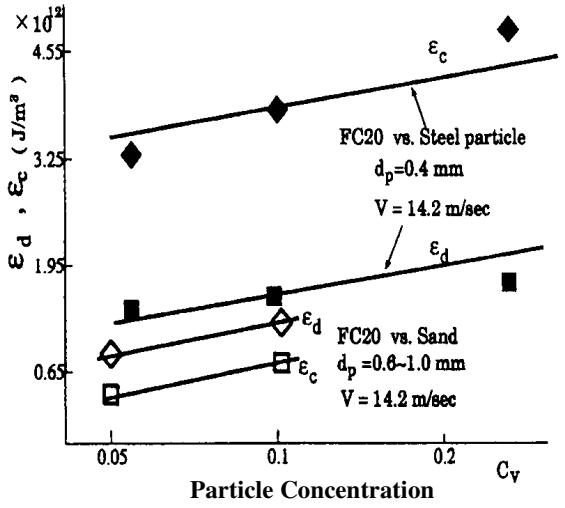


Figure 2.7: Effect of particle concentration (C_v) (Zhong, 1996).

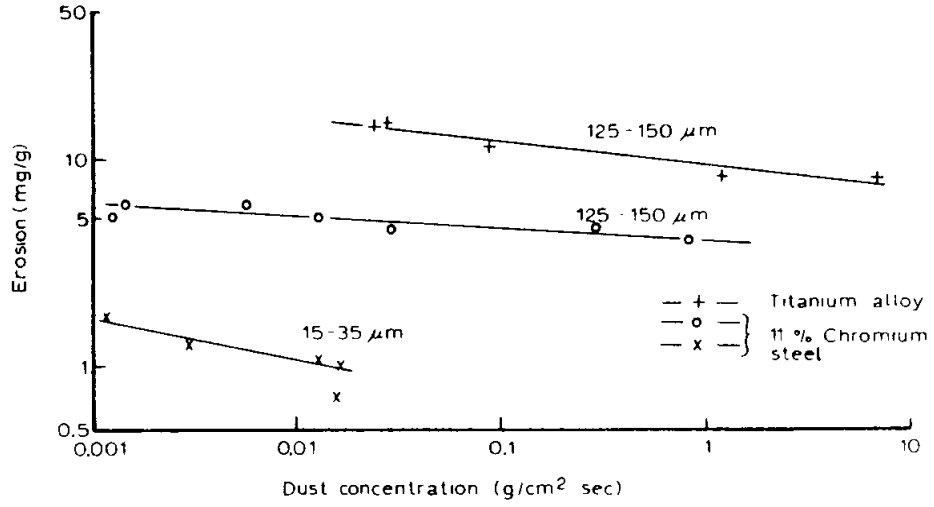


Figure 2.8: Influence of dust concentration on erosion (Tilly, 1970).

2.1.6 Temperature Effects of the Two Phase Flow

Tabakoff and Wakerman (1979) investigated the effect of temperature on erosion. The results are presented in Figure 2.9. From the two curves of Figure 2.9, it can be seen that for both velocities the erosion rate decreases very slightly for increased temperature between the ambient temperature and 150°C. The predominant influence of the temperature on erosion is observed, however, at temperatures above 150°C. With increased temperature, the erosion rate is found to increase initially at a lower rate up to about 316°C, and then to increase at a higher rate.

Levy and Chik 1(982) investigated the changes in wear rates for temperature up to 550°C, as shown in Figure 2.10. It can be seen that both silicon carbide, SiC, and silica, SiO_2, particles cause a marked increase in wear rate with temperature, particularly above 300 - 400°C. The erosion rate when using ash increased only slightly with temperature.

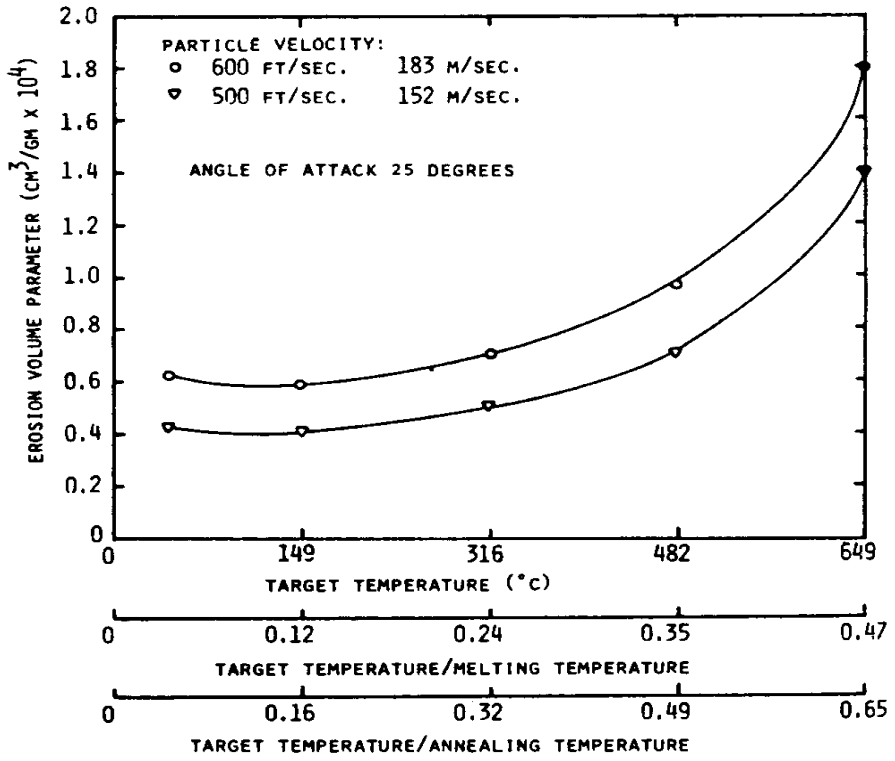


Figure 2.9: Effect of temperature on erosion (Tabakoff, 1979).

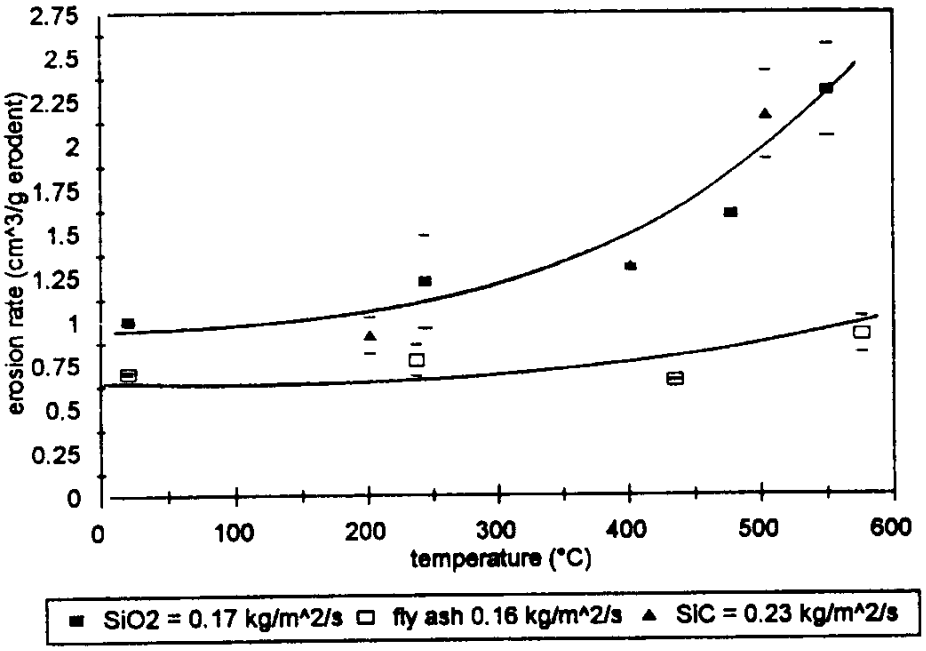


Figure 2.10: Differences in particle erosivity at a constant particle velocity 24±2 m/s, (Levy and Chik, 1982)

2.1.7 Nature of Material Removal

In most of the studies carried out on the erosion of materials by small particles entrained in moving fluids, it was found that the particle shape plays a major role in the form of material removal. Angular particles have been found to erode materials by cutting, while spherical particles erode materials by plastic deformation.

Finnie *et al.* (1967) carried out tests on both ductile and brittle materials eroded by silicon carbide particles. In their investigation they carried out tests for individual materials at the same velocity of 76.20 m/s. They bombarded the material surface with a flow stream of silicon carbide particles. They found that out of the ten materials they tested eight experienced peak erosion rate at the same angle of attack, 25 º, with the other two experiencing peak erosion also at the same angle of attack, 90 º. The eight materials that experienced erosion at 25 º are ductile materials. Their findings are shown in Figure 2.11. This shows that the ductile material experiences severe erosion

when the particles cut into the target surface. When the particles attack the target surface they remove material in the chip form.

Tilly and Sage (1970) suggested that erosion occurs by a two-stage process. In the first stage, for brittle materials the mechanism of material removal appears to be cracking upon impact, while for predominantly ductile materials the situation is more complex because impaction causes pronounced pitting and extrusion of material in the direction of motion of the particle, to form a hump or lip. The second stage occurs as fragments of the particle cause the radial or secondary scars.

Levy and Chik (1982) observed that the loss of metal from an eroding surface appears to occur by a combined extrusion-forging mechanism. The erosion occurs by the generation of and loss from the surface of the plate-like pieces of metal. The effect of particle velocity on the platelet formation process is shown in Figure 2.12. The increased size of the platelets is caused by the marked increase in the force imparted to the surface by the much faster moving particles. The increased particle velocity does not change the erosion mechanism but only the size of the platelets. The larger size platelets result in the peak erosion rates.

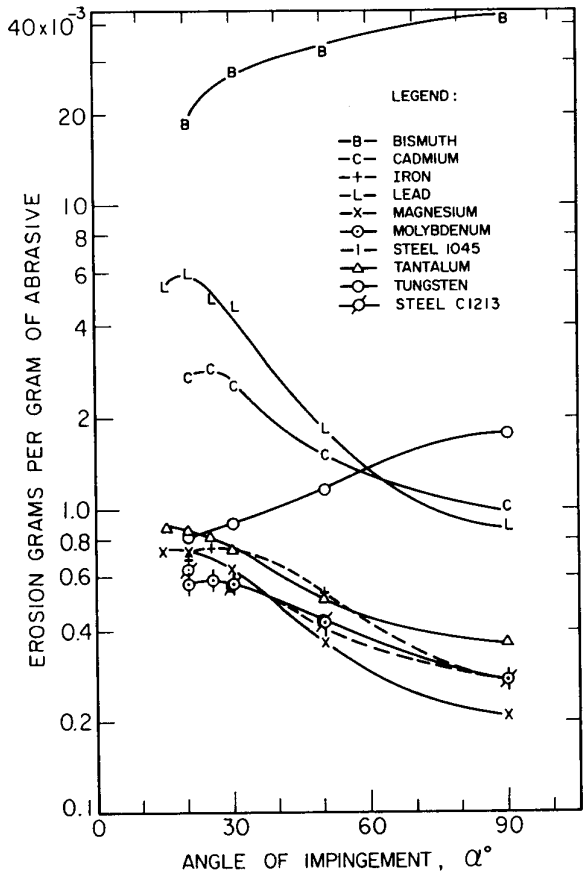


Figure 2.11: Weight removed by erosion as a function of angle for a number of metals eroded by silicon carbide particles at 76.20 m/s, (Finnie *et al.*, 1967).

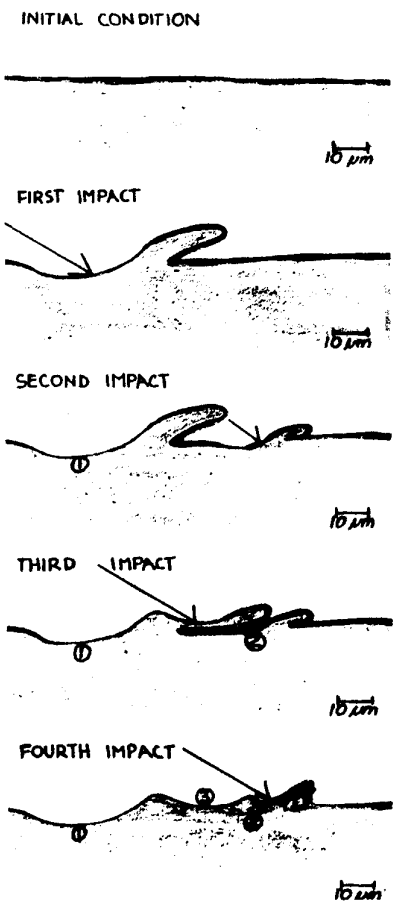


Figure 2.12: Platelet formation on metal surface (Levy and Chik, 1982).

2.2 Summary of the Findings from the Literature Review

The literature highlights factors that have significant influence in the material removal on a target surface. These factors include material of the target surface, chemical composition and particle size and shape of the erodent, the particle velocity and angle of attack. The ductile mild steel material experiences the most severe material erosion. This is backed by a number of investigations done over the years.

The literature also indicates that the critical angle of attack is between 20º and 30º. Most investigations in the literature found the critical of angle attack to be in the range between 25º and 30º. A lot of work has been done in this regard to determine the critical angle of attack. It also shows that most erosive chemical elements are quartz and abrasive materials. The particle size and shape also have a significant effect in the

erosion of the target material. The particle velocity also influences the erosion of the target material. The literature shows that erosion rate increases with increasing velocity. The other factor that influences erosion of the target material is the particle concentration. The erosion rate also increases with increasing concentration. The literature found that these relationships, erosion rate and particle velocity and erosion rate and particle concentration, are related by a power law.

3 DESIGN OF THE TEST FACILITY

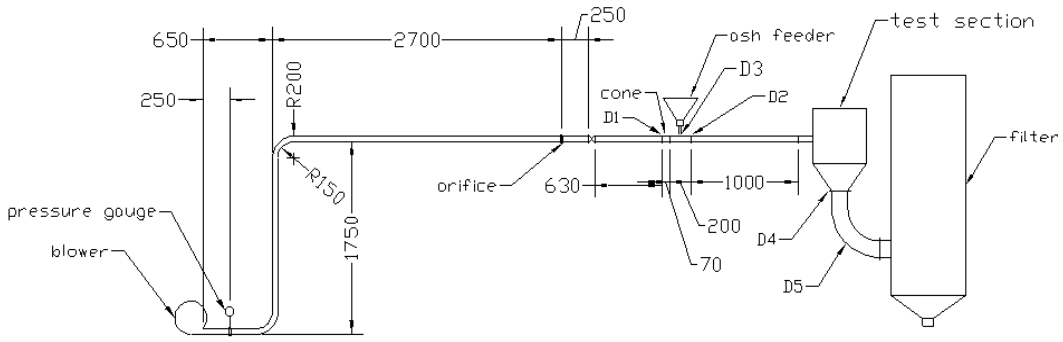


Figure 3.1: Layout of the test facility.

Figure 3.1 shows a layout of the test facility that was used to carry out the investigations in this study. The test facility was designed and constructed at the University of the Witwatersrand in the School of Mechanical, Industrial and Aeronautical Engineering. The manufacturing of the test facility was also done at the school. The manufacturing drawings of the test facility are attached in Appendix A.

The layout shows the complete assembly of the test facility as it was in full operation during the tests. The sequence of operations in the test facility is as follows:

- The blower pumps air into the pipeline at a particular velocity. This velocity is regulated by a speed controller that is connected directly to the blower motor main power supply line.
- The pressure gauge in front of the blower indicates the pressure reading of the air flowing in the pipeline coming from the blower.
- The air flows through the vertical section and horizontal section of the pipeline. In the latter section of the pipeline the air flows through the orifice meter.
- After the orifice meter there is another constriction, a venturi, in the conical section from D1 to D3, see Figure 3.1. In this section of the pipeline ash particles are fed into the pipeline by the ash feeder. The air that is pumped into

the pipeline by the blower carries these ash particles through the acceleration section of the pipeline where the mixture is allowed to attain the velocity of the air.

- At the end of the acceleration section there is a test section where the target surface is mounted. The flow stream of the ash particles coming out of the acceleration section impacts on the target surface in the test section.
- After the ash particles have impinged on the target surface they come out of the test section through the ducting at the bottom of the test section. These ash particles get collected in the filter.
- The filter collects ash at the bottom allowing air to exit at the top of the filter. Small ash particles that get entrained in the air collect on the sides of filter bags inside the filter. An extractor fan was mounted in a window facing the exit of the filter to draw the entrained ash particles out of the laboratory. This fan provides good ventilation in the laboratory.

3.1 TEST FACILITY REQUIREMENTS

A test facility needed to be designed and constructed to meet the objectives of this investigation. The most important criterion that had to be addressed was the data to be provided by the test facility. The test facility should provide measurable erosion of material when the target surface is hit by a flow stream of the ash particles. The test facility should provide accelerated erosion of material on the target surface. The amount of the ash fed into the main pipeline by the ash feeder should be accurately measured. The facility should be able to provide variable flow velocity in the flow stream of the ash particles that hit the target surface. The test specimen was also another design factor of the test facility. The sizing of the test specimen could also be derived from the size of the facility. The facility should provide variable angle orientation of the test specimen.

All these requirements needed to be taken into consideration when deciding on the final layout of the test facility. There were other constraints that had to be dealt with in order to design the test facility that was going to meet the stated requirements. These constraints are space available in the laboratory that was identified to be used to build and commission the test facility, storage of the ash samples that were going to

be used to run the tests, collection of the ash after the tests and ventilation in the laboratory to prevent health hazards. The other constraints were budget and time allocated for the study. The budget constraint saw the use of already available equipment for the main air supply and measurement of the pressure difference across the orifice meter. The time limitation dictated the type and number of tests that had to be done.

3.1.1 BLOWER

The main air supply in the pipeline was provided by the blower. The budget constraint led to the selection of this blower. This blower was suitable for the type of tests that were carried out in the study. The maximum velocity that could be achieved with the blower was 27 m/s. This velocity is almost three times the actual flue gas velocity of 10 m/s that flows through the air preheater at power station boilers. For accelerated erosion test purposes the velocity range that could be achieved by the blower was adequate. The variable speed of the blower was controlled by the use of a speed controller. This type of speed controller is called Siliconics, PWM Inverter-ACD. The speed controller was regulating the speed of the three phase power motor that was coupled to the blower. The regulation of the speed was done by changing the frequency in the speed controller that could produce the variable speed. The speed controller and motor were also readily available with the blower. Using them in this study also helped in the cost cutting exercise.

The blower specification on the name plate that was attached to it read as follows:
Davidson & Co.
Fan Number: 96978
Belfast
Northern Ireland
Size: 17 ½''
Fan Number: 10332 (RSA)

The motor specification on the name plate that was attached to it read as follows:

Size	: C184
Power	: 3 Hp
Speed	: 1420 RPM

Number of cycles : 50

Current : 5.36 Amps

BS 2960: 1958

3.1.2 ORIFICE METER

Along the main pipeline there were pipe constrictions and fittings that allowed pipe diameter changes. One of these items was the orifice meter that was fitted before the point of introduction of the ash particles into the main pipeline. The orifice meter was designed in accordance with design information from Douglas (1987). The pressure difference across the orifice meter was measured by the use of a pressure manometer. After the orifice there was a ball valve that was used to regulate air flow downstream. The ball valve was opened in stages like partially open up to fully open position. This was done so to provide different velocities in the flow stream. When the ball valve was partially open the flow stream velocity was low and increased with the valve moving to the fully open position.

3.1.3 ASH FEEDER

One of the test facility requirements was to accurately measure the amount of ash that was fed into the main pipeline to be carried into the test section by air. The feeder had to introduce ash that would be enough to form a good mixture with the air supply and be able to hit the target surface in the test section. The ash from the feeder was fed into the main pipeline through a venturi that was designed in accordance with design information from Douglas (1987). The feeder had a variable speed controller that made it possible to regulate feed rate. The type of speed controller used is called Siemens Micromaster. The feed rate in the feeder was regulated by varying the frequency in the speed controller, hence the feed rate would change.

The feeder was built onto load cells that were used to accurately measure the amount of ash fed into the main pipeline. This configuration of the feeder is known as a weight loss metering unit with a screw. This feeder could give the initial quantity of the ash, amount of ash fed into the main pipeline and the final mass left in the feeder after each test run.

The feeder was purchased from a South African supplier called Alkamee cc. The original equipment manufacturer of the feeder was Torex S. R. L., Medolla (MO)

Italy. The specification of the feeder is attached in Appendix B. The description of the feeder is as follows:

Description	: Screw Feeder "DCC32/S" Type
Type	: DCC
Size	: 32
Serial Number	: 01102501
Job	: 2188/1
Construction Year	: 2001

3.1.4 TEST SPECIMEN

The test specimen was made out of mild steel material. This material is the most commonly used in air preheater plates at fossil-fuelled power stations. This could give results that are representative to a certain degree of the real situation at fossil-fuelled power stations. The test specimen should produce measurable erosion rate using the accelerated test facility. Its target surface that was going to be exposed to the flow stream of ash particles should allow all the ash particles entrained in the flow stream to impact on it. This meant that the ash stream issuing from the last pipe section impacted on the test specimen before collecting at the bottom of the test chamber.

The last pipe section had a major influence in sizing of the test specimen. The thickness of the test specimen was also chosen according to the reasonable erosion that could be experienced by the target surface. The test specimen size was 100mm square with 2mm thickness.

3.1.5 DATA ACQUISITION

One of the requirements of the test facility was the gathering of measurable data from the tests. This facility provided different types of data that were used in the investigation conducted in this study. The pressure in the main pipeline was measured by the use of pressure gauge and manometer. The pressure gauge was used to measure the pressure in the air supply coming from the blower. It was mounted in front of the blower. The pressure manometer was used to measure pressure difference across the orifice meter.

The amount of ash in the feeder hopper was measured by the load cells in the ash feeder. The feed rate and the final ash quantity left in the feeder left after each test run

was also measured by the load cells in the feeder. All this data was displayed in a display unit called Microcontroller 9300 NS. This equipment was also supplied by Alkamee cc. In this unit the amount of ash used throughout the test programme could be retrieved. This unit could also be programmed to control the operations in the feeder. There was also an option to toggle between functions and desired display of results while the test was still running.

The amount of wear experienced by the test specimen had to be measured after each test run. This was done by weighing the test specimen before the test and after the test. The difference between these two parameters was the amount of material eroded by the flow stream of the ash particles. This amount of eroded material was in milligrams. In order to measure this quantity a reasonably small balance scale had be acquired. The type of the balance scale that was used for this exercise was called ADA 210LE. This equipment was supplied by Adam Equipment. The specification of this equipment is attached in Appendix C.

3.1.6 SIZING OF THE TEST FACILITY

The main air supply was decided by the blower which was a readily available unit that was to be used in the test facility. Dimensions at the outlet of the blower were used as the basis of sizing the facility. This section of the blower allowed a 50mm diameter pipe to be joined onto it. This pipe diameter was used to get the right pipe material that could be used in the joint. A PVC pipe was chosen because it is light, cheaper, lasts long and is wear resistant, besides that PVC is the best selection for usage in pneumatics.

Other pipework used were 32mm diameter and 22mm diameter stainless steel pipes. Since this section was exposed to the mixture of air from the blower and ash particles from the feeder, a wear resistant material selection was necessary. Stainless steel was chosen in this section. Pipe constrictions were used to step down from big diameter pipe size to small diameter pipe size. The type of pipe constriction used in particular was a venturi. Stepping down in pipe sizes was also used to accelerate the flow stream in the pipework.

The size of the test specimen was decided on 100 x 100 x 2 mm. The flow stream coming out of the 22 mm diameter pipe could hit this size test specimen at the test section. This size took into consideration the target surface that would be hit by the

flow stream at all angular positions. The other consideration was mounting of the test specimen and still have enough target surface with no obstructions.

3.1.6.1 Parameters Used in the Sizing of the Test Facility

The test facility sizing had a direct influence in the type of flow that could be achieved by the ash particles downstream. The blower size dictated the whole sizing exercise of the test facility. Since the blower dictated the pipeline sizing the velocity range that could be achieved had to be determined using the pipeline size parameters. This section gives theoretical derivations that were used to determine the possible velocities that the mixture could attain downstream. The values used were taken from known properties of air at room temperature of 20ºC. It should be noted that the theoretically calculated velocity values differ significantly to the velocity values from the actual test.

Density of air, $\rho_{air} = 0.993 kg/m^3$

Gravitational acceleration, $g = 9.81 m/s^2$

Viscosity of air, $\mu_{air} = 18.12 \times 10^{-6} Ns/m^2$

PVC pipe diameter, $D = 46.6mm$

Acceleration section pipe diameter, stainless steel pipe, $d_m = 22.2mm$

Acceleration length, $L_m = 1m$

PVC pipe length, $L = 4m$

Mass load ratio, $$\mu = \frac{m_{pl}}{m_{al}} = 0.1 \qquad (3.1)$$

Where m_{pl} and m_{al} are ash particles and air mass flow rates respectively.

Ash particles mean diameter, $d_p = 35\mu m$

Diameter of orifice meter mounted in the PVC pipe, $d_o = 32mm$

Air velocity in the PVC pipe, this value came from blower dry test, $V_1 = 16m/s$

Bulk density of ash particles, $\rho_{ash} = 720 kg/m^3$

Mass flow rate of ash particles, $m_p = 0.007 kg/s$

Using continuity equation of flow, $Q = A_1V_1 = A_2V_2$, velocity of air passing through the orifice can be calculated and velocity of the mixture in the acceleration section can also be calculated assuming that the mixture will attain velocity of air.

Velocity of air passing through the orifice is given by the following equation,

$$V_o = \frac{A_1}{A_o}V_1 = \frac{46.4^2}{32^2}16 = 33.64 m/s \quad (3.2)$$

This velocity is more than the actual velocity for the tests. Assuming that in the acceleration section the mixture will attain the velocity of air, then the mixture flow velocity can be calculated using continuity equation of flow as follows;

$$A_1V_1 = A_mV_m \quad (3.3)$$

$$V_m = \frac{A_1}{A_m}V_1 = \left(\frac{46.4}{22.2}\right)^2 16 = 69.90 m/s$$

This could be the maximum velocity attained by the flow stream when it reached the test section. These velocity calculations were used in the estimation of the possible pressure drop in the main pipeline of the test facility when in operation. These were purely theoretical predictions, but the real scenario produced a maximum velocity of 27 m/s.

3.1.6.2 Pressure Drop in the Test Section

There is a drop in pressure when the air suddenly expands as it enters the test section. Wallis (1961) gives a range of pressure drop factor to be 30 to 50% of the mean dynamic head downstream of the flow. Taking a factor of 50%, the maximum pressure drop due to the sudden expansion of the air is given by;

$$\Delta P_{t1} = 0.5\frac{\rho_{air}V_m^{\ 2}}{2} = 0.5\frac{0.992(69.90)^2}{2} = 1213 Pa \quad (3.4)$$

3.1.6.3 Pressure Drop in the Acceleration Section

The ash particles injected into the main air stream are kept afloat by the drag and buoyancy forces. However, at low values of the air velocity, the gravitational force causes the particles to fall to the bottom of the main pipeline. Saltation velocity is the minimum velocity of the air below which the particles entrained in the air stream will separate from the air stream and fall to the bottom of the pipeline. Marcus *et al.* (1990) give the acceleration length, L_a, as follows;

$$L_a = 0.527 d_m \left(\frac{d_m}{d_p} \right)^{-1.26} (1+\mu) \mathrm{Re}_2 \qquad (3.5)$$

where,

μ = mass load ratio = 0.1

d_m = pipe diameter = 22.2mm

d_p = particle diameter = 35μm

Re_2 = Reynolds Number

$$\mathrm{Re}_2 = \frac{\rho V_m d_m}{\mu_{air}} = \frac{0.993 x 69.90 x 22.2 x 10^{-3}}{18.12 x 10^{-6}} = 8.5 x 10^4 \qquad (3.6)$$

Therefore, substituting all these values back into the acceleration equation, the acceleration length is found to be,

$$L_a = 0.527 d_m \left(\frac{d_m}{d_p} \right)^{-1.26} (1+\mu) \mathrm{Re}_2 = 0.527 x 22.2 x 10^{-3} \left(\frac{22.2 x 10^{-3}}{35 x 10^{-6}} \right)^{-1.26} (1+0.1) 8.5 x 10^4 = 0.322 m$$

In order to allow for adequate smoothing of the flow, the length of the pipeline between the test section and the point at which the ash particles are injected into the air stream was made to be 1.0m.

The friction factors, f_l and λ_l, for air and ash particles respectively, are given (Marcus *et. al.*, 1990) by the following equations;

$$f_{l2} = 0.0014 + 0.125(\mathrm{Re})^{-0.32} \qquad (3.7)$$
$$= 0.0014 + 0.125(8.5 \mathrm{x} 10^4)^{-0.32}$$
$$= 0.00471$$

$$\lambda_a = 0.0285 \frac{\sqrt{g d_m}}{V_m} = 0.0285 \frac{\sqrt{9.81 x 22.2 x 10^{-3}}}{69.90} = 0.00019 \qquad (3.8)$$

The pressure drop in the pipeline between the test section and the point at which the ash particles are injected into the air stream is given by the following;

$$\Delta P = L_a f_{l2} \frac{\rho_{air} V_m^2}{d_m} = 1.0x0.00471 \frac{0.993x69.90^2}{22.2x10^{-3}} = 1029Pa \quad (3.9)$$

It is assumed that the initial velocity of the ash particles as they are released into the air stream is zero. It is assumed that before striking the test specimen, the ash particles will have attained the velocity of the air in the acceleration section. The rate of increase in the momentum of the ash particles will be equal to the rate of decrease in the momentum of the air. The pressure drop due to ash particles is given by the following;

$$\Delta P_p = \frac{m_p V_m}{A_m} = \frac{0.007x69.90}{\frac{\pi}{4}x(22.2x10^{-3})^2} = 1264.09Pa \quad (3.10)$$

The Reynolds Number in the PVC pipe, airside, is given by the following;

$$\mathrm{Re}_1 = \frac{\rho_{air} V_1 D}{\mu_{air}} = \frac{0.993x16x46.6x10^{-3}}{18.12x10^{-3}} = 4.07x10^4 \quad (3.11)$$

The friction factor, f_l, for the air flowing in the PVC pipe is given by the following;

$$f_{l\,1} = 0.0014 + 0.125(\mathrm{Re}_1)^{-0.32} = 0.0014 + 0.125(4.07\mathrm{x}10^4)^{-0.32} = 0.0056 \quad (3.12)$$

The pressure drop in the PVC pipe is given by the following;

$$\Delta P_1 = l_1 x2 f_{l1} \frac{\rho_{air} V_1^2}{D} = 4x2x0.0056x \frac{0.993x16^2}{0.0464} = 245Pa \quad (3.13)$$

The pressure drop in the orifice plate, ΔP_o = 4Pa, from Ower and Pankhurst (1977).

4 EXPERIMENTAL PROCEDURE

The first two objectives, construction of the test facility and collection of ash samples from the three power stations, were carried out successfully and after their completion the tests programme had to be carried out. The initial tests programme was drawn up as shown in Table 4.1. This was the anticipated tests programme that would probably be taken through the investigation in the study. In this programme the test for the determination of the critical angle of attack was going in the range between 15º and 90º. Between 15º and 50º the angular position of the test specimen was going to be increase by 5º increments, then by 10º increments thereafter up to 90º. This setup would see a total number of 36 tests of three hours each just for the determination of the critical angle of attack test alone. A decision was taken to reduce the total number of tests from 36 to 21. The number of tests in each angular position of the test specimen was kept at three and the duration of each test run was also kept at three hours. The range of angular position that was going to be tested for critical angle of attack was reduced. In the process of reducing this range the investigations that were done before by others and their findings were taken into consideration. In most investigations it was found that the critical angle of attack that gives maximum erosion is between 20º and 30º with a few finding it to be between 30º and 40º. The other parameter that was considered in the selection of the range of angular position of the test specimen was the mechanism of erosion experienced by the target surface at different angular positions. In the investigations done by others there were findings about different erosion mechanisms experienced at each angular position. After taking all this into consideration a new tests programme for the determination of the critical angle of attack was drawn up. This tests programme is shown in Table 4.2.

The velocity and concentration tests needed a predefined critical angle of attack that gives maximum erosion. The critical angle of attack that was found from the tests programme of determining the critical angle of attack was used in the velocity and concentration tests programmes. In drawing up these tests programmes the limitations of the velocity range that would be provided by the blower was taken into consideration. The velocity range that was found possible to test in these tests programmes was between 18.50 m/s and 27.66 m/s. In this velocity range five

velocities were tested. Again in these tests programmes the duration of each test run was kept at three hours and three test runs were done in each velocity. These tests programmes are shown in Tables 4.3 through 4.5.

Table 4.1: Initial tests programme, determination of the critical angle of attack.

Test Number	Temp(˚C)	Velocity (m/s)	Orientation (Degrees)	Concentration (kg/m^3)	Duration of Test(h)	Weight of Test piece (g)		Erosion Rate [weight lost(mg)/ash(kg)]
						Before	After	
1	20		15		3			
	20		15		3			
	20		15		3			
2	20		20		3			
	20		20		3			
	20		20		3			
3	20		25		3			
	20		25		3			
	20		25		3			
4	20		30		3			
	20		30		3			
	20		30		3			
5	20		35		3			
	20		35		3			
	20		35		3			
6	20		40		3			
	20		40		3			
	20		40		3			
7	20		45		3			
	20		45		3			
	20		45		3			
8	20		50		3			
	20		50		3			
	20		50		3			
9	20		60		3			
	20		60		3			
	20		60		3			
10	20		70		3			
	20		70		3			
	20		70		3			
11	20		80		3			
	20		80		3			
	20		80		3			
12	20		90		3			
	20		90		3			
	20		90		3			

Table 4.2: Determination of the critical angle of attack, Matimba Ash Sample.

Test Number	Temp(°C)	Velocity (m/s)	Orientation (Degrees)	Concentration (kg/m^3)	Duration of Test(h)	Weight of Test piece (g)		Erosion Rate [weight lost(mg)/ash(kg)]
						Before	After	
1	20	26.59	20		3			
	20	26.59	20		3			
	20	26.59	20		3			
2	20	26.59	25		3			
	20	26.59	25		3			
	20	26.59	25		3			
3	20	26.59	35		3			
	20	26.59	35		3			
	20	26.59	35		3			
4	20	26.59	45		3			
	20	26.59	45		3			
	20	26.59	45		3			
5	20	26.59	55		3			
	20	26.59	55		3			
	20	26.59	55		3			
6	20	26.59	70		3			
	20	26.59	70		3			
	20	26.59	70		3			
7	20	26.59	90		3			
	20	26.59	90		3			
	20	26.59	90		3			

Table 4.3: Effect of particle velocity and concentration, Matimba Ash Sample.

Test Number	Temp(°C)	Velocity (m/s)	Orientation (Degrees)	Concentration (kg/m^3)	Duration of Test(h)	Weight of Test piece (g)		Erosion Rate [weight lost(mg)/ash(kg)]
						Before	After	
1	20	19.41	27		3			
	20	19.41	27		3			
	20	19.41	27		3			
2	20	21.86	27		3			
	20	21.86	27		3			
	20	21.86	27		3			
3	20	24.70	27		3			
	20	24.70	27		3			
	20	24.70	27		3			
4	20	25.55	27		3			
	20	25.55	27		3			
	20	25.55	27		3			
5	20	26.59	27		3			
	20	26.59	27		3			
	20	26.57	27		3			

Table 4.4: Effect of particle velocity and concentration, Lethabo Ash Sample.

Test Number	Temp(˚C)	Velocity (m/s)	Orientation (Degrees)	Concentration (kg/m^3)	Duration of Test(h)	Weight of Test piece (g)		Erosion Rate [weight lost(mg)/ash(kg)]
						Before	After	
1	20	19.41	27		3			
	20	19.41	27		3			
	20	19.41	27		3			
2	20	21.86	27		3			
	20	21.86	27		3			
	20	21.86	27		3			
3	20	24.70	27		3			
	20	24.70	27		3			
	20	24.70	27		3			
4	20	25.55	27		3			
	20	25.55	27		3			
	20	25.55	27		3			
5	20	26.59	27		3			
	20	26.59	27		3			
	20	26.57	27		3			

Table 4.5: Effect of particle velocity and concentration, Matla Ash Sample.

Test Number	Temp(˚C)	Velocity (m/s)	Orientation (Degrees)	Concentration (kg/m^3)	Duration of Test(h)	Weight of Test piece (g)		Erosion Rate [weight lost(mg)/ash(kg)]
						Before	After	
1	20	19.41	27		3			
	20	19.41	27		3			
	20	19.41	27		3			
2	20	21.86	27		3			
	20	21.86	27		3			
	20	21.86	27		3			
3	20	24.70	27		3			
	20	24.70	27		3			
	20	24.70	27		3			
4	20	25.55	27		3			
	20	25.55	27		3			
	20	25.55	27		3			
5	20	26.59	27		3			
	20	26.59	27		3			
	20	26.57	27		3			

4.1 Test Facility

4.1.1 Test Specimen

1. The test specimens are 100mm square and 2mm thick. They are constructed from mild steel plates (BS144-CR4).
2. Keep test specimens in dust free environment and should not be exposed to moisture.
3. The surface of the test specimen should be kept clean.
4. Use soft cloth to clean the surface of the test specimen.
5. After cleaning it, weigh it and record its mass then mount it in the test section.
6. Keep it in the test section throughout the test.
7. After the duration of the test take it out of the test section.
8. Clean its surface using the soft cloth and make sure that the surface is dust free.
9. Weigh it and record its mass.
10. Keep it in a dust free environment and should not be exposed to moisture.

4.1.2 Test Section

1. The test section should be kept clean at all times before and after the test.
2. The test specimen holder in the test section should be kept clean at all times, this is done so to prevent subjecting the test specimen to wear and corrosion before starting the test..
3. Orientation of the test specimen should be set after the test specimen has been mounted otherwise it will be cumbersome if it is done other way round. The angular is set by turning the protractor on the side of the test box to the desired position. Once the desired position has been reached then the protractor can be locked into that position by the use of a bolt on the side of the test box inside the slot of the protractor.
4. The window on the side of the test box should be kept clean so that the test specimen can be viewed during the test.
5. The test section should be sealed properly to prevent dust from oozing out of the test box. Sealing gaskets should be fitted between flanges and the lid in the test section should be in place when running the test.

6. Every time when the test is stopped for refill of the ash in the feed line, the ash that might have deposited on the sides of the test box should be taken out of the test section via the filter at the exit. This should be done repeatedly until the completion of the test.

4.1.3 Ash Filter

1. The filter should be switched off during tests. If this is not done it will cause vibration in the test facility.
2. Each time when refilling ash in the hopper the filter has to be switched on to shake off dust that might have accumulated on the sides of the filter bags.
3. When the filter is switched on other apparatus have to be stopped because vibration that comes out of the filter might disturb the working condition of those apparatus which might result in an error in the results.
4. In order to maintain high efficiency of the filter dust accumulation in the filter bags should be avoided.
5. The filter has a ball valve that is used to close the filter for the ash to collect at the bottom, and also used to get rid of the ash by opening it to release the accumulated ash.

4.1.4 Ash Hopper

1. Clean the hopper before commencing tests.
2. Check the rubber seal at the interface between the hopper and the feeder to ensure that it is sealing properly.
3. Fill the hopper with ash.
4. Keep an eye in the hopper to make sure that when the test is running the volume of ash decreases with time. This serves as an indication that the feeder is working and that there are no blockages in the pipeline.
5. When there is little ash remaining in the hopper, stop the test and refill.
6. After refilling run the filter to clear the ash from the test box and sides of the filter bags.
7. Switch off the filter and resume running the tests.

4.1.5 Ash Feeder

1. Check the feeder before every test to see if it is properly working. This can be done by running it empty to see if it is working, then add ash that will be enough to cover the feeder just to see if it can feed that material through.
2. Record the initial load in the feeder.
3. Program the feeder to the desired feed rate.
4. The feeder should be delayed when starting the test. The main air line that is used to carry the ash particles should be started first to fill the pipeline. Once this has been done the air in the pipeline will have momentum that can be used to carry the ash particles to the test section. This also prevents clogging in the test ducting and or to maintain a dilute two-phase flow in the pipeline.
5. When there is insufficient ash in the hopper the feeder should be stopped.
6. Record the final load in the feeder before refilling.
7. Refill the hopper and record the new load in the feeder.
8. Resume running the tests after the refill.
9. Repeat this procedure until the completion of the test.

4.1.6 Orifice Meter

1. Check that the pressure manometer is working before starting the test.
2. Connect the manometer across the orifice.
3. Take note of the reading appearing on the manometer's display and record it.
4. Record the pressure before the introduction of the ash particles.
5. Record the pressure after the introduction of the ash particles.
6. Take note of pressure readings during the test.

4.1.7 Blower

1. Check the pressure gauge at the exit of the blower if it is properly working before starting the test.
2. Set the blower to the desired speed by varying frequency in the blower motor.
3. Start the blower.
4. Record the pressure reading indicated on the pressure gauge when the pressure settles at a particular value.
5. Start the feeder once the desired speed has been reached.

6. Stop the blower when refilling the ash hopper.
7. Do not switch on the blower when the filter is still running.
8. Resume the test.
9. Repeat this procedure until the completion of the test.

4.2 Overall Experimental Procedure

1. Check that all instrumentation that will be used in the test is in a proper working condition.
2. Weigh the test specimen and record its initial weight.
3. Mount the test specimen in the test specimen holder in the test section.
4. Set the test specimen in the desired orientation and lock it into that position.
5. Close the test section properly to prevent dust from oozing out.
6. Put a bag at the exit of the filter to collect dust.
7. Tie the mouth of the bag around the exit of the filter.
8. Record the mass reading displayed in the micro controller before loading ash in the hopper.
9. Load ash into the hopper.
10. Record the new reading of the load in the hopper.
11. Program the feeder to the desired feed rate.
12. Record the pressure reading in the manometer across the orifice.
13. Set the blower to the desired speed.
14. Start the blower.
15. Record the pressure reading displayed in the pressure gauge when the blower reaches the desired speed.
16. Record the pressure reading across the orifice as indicated in the manometer.
17. Start the feeder.
18. When the desired feed rate is reached record the pressure across the orifice as indicated in the pressure manometer.
19. When there is little ash remaining in the hopper, stop the feeder first, then stop the blower.
20. Record the load remaining in the hopper.
21. Refill the ash in the hopper.
22. Switch on the filter to clear the ash from the test section and filter bags.

23. Stop the filter.
24. Repeat the same procedure as from 10 above.
25. Repeat this procedure until the completion of the test.

4.3 Scanning Electron Microscope (SEM)

The scanning electron microscope was used to gain the insight into a microscopic view of the erosion process occurring on the test specimen. This was done in Biology laboratory at the University of the Witwatersrand. The samples used were obtained from the eroded test specimens.

1. The test specimen was machined into a 100mm diameter sample in order to fit it into the SEM.
2. The samples were then cleaned by alcohol to prepare their surface for testing.
3. The samples were put in the SEM and scanned.

4.4 Method of Analysis of the Eroded Plates

A JEM-840 Scanning Electron Microscope (SEM), JEOL, set at 20kV, was used in the examination of the eroded mild steel plates. The eroded plates were cleaned by alcohol before scanning them.

Fly ash analysis was done by Set Point Laboratories, a specialist laboratory in Wynberg, Johannesburg. All this analysis is available in Appendix D. The quantities measured were: particle size, particle and bulk densities and chemical composition of the ash.

Chemical analysis of the mild steel plates was done by Scrooby's Laboratory Services, Johannesburg. This analysis is shown in Appendix F. The intention of this exercise was to do a full analysis in terms of chemical composition of the mild steel. This was done to determine what grade of the mild steel material was tested. Since the mild steel is commonly used in the air preheaters on both hot and intermediate layers the analysis will help in the comparison of the tested material and the manufacturing material of the air preheater pack elements. The other work that was done by Scrooby's Laboratory was the mechanical test in the mild steel plates. This test was done to determine mechanical properties of the plates like yield stress, tensile strength and elongation.

5 RESULTS AND DISCUSSION

The objectives of the study culminated in the set of results from the three ash samples, Matimba, Lethabo and Matla. The test facility was constructed that was used to run the tests programme. The three ash samples were collected from the power stations in order to carry out the desired tests. After these two objectives were completed the tests programme then started. The data that was gathered in the tests was used for the presentation of the test results. In this section the test results are presented and compared to other work done by others in their investigations. Analysis of the ash samples from the three power stations are attached in Appendix D. There is also a daily coal analysis report from Matimba Power Station that was sampled and tested by the power station. This report and e-mail communication between the power station analyst and the author are attached in Appendix E.

The degree of accuracy of the results is detailed in the uncertainty analysis attached in Appendix G. The author would like to acknowledge Mbabazi (2004) for his contribution in this analysis. He used part of this work in his computational fluid dynamics (CFD) study to predict erosion on boiler air heater plate elements.

5.1 Determination of Critical Angle of Attack

The test specimen was bombarded by a flow stream of ash particles. The ash particles hitting the test specimen were in a range of 0.1 to 300 μm in size. The mean diameter of the ash particles was 57.46 μm. These ash properties are taken from ash analysis that was done by Set Point Laboratories. The full ash analysis is available in Appendix B.

The tests were done at room temperature conditions. The velocity that was used in the tests is 27 m/s. This is the maximum velocity that could be achieved using the air supply, the blower. A decision was taken to use this blower because it was readily available and could help in cutting down costs. Orientation of the test specimen was varied from 20° through 90°. The results are shown in Figure 5.1 below. A sharp increase in erosion is seen between 20° and 25°. Between 25° and 30° the figure changes shape with maximum erosion noticed in this region. The erosion rate seems

to reach its peak just before the centre point between 25° and 30°. From the figure the angle of attack that gives maximum erosion is approximately 27°±3°. Tabakoff and Wakerman (1979) found the critical angle of attack to be 25° which is 2° below the finding in this investigation. Above 30° erosion rate decreases with the least erosion rate experienced at 90°.

The test specimen showing erosion after being subjected to the different orientation tests is shown in Figures 5.2 through 5.15. The figures show macroscopic and microscopic erosion. The difference between the two is that macroscopic erosion is visual inspection whereas microscopic is taken under a scanning electron microscope. The figures show the test specimen orientation from 90° through 20°. They show that least erosion is experienced at 90°. The scanning electron microscopic (SEM) figures show different types of material removal mechanisms that were experienced by the test specimen in each orientation. At 90° the test specimen target surface was dented by the flow stream of the ash particles and the form of material removal mechanism experienced is pitting. At 70° orientation there was more significant erosion experienced by the test specimen. This orientation also showed a significant change in the form of material removal on the target surface. The ash particles hit the target surface and removed the material forming something like a lip. When the test specimen is continuously hit by the flow stream of the ash particles the lip formed something like a platelet. This form of material removal mechanism is called platelet mechanism. This form of material removal mechanism was also seen at 55° orientation. At 45° orientation there was another form of material removal that started developing on the target surface. The platelet mechanism was still showing with the new form of material removal mechanism. The new material mechanism that was seen is cutting. This form of material removal mechanism was became more clear from 35° down to 20°. This mechanism showed that as the flow stream of the ash particles hit the target surface they were cutting into the test specimen thus removing more material from the test specimen. This mechanism produced the highest erosion rates on the test specimen. When the ash particles have sharp edges they leave open cuts on the target surface. This is another characteristic of the ash particles that shows that erosion rate is also influenced by the shape of the ash particles.

As the test specimen orientation decreases more and more significant material removal is experienced. Between 35° and 20° the most significant material removal is experienced. This interval shows that almost all ash particles in the flow stream attack material surface. The microscopic figures show the 25° test specimen orientation with the deepest and biggest cut into the material. This shows that most material removal is the result of the cutting into the material surface.

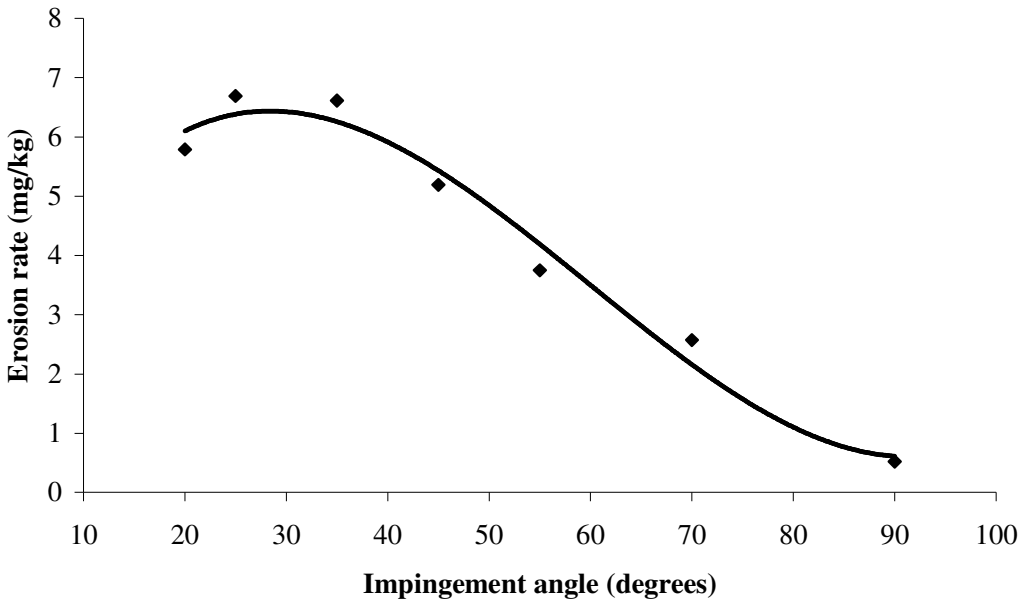


Figure 5.1: Effect of angle of attack.

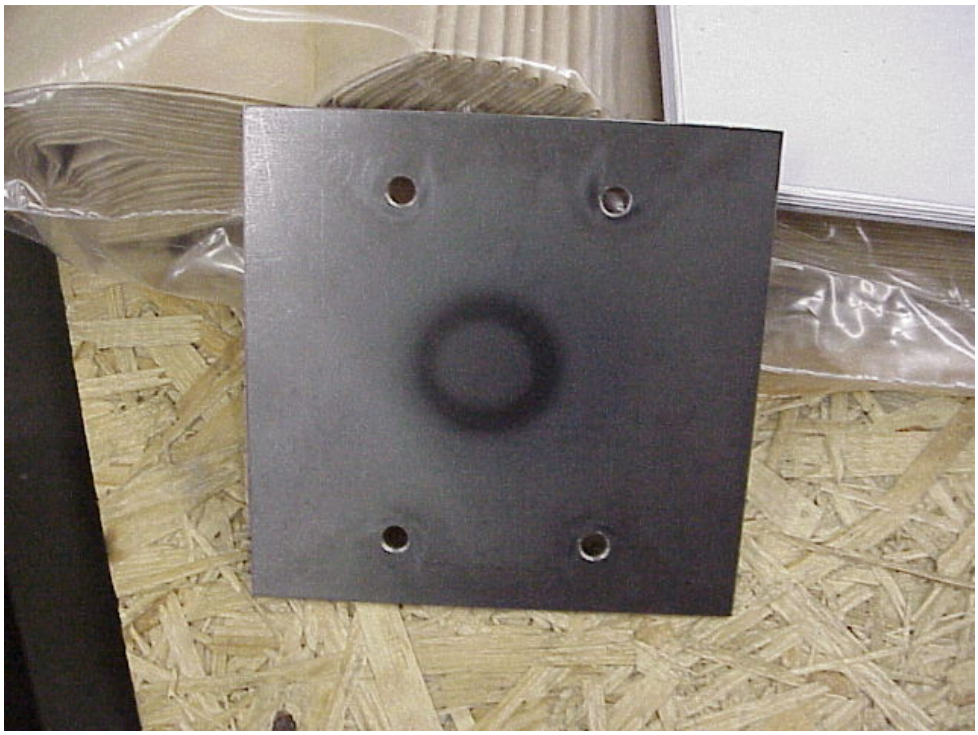


Figure 5.2: 90 degrees orientation.

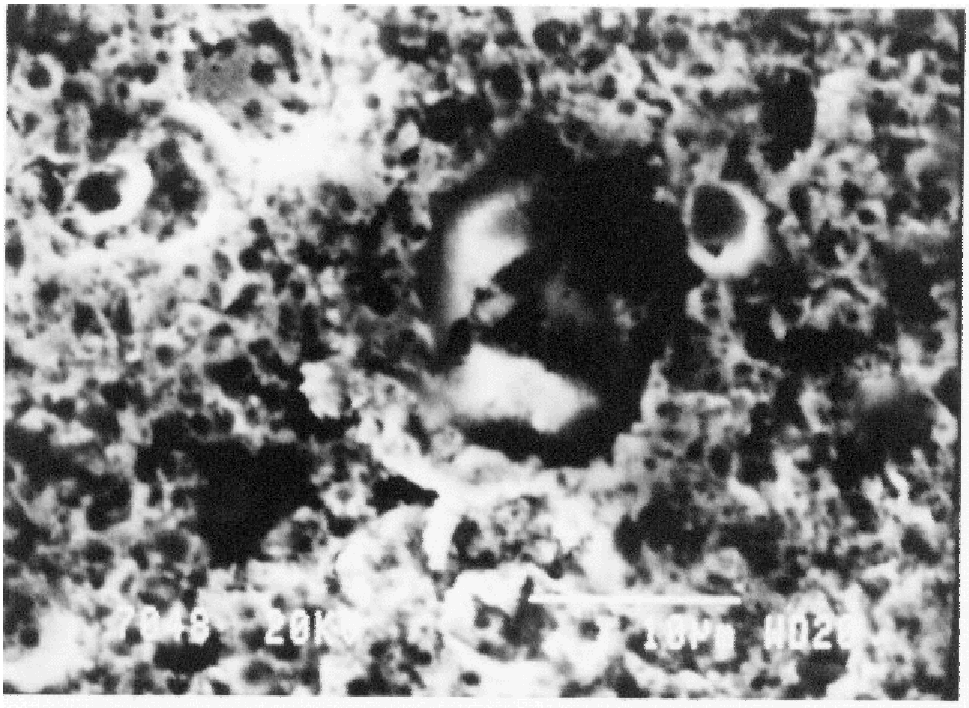


Figure 5.3: 90 degrees orientation.



Figure 5.4: 70 degrees orientation.

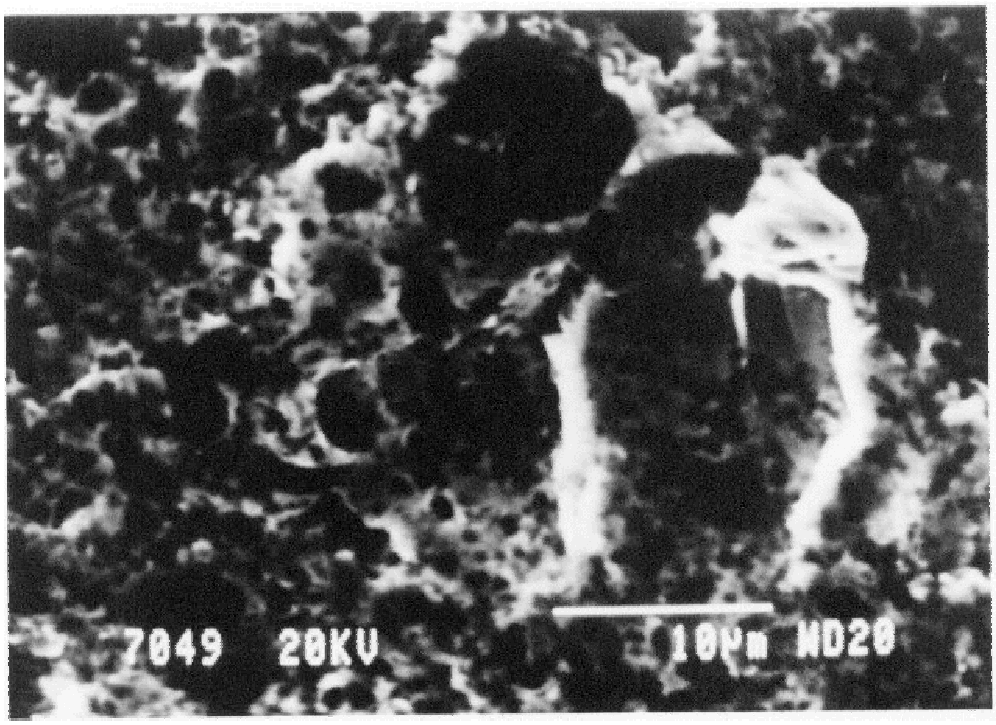


Figure 5.5: 70 degrees orientation.

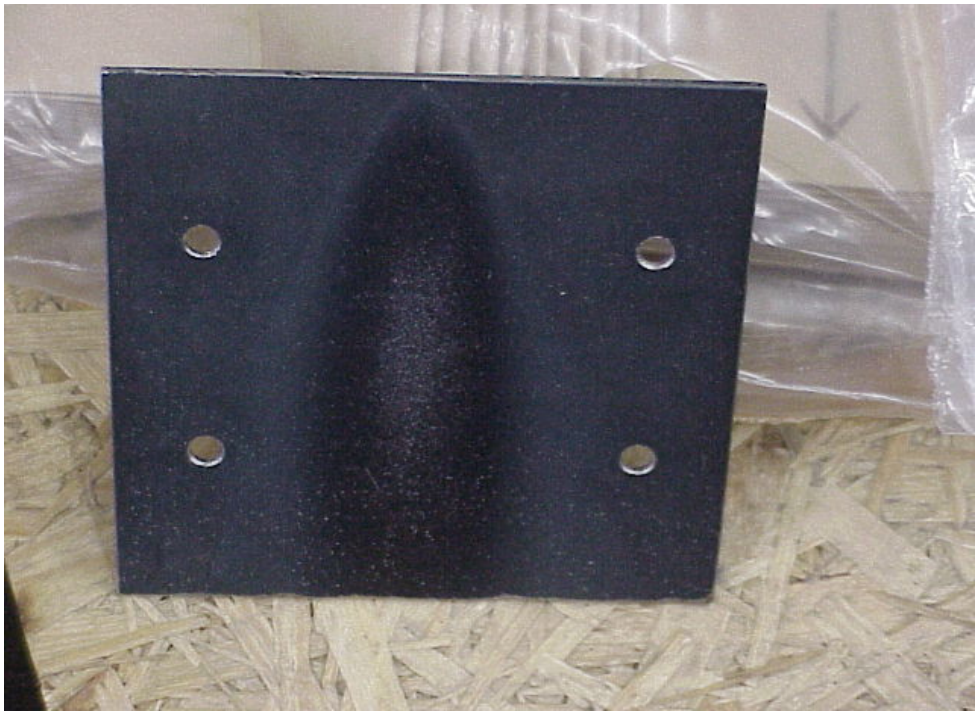


Figure 5.6: 55 degrees orientation.

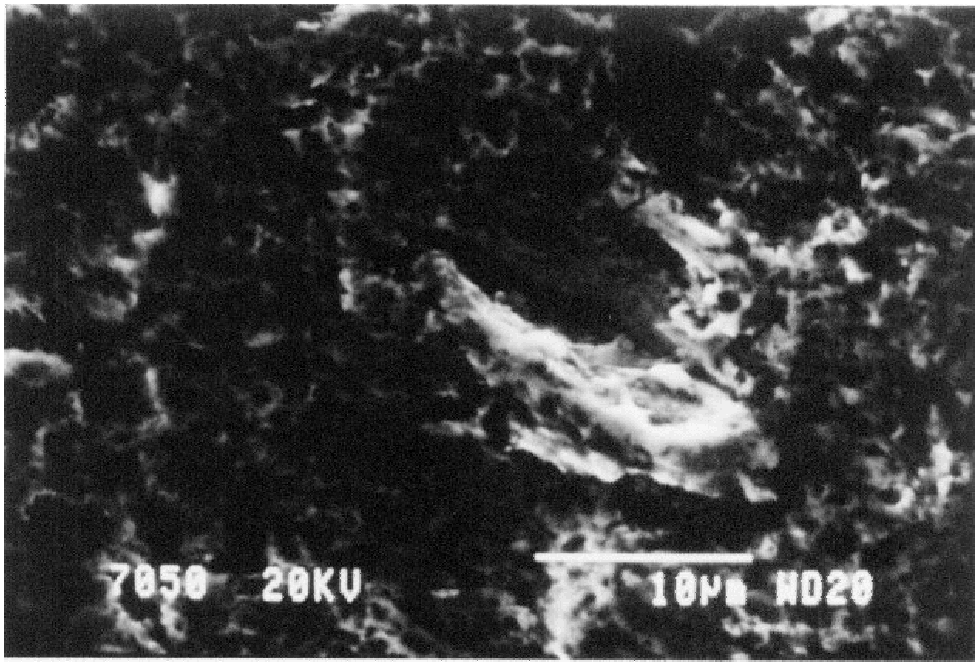


Figure 5.7: 55 degrees orientation.

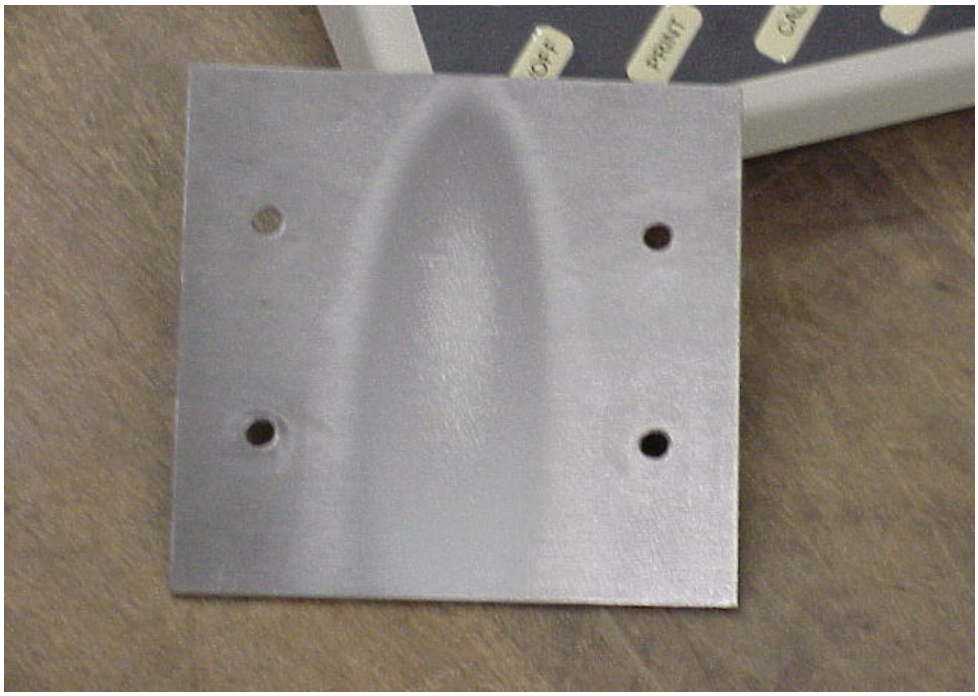


Figure 5.8: 45 degrees orientation.

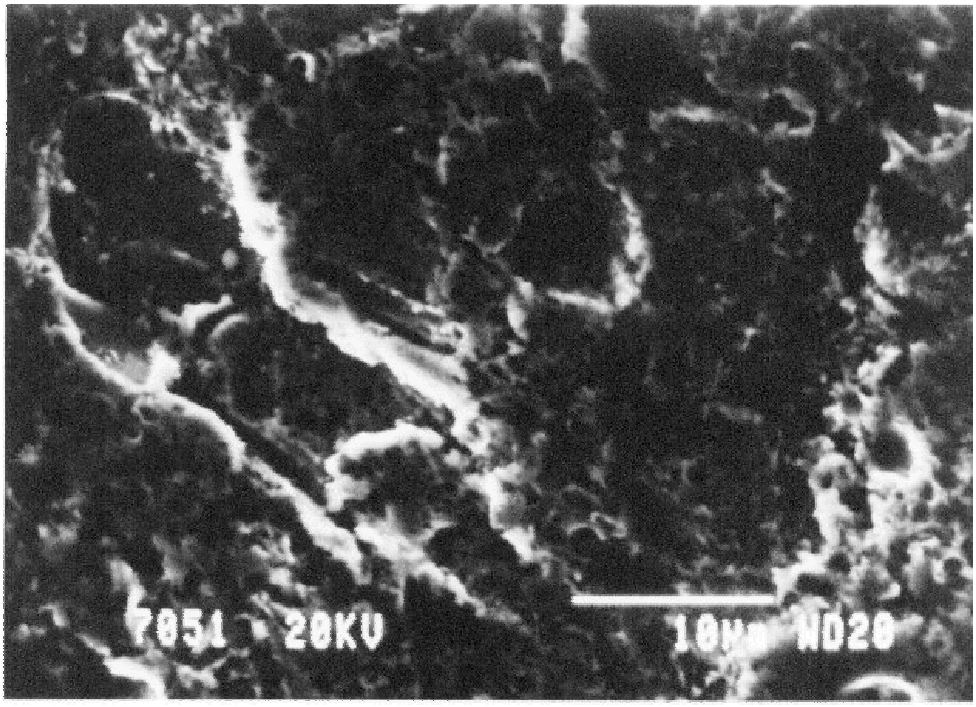


Figure 5.9: 45 degrees orientation.

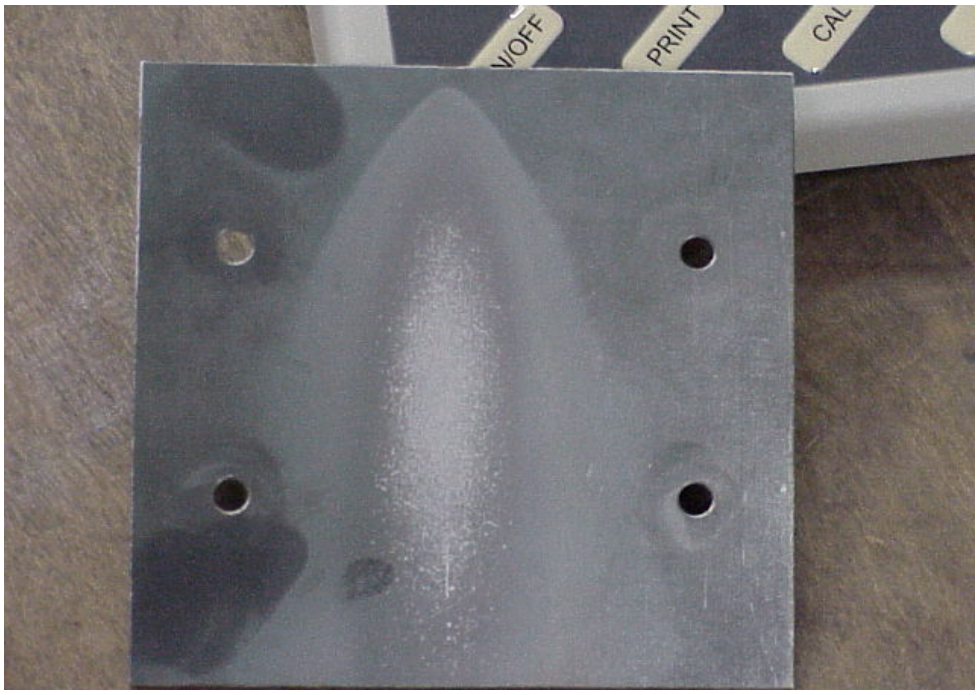


Figure 5.10: 35 degrees orientation.

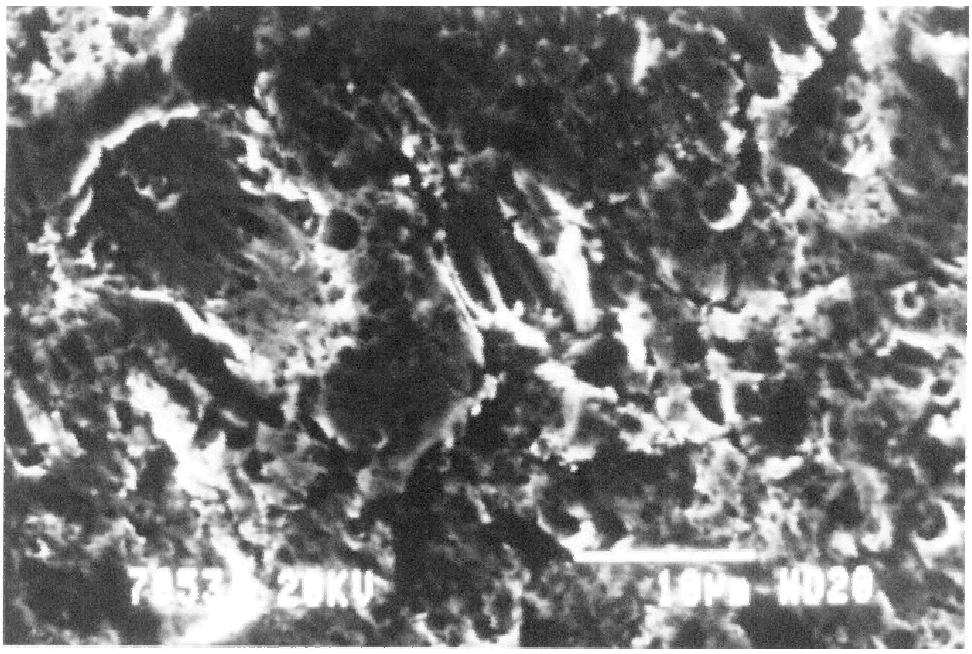


Figure 5.11: 35 degrees orientation.



Figure 5.12: 25 degrees orientation.

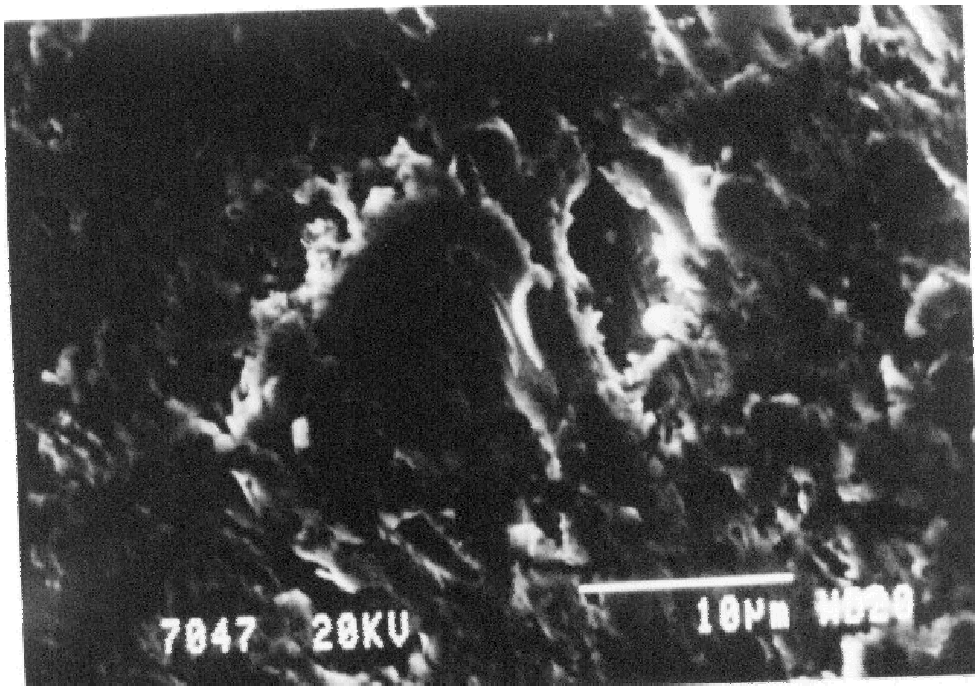


Figure 5.13: 25 degrees orientation.

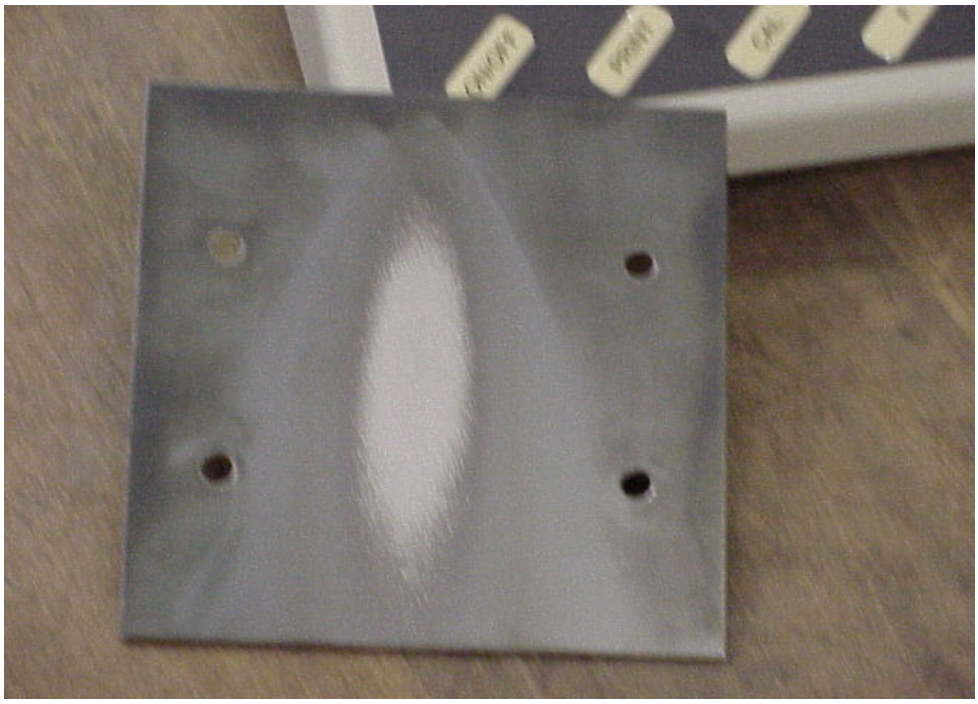


Figure 5.14: 20 degrees orientation.

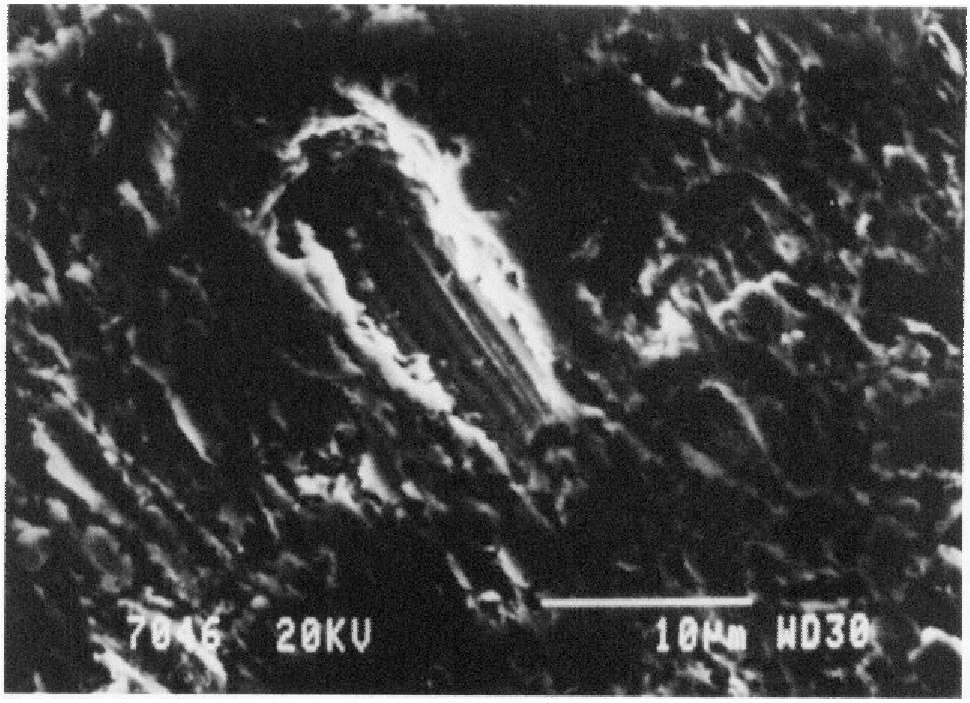


Figure 5.15: 20 degrees orientation.

5.2 Effect of Particle Velocity, Shape and Size

The effect of particle velocity becomes more significant owing to the shape and size of the ash particles. The small hard particles can cause significant material removal on the target surface when traveling at high velocity. Big particles need to be accelerated to higher velocity in order to achieve the same erosion like small particles.

The ash particles with sharp edges can cause even more significant material removal on the target surface. The sharp edges cut into the target surface leaving the test specimen with open cuts. When the flow stream of the ash particles continuously attack these open cuts the test specimen experiences accelerated erosion.

The ash samples used in this study were scanned under an electron microscope to see their particle shape. The results of these samples are shown in Figures 5.16 through 5.18. The ash sample from Matimba Power Station had ash particles with sharp edges. This is a characteristic of most erosive ash particles. The sample from Matla Power Station had round ash particles. This is another characteristic of ash particle size that influences erosion rate. In this sample there was a good mix between big and small ash particles. The ash sample from Lethabo Power Station also had round particles but they were very small.

The ash particles can produce more significant erosion rates owing to their chemical composition. There are compounds like silica that have been found to be the most erosive erodents. The form of silica that was found to be most erosive erodent is quartz. The chemical composition of the three ash samples is shown in Table 5.1. The ash sample from Matimba Power Station had the highest silica content followed by the ash samples from Lethabo Power Station and Matla Power Station. The silica content was found to be 60.10%, 55.20% and 46.30% for the three samples, Matimba, Lethabo and Matla; respectively.

The particle velocity has a big influence in erosion experienced by a target surface. At higher velocity the erosion on the target surface is also high. This erosion is accelerated by the shape and size of the ash particles and the silica content in the ash.

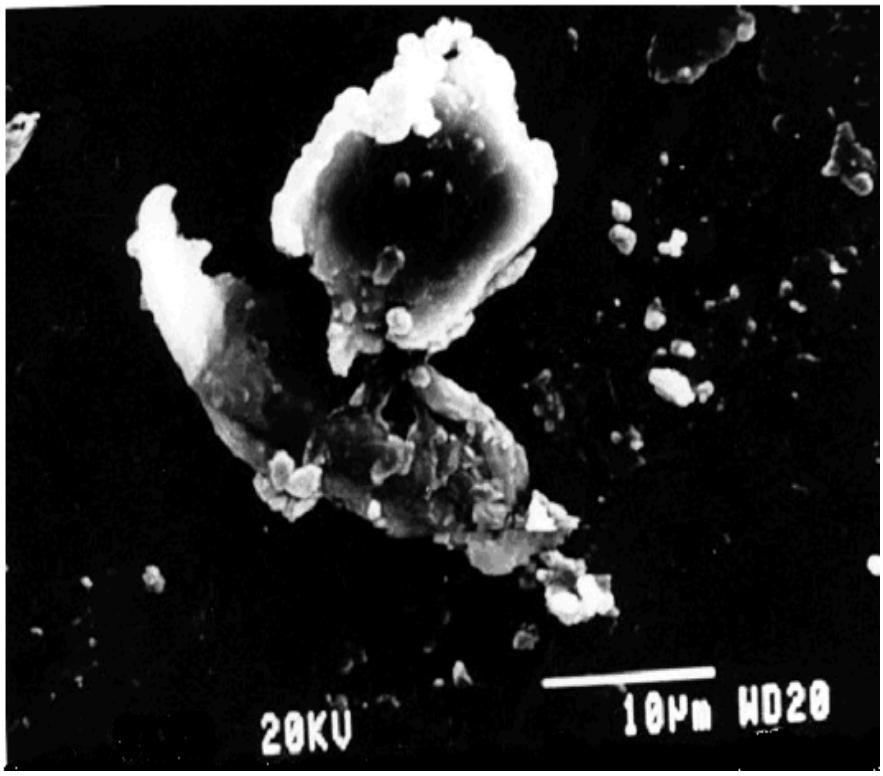


Figure 5.16: Particles in the ash sample from Matimba Power Station.

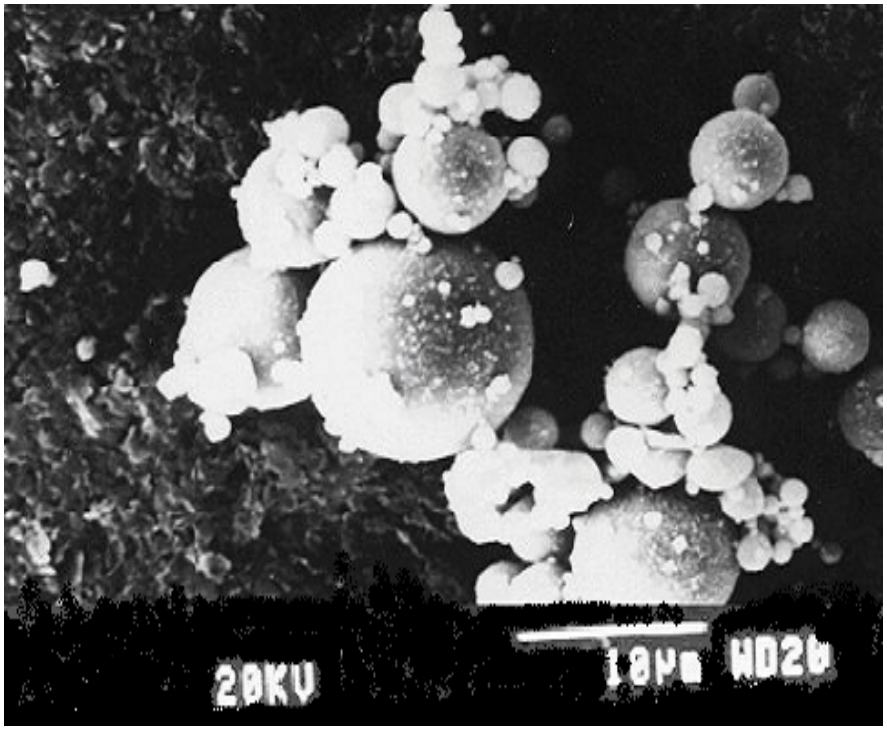


Figure 5.17: Particles in the ash sample from Matla Power Station.

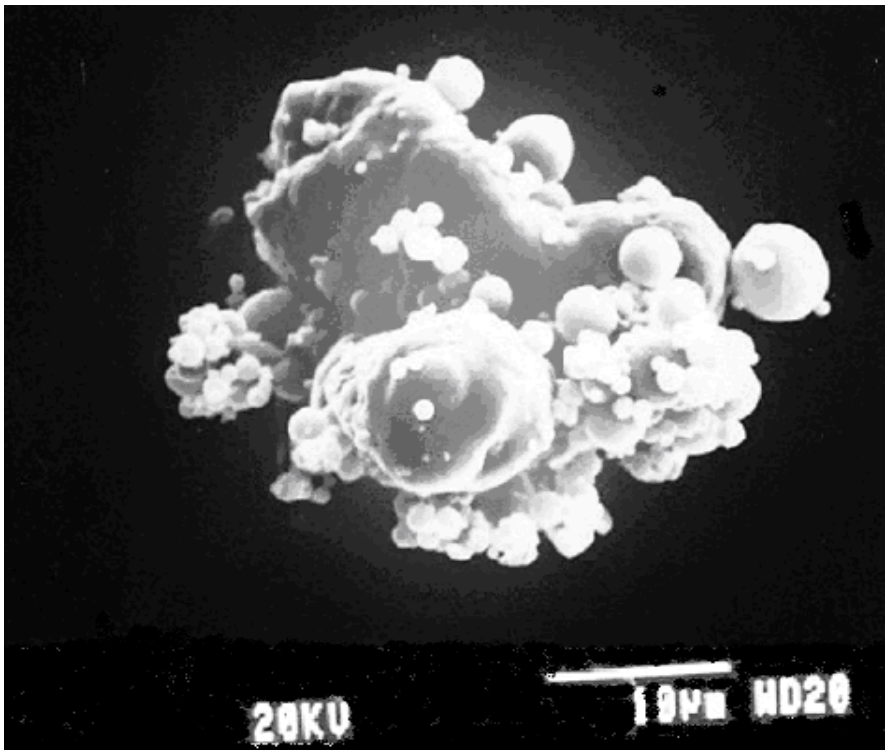


Figure 5.18: Particles in the ash sample from Lethabo Power Station.

Table 5.1: Chemical (elemental) composition of the three ash samples.

Element	Compound occurring in ash	Percentage composition		
		Lethabo	Matimba	Matla
Silicon	Silica (SiO_2)	55.20	60.10	46.30
Aluminium	Aluminium Oxide (Al_2O_3)	30.80	26.50	29.50
Iron	Iron Oxide (Fe_2O_3)	3.67	5.64	4.55
Titanium	Titanium Oxide (TiO_2)	1.61	1.26	1.73
Phosphorus	Phosphorus Pentoxide (P_2O_5)	0.35	0.31	1.12
Calcium	Calcium Oxide (CaO)	5.01	2.95	10.70
Magnesium	Magnesium Oxide (MgO)	1.40	0.70	2.40
Sodium	Sodium Oxide (Na_2O)	0.20	0.10	0.50
Potassium	Potassium Oxide (K_2O)	0.73	0.75	0.88
Sulphur	Sulphur (S)	0.20	0.10	0.70
Manganese	Manganese Oxide (MnO)	0.03	0.06	0.05
	$SiO2 + Al_2O_3 + Fe_2O_3$	89.67	92.24	80.35

The determination of the critical angle of attack test had to be done so that a fixed orientation of the test specimen could be maintained at different velocity tests. The critical angle of attack was kept at 27°. The maximum velocity that could be provided by the blower was already known to be 27 m/s. Since this was the case, it was decided to identify a velocity range that would provide significant material removal. This was experimentally done by determining the minimum velocity at which the least material removal is experienced. At very low velocities fewer ash particles reach the target surface of the test specimen with the bulk of the ash particles accumulating in the pipeline thus causing blockage in the pipeline. This situation was prevented by choosing the velocity range to be between 18 m/s and the maximum velocity of 27 m/s. The test results in this velocity range are shown in Figures 5.19 through 5.21.

The results show that erosion rate increases with increasing velocity. The test results produced a power relationship between erosion rate and ash particle velocity.

The Matimba velocity test results produced the following equation:

$\varepsilon = 0.0004V^{3.09}$ (5.1)

where ε is the erosion rate and V is the particle velocity. These results produced an erosion constant to the value of 0.0004 (4 x 10^{-3}). The velocity exponent was found to be 3.09, Mbabazi (2004) found the velocity exponent to be 3 in his erosion prediction model. This finding also concurs with what Grant and Tabakoff (1980) discovered. At 20° angle of attack they found the velocity of exponent to be 2.8 and at 90° angle of attack they found the velocity exponent to be 4. The finding in this study is within the range of their findings.

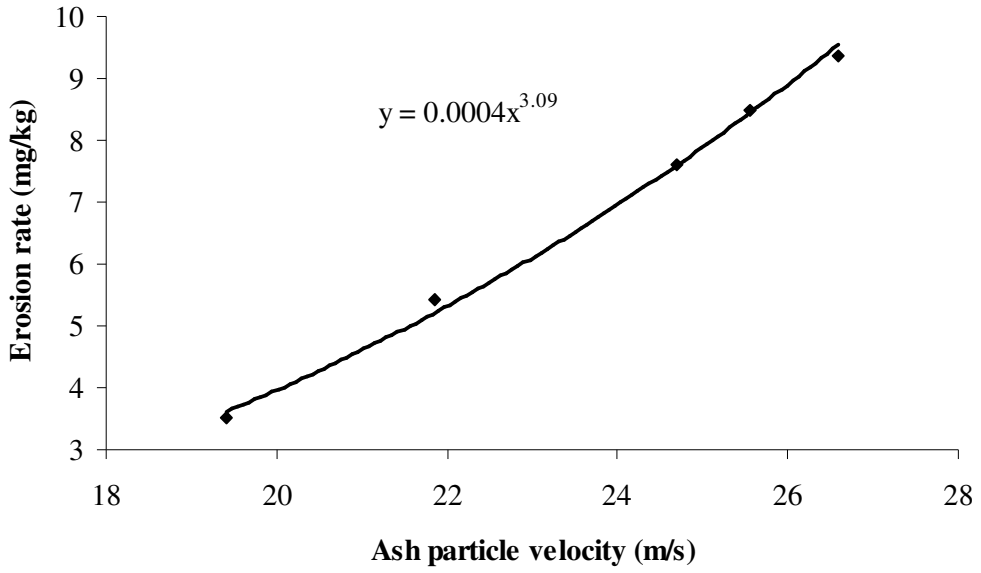


Figure 5.19: Effect of particle velocity, Matimba ash.

The Lethabo velocity test results also produced a power relationship. These results produced the following power equation:

$\varepsilon = 0.002V^{2.42}$ (5.2)

where ε is the erosion rate and V is the particle velocity. The erosion rate constant was found to be 0.002 (2 x 10^{-3}). The velocity exponent was found to be 2.42. This finding is very much interesting when compared to what other investigations have produced.

In the investigation done by Sheldon and Kanhere (1972) they found the velocity exponent to be 2.41. The difference between theirs and from this study is only 0.01. In another investigation done by Tilly and Sage they found the velocity exponent to be 2.3. In another investigation done by Raask (1969) he found the velocity exponent to be 2.5 where a mild steel target surface was hit by a flow stream of quartz particles. The findings from these investigations concur with the finding in this study.

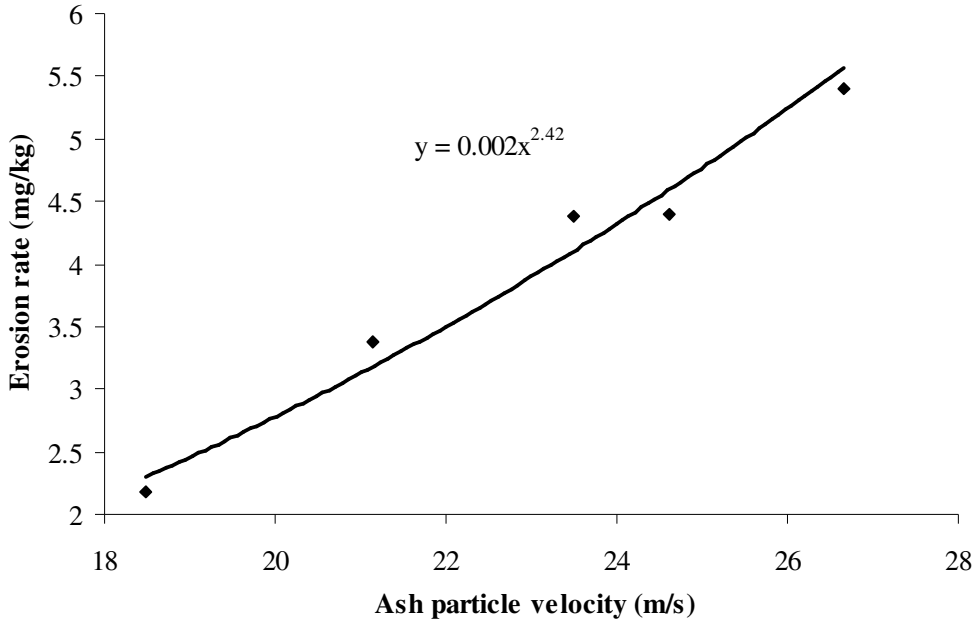


Figure 5.20: Effect of particle velocity, Lethabo ash.

The Matla velocity test results also produced a power relationship between erosion rate and particle velocity. This relationship is presented by the following power equation:

$$\varepsilon = 0.00002V^{3.64} \quad (5.3)$$

where ε is the erosion rate and V is the particle velocity. In these tests the erosion rate constant was found to be 0.00002 (2×10^{-5}). The velocity exponent was found to be 3.64. This finding is also backed by the finding from the investigation done by Grant and Tabakoff (1980) where they found the velocity exponent to be 4 at 90° angle of attack. These results are also of great interest since the difference between their finding and from this study is only 0.36, this is a great achievement.

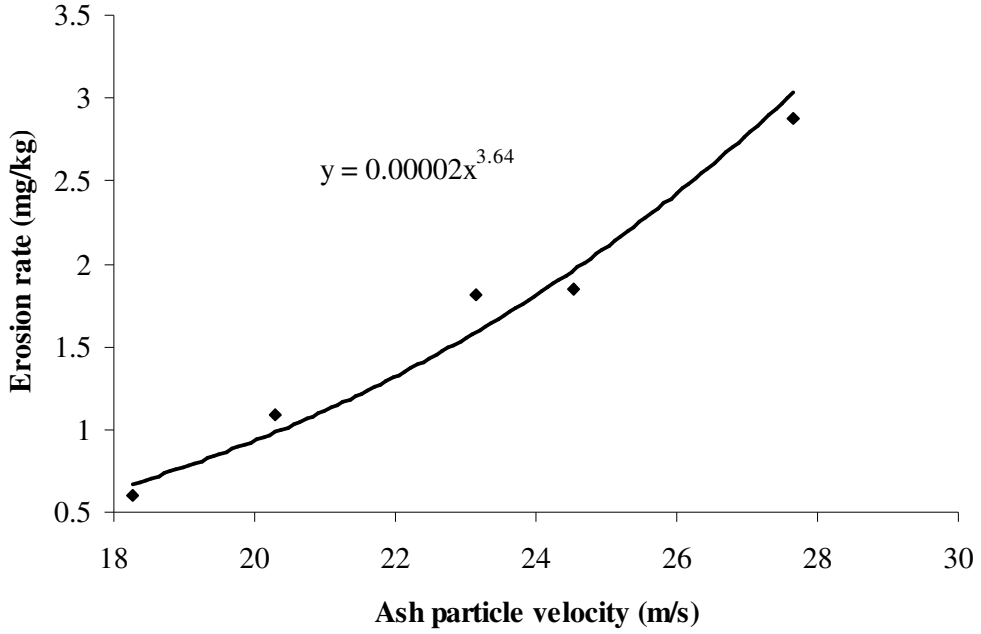


Figure 5.21: Effect of particle velocity, Matla ash.

The summary of the velocity test results from the three ash samples are presented in Figure 5.22 with their uncertainties presented in Figure 5.23. The results show Matimba ash as the most erosive. The Matimba results produced the highest erosion rates. This result justified the effect of particle shape. In the photos taken under the scanning electron microscope the Matimba ash had sharp edges. This means that the target surface of the test specimen was exposed to more cutting form of material removal mechanism thus resulting in higher erosion rate. This form of material removal mechanism is known to be the most severe erosion that a target surface can be exposed to. The other factor that made a significant contribution to these Matimba high erosion rates was silica (quartz). The silica content in the ash composition was found to be 60.10%. The effect of this high silica content is also seen in the high erosion rates from the Matimba test results.

The Lethabo test results brought about very interesting findings which concur with what other investigations came up with before. When looking at the summary of the test results it can be seen that the highest erosion rate achieved in the Lethabo tests is almost half of the highest erosion rate achieved from Matimba tests. This can be related to the ash particle size and shape and silica content. The photos of the Lethabo

ash that were taken under an electron microscope showed that the ash particles were round and small. The round particles can cause severe erosion if they are hard and traveling at high velocity. The silica content was relatively high at 55.20% but less than that of Matimba ash. This was another contributing factor to the high erosion rate in the Lethabo results.

The Matla results showed the least erosion rates of the three ash samples. In the results summary figure these results show the highest erosion rate achieved that is almost half of the Lethabo highest erosion rate achieved.

The results shown in Figure 5.22 clearly indicate that erosion rate is influenced by the following factors:

- Particle size – small particles cause more erosion on the surface of the target material as compared to big particles.
- Particle velocity – big particles will have to be accelerated to a higher velocity in order to produce the same erosion rate as the small particles.
- Particle shape – particles with sharp edges cause more erosion on the surface of the target material as compared to round particles.
- Ash chemical composition – high silica content causes more erosion.

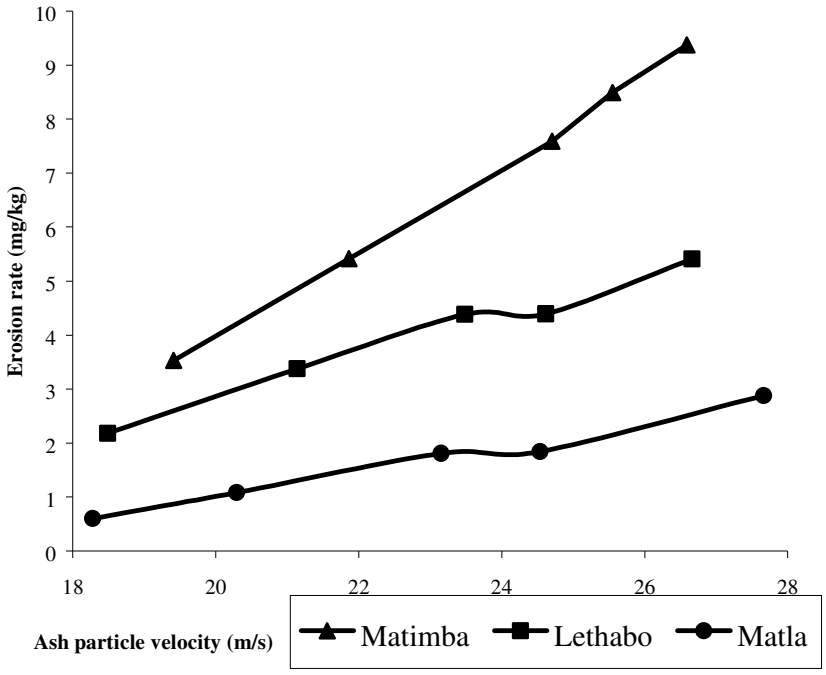


Figure 5.22: Velocity test results for the Matimba, Lethabo and Matla.

The test results degree of accuracy was measured by the uncertainty in the results. The uncertainty analysis showed that the uncertainty in the erosion rate was relatively constant at 0.01 mg/kg. The only significant uncertainty experienced was on the velocity results. The Matimba results produced an uncertainty ranging between 0.22 and 0.30 m/s of the velocity range tested during the velocity tests. The Lethabo test results also produced an uncertainty ranging between 0.22 and 0.30 m/s in the velocity range tested. The Matla test results produced an uncertainty ranging between 0.21 and 0.31 m/s in the velocity range tested. These velocity test results produced an overall velocity uncertainty of about ±1%. This is a good indication of the working condition of the apparatus used for data acquisition and the way the whole investigation was carried out.

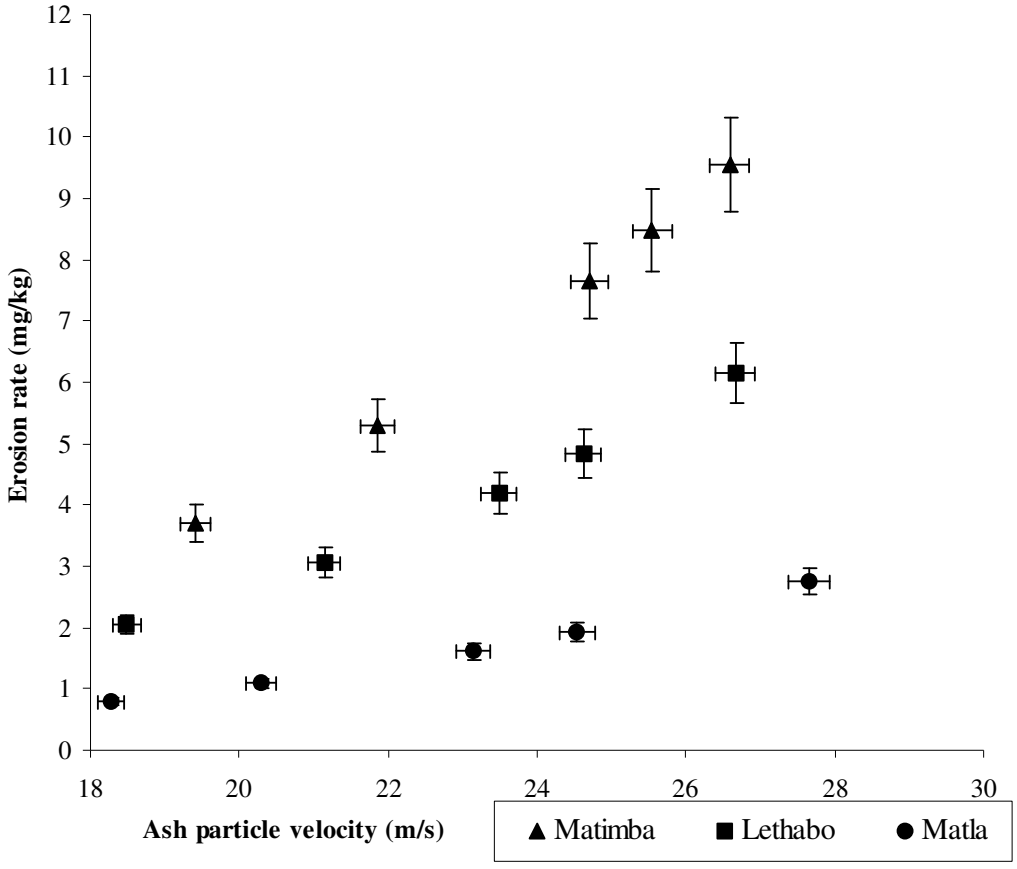


Figure 5.23: Uncertainties in the test results for the Matimba, Lethabo and Matla ash.

5.3 Effect of Particle Concentration

This test needed a predefined angle of attack that gives maximum material removal. The orientation of the test specimen was kept at 27°. This test was done in the same velocity range as in the velocity tests, 18 to 28m/s. The test results are shown in Figure 5.24. It can be seen from the results presented that erosion rate increases with increasing concentration. The results produced a linear relationship between erosion rate and particle concentration. This relationship was presented by the following equation:

$$\varepsilon = 0.5552C_v - 30.307 \quad (5.4)$$

where ε is the erosion rate and C_v is the particle concentration. These results produced a gradient to the value of 0.555223 ± 0.118(mg/kg)/(kg/m^3) with an intercept to the value of -30.3068 ± 7.927mg/kg. The coefficient of determination, R^2, was found to be 0.8799. This finding concurs with the findings from other investigations done before by other researchers.

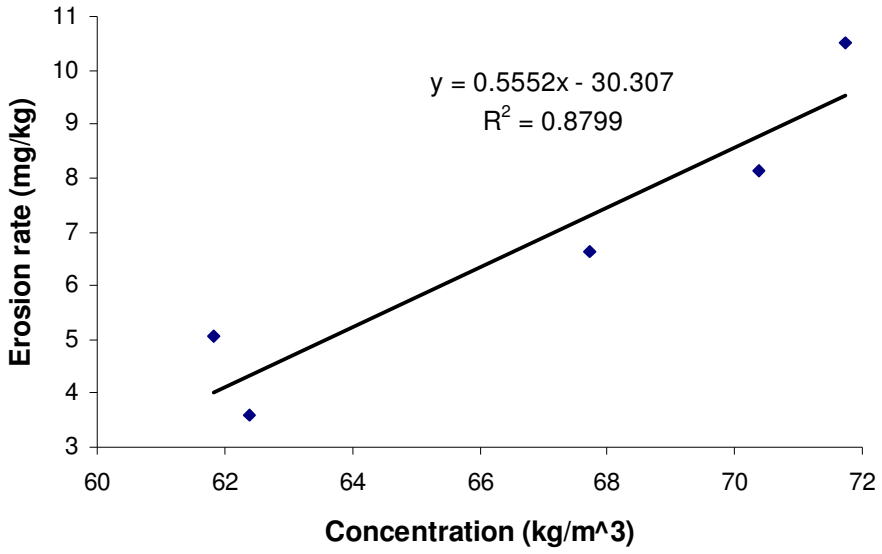


Figure 5.24: Effect of particle concentration.

6 CONCLUSIONS AND RECOMMENDATIONS

6.1 CONCLUSIONS

When this study was taken up there were four main objectives that had to be carried out. The objectives of the study were as follows:

- Construction of the test facility that could produce measurable data in erosion experienced by a mild steel target material. A test facility had to be built using a space available at the university laboratory. This was a primary objective that could make it possible to carry out other objectives of the study as well as future work.
- Collection of ash samples – ash samples were needed to carry out the tests using the test facility in a laboratory environment.
- Determination of critical angle of attack – once the abovementioned objectives were completed this was the first test to be carried out. This was done so because the angle of attack was used as a predefined angle in other tests that follow.
- Effect of particle velocity – this test was going to give an indication as to how does particle velocity influence erosion of target material.

Since the erosion experienced by air preheater elements in a boiler at a power station takes long to take effect due to low flue gas velocity of 10m/s passing through the air preheater this test facility had to produce accelerated erosion with minimum of about 18.50 m/s which is almost double the velocity at which flue gas flows inside an air preheater. There were two constraints that had to be dealt with in the process of the test facility construction. These constraints were budget and space available in the laboratory. The budget constraint saw this study making use of some of the already available equipment that was needed in the tests. This equipment could provide velocity range between 18.50 and 27m/s that was used in the tests. This velocity range was found suitable to carry out the tests.

The test facility had to be designed to fit the space available in the laboratory and leave enough room for storage of the ash samples, experiment apparatus, and other activities. These objectives were carried out successfully leading to the collection of the ash samples from the three power stations.

The ash samples had to be collected from the three power stations, which is one of the four main objectives of the study. The logistics involved in getting ash from the power stations and transporting them to the laboratory were a serious challenge.
The ash circulation system at power stations makes it cumbersome to tap samples of ash. Almost all fossil-fuelled power stations have never had a situation where they had to tap huge quantities of ash samples from their ash circulation system. This was a first time experience that required more thought to be put into it. This had to be done without interrupting the usual operations in the power plant. Plans were made and the required amount of the ash samples were collected from the power stations. The most expensive collection was from Matimba Power Station because they were furthest of them all. The ash samples from Matimba had to be transported over a 400 km distance to the laboratory. The distance between the laboratory and the other two power stations Lethabo and Matla was 150 and 190 km, respectively.

The test programme was put together to determine the type of tests that could be done with the available ash quantity collected from the power stations. This section saw the third objective of determining erosion rates being carried out. This objective was broken down into other smaller objectives that had to be carried out to effect this major objective. These objectives are the determination of the critical angle of attack, determining the effect of particle size and shape, velocity and concentration. The first test that was done was the determination of the critical angle of attack that gives maximum erosion on the target surface. This angle was found to be 27º ± 3º. This angle of attack is within the range of what other researchers have come up with in their investigations. Most investigations found the critical angle of attack that gives maximum erosion to be 25º with a few that found it to be 20º and 30º.
The other objectives needed this predefined angle in order to be carried out. The velocity test results were carried. These results also produced a remarkable finding in the effect of particle size and shape and the chemical composition of the ash particles. At the completion of these results it was found that the particle size and shape had a major influence in the erosion rates. The other finding which was known from the investigations from other researchers which was confirmed in this study that is the influence of the silica (quartz) in the erosion rate experienced by the target material.

The higher the silica content in the ash particles the more erosive they become. This is one of the greatest findings that came out of this study.

The results from the tests produced very good findings that compare well with the work from the investigations done by other researchers. The effect of particle velocity in the erosion of the target surface was found to have a power relationship. This power relationship produced three power equations from the three ash samples. These equations are as follows:

$$\varepsilon = 0.0004V^{3.09} \quad (6.1)$$

$$\varepsilon = 0.002V^{2.42} \quad (6.2)$$

$$\varepsilon = 0.00002V^{3.64} \quad (6.3)$$

These equations 6.1 – 6.3 are for Matimba, Lethabo and Matla test results; respectively. The findings in the velocity exponent are within the range of what other investigations came up with. The investigations that were done by others in their work produced velocity exponents ranging from 2 to 4. In this study the velocity exponent ranges between 2.42 and 3.64.

The other finding that this study produced was the effect of particle concentration on the erosion of the material of the target surface. This finding also produced a linear relationship between the erosion rate of the target surface and the particle concentration of the particle that hit the target surface. This linear relationship produced the following linear equation:

$$\varepsilon = 0.5552C_v - 30.307 \quad (6.4)$$

These results also showed a proportional relationship between erosion rate and ash particle concentration. Other researchers also came up with similar findings that erosion rate increases with increasing particle concentration.

The results of this study were published in a Wear technical paper, it is attached in Appendix H.

6.2 RECOMMENDATIONS

The objectives of this study were completed and results presented. These results could serve as basis for more future work that can still be carried out. In this study only three ash samples were tested from three Eskom fossil-fuelled power stations. All in all there are about thirteen Eskom fossil-fuelled power stations that also experience erosion in their air preheaters even though the scale is not the same as the tested ones. It could be of great interest to carry out this same study for all other power stations that were not tested in this study. The same programme of the tests done in this study should be rolled out to all those power stations.

The material of the target surface that was used in this study was mild steel. The future work should explore other material types to see if the same erosion trends stay the same. This could produce some very remarkable results on the effect of the selection of the material of the target surface to the erosion rate experienced by the target surface.

In this study the velocity range tested was limited to the maximum velocity of 27 m/s. In future work these tests should be done at higher velocity range than the case in this study. This will also serve as a comparison of erosion trends if they stay the same at higher velocity range.

There could also be a need of doing more particle concentration tests in future to take the investigation of the particle concentration effect further. Very little has been done in this regard by others in their work to determine the effect of particle concentration in the erosion rate. If more work could be done at least this study will have more investigations to be compared with it.

There should be more tests done to determine the critical angle of attack that gives maximum erosion on the target surface. It could e interesting to see if the same result could be found in another investigation. This result has always been found to hovering around 25º. This is because in each investigation done the erodent was not the same. In these tests at least the erodent will be ash from different power stations.

The other work that can be carried out in future would be determining different forms of silica that are found in ash. In most investigations they did not do the mineralogy of the silica to find out what other forms of silica influence erosion on the material of the target surface.

References

Blackburn, W. and Rhodes, R., Electric Power Research Institute, Fossil Plant Maintenance Conference, N Y, 1996.

Borman, F.V., *Research Into the Improvement of the Performance and Operation of Regenerative Air Heaters: Commissioning of the Test Facilities*, Technology and Research Investigations (TRI) Report No. TRR/P94/101,1995.

Bosch, F.J., *Particulate Emission Control Evaluation and Database Report*, Technology and Research Investigations (TRI) Report No.TRR/P93/034, 1993.

Crookes, R. A., *Erosion by fly ash of regenerative air preheater elements in power stations,* MSc (Eng) Dissertation, University of the Witwatersrand, 2000.

de Klerk, G. B., *An improved simulation model for rotary regenerative air heaters*, MSc (Eng) Dissertation, University of the Witwatersrand, 2001.

Douglas, J. F., *Solving Problems in Fluid Mechanics, Volume 2*, John Wiley & Sons, Inc, 1987.

Finnie, I., Wolak, J. and Kabil, Y., *Erosion of metals by solid particles, Journal of Materials*, Vol. 2, Number 3, September 1967, pp. 682 – 700.

Grant, G. and Tabakoff, W., *Erosion precision in turbomachinery resulting from environmental solid particles, Journal of Aircraft*, Vol. 12, Number 5, January 1980, pp. 148 – 152.

Lee, B.E., Fletcher, C.A.J., and Behnia, M., *Computational prediction of tube erosion in coal fired power utility boilers, Journal of Engineering for Gas Turbines and Power,* Vol. 121, 1999, pp. 746-750.

Levy, A. V. and Chik, P., *The Effects of Erodent Composition and Shape on the Erosion of Steel*, University of California, USA, 1982.

Levy, A. V., *The Platelet Mechanism of Erosion of Ductile Materials*, Wear, 180, pp. 1 – 21, University of California, USA, 1985.

Mabena, B. S., *Fouling in Boiler Regenerative Air Preheaters*, MSc. (Eng.) Dissertation, University of the Witwatersrand, 2003.

Maji, J., Sheldon, G. L., "Mechanics of Erosion of a Ductile Material by Solid Particles," *Erosion: Prevention and Useful Applications. ASTMP STP 664*, W. F. Adler, Ed., American Society for Testing and Materials, 1979, pp. 136 – 147.

Marcus, R.D., Leung, L.S., Klinzing, G.E., and Rizk, F., *Pneumatic Conveying of Solids*, Chapman and Hall Publishers, 1990.

Mbabazi, J. G., *Prediction of Erosion by Fly Ash of Boiler Air Heater Plate Elements*, Ph. D (Eng) Thesis, University of the Witwatersrand, 2004.

Meriam, J.L., and Kraige, L.G., *Engineering Mechanics, Volume 1: Statics, 3rd Ed.*, John Wiley and Sons Publishers, 1998.

Oka, Y. I., Ohnongi, H., Hosokawa, T. and Matsumura, M., *The Impact Angle Dependence of Erosion Damage Caused by Solid Particle Impact*, Hiroshima University, Japan, 1997.

Ower, E, and Pankhurst, R.C., *The Measurement of Air Flow, 5th Ed.*, Pergamon Press, 1977.

Raask, E., Mineral Impurities in Coal, Behavior, Problems, and Remedial Measures, Hemisphere Publishing Corporation, 1985.

Raask, E., Tube Erosion by Ash Impaction, Central Electricity Research Laboratories, Leatherhead, Surrey (Gt. Britain), Wear 13, 1969, pp. 301 – 315.

Sheldon, G. I. and Kanhere, A., *An Investigation of Impingement Erosion Using Single Particles*, Wear, 21, pp. 195 – 209, Washington State University, 1972.

Shigley, J.E., *Mechanical Engineering Design, First Metric Edition*, McGraw-Hill Book Company, 1986.

Singh, T., Tiwari, S. N. and Sundararajan, G., *Room Temperature Erosion Behaviour of 304, 316 and 410 Stainless Steel*, Banares Hindu University, India, 1990.

Suckling, M. and Allen, C., *Critical Variables in High Temperature Erosive Wear*, MSc. (Eng.) Dissertation, University of Cape Town, RSA, 1997.

Tabakoff, W., Kotwal, R. and Hamed, A., *Erosion study of different materials affected by coal ash particles, Wear* 52, 1979, pp. 161 – 173.

Tabakoff, W., Wakerman, T., *The test facility for material erosion at high temperature, Erosion Prevention and Applications, ASTM 664, American Society for Testing and Materials,* 1979, pp. 123 – 135.

Tilly, G. P. and Sage, W., *The Interaction of Particle and Material Behaviour in Erosion Processes,* 1970.

Wallis, R.A., *Axial Flow Fans, Design and Practice*, William Clowes and Sons Ltd. Publishers, 1961.

Wilson, R. W., *Erosion prediction in rotary regenerative boiler air preheaters,* MSc. (Eng.) Dissertation, University of the Witwatersrand, 1999.

Zhong, Y. and Minemura, K., *Measurement of Erosion Due to Particle Impingement and Numerical Prediction of Wear in Pump Casing,* Nagoya University, Japan, 1996.

APPENDIX A

ENGINEERING DRAWINGS OF THE TEST FACILITY

APPENDIX B

ASH FEEDER TECHNICAL SPECIFICATION

APPENDIX C

MASS BALANCE SCALE TECHNICAL SPECIFICATION

APPENDIX D

ASH ANALYSIS FOR THE THREE POWER STATIONS

Table D.1: Matimba Power Station Ash Chemical Composition

MATIMBA ASH ANALYSIS REPORT

Attention:	**Mr Richard Shandu**	**SPL Report No:**	**2/2216**
Company:	**Wiwatersrand University**	**Date:**	**13/09/20021**
Order No:			
Address:	**Private Bag 3**		
	Wits		
	2050		

SAMPLE NAME	Fe2O3 %	MnO %	Cr2O3 %	V2O5 %	TiO2 %	CaO %	K2O %	P2O5 %	SiO2 %	Al2O3 %	MgO %	Na2O %	CL %	S %	L.O.I %	H2O- %
MATIMBA	5.64	0.06	0.02	0.04	1.26	2.95	0.75	0.31	60.1	26.5	0.7	0.1	0	0.1	0.90	0.18

SAMPLE NAME	Bulk Density g/cm³	S.G
MATIMBA	0.76	2.46

Dr CJ Rademeyer
(Managing Director)

Margaret Farrell
(Spectroscopist)

While every effort is made to provide analysis of the highest accuracy, the liability of **Set Point Laboratories** is restricted to the cost of the analysis

Table D.2: Matimba Power Station Ash Analysis (Particle Size)

Result: Analysis Table

ID: 1020900735	Run No: 10	Measured: 13/9/2002 08:31PM
File: 20900735	Rec. No: 9	Analysed: 13/9/2002 08:31PM
Path: C:\SIZERS\DATA\		Source: Analysed

Range: 300RF mm	Beam: 2.40 mm	Sampler: MS17	Obs': 18.5 %
Presentation: 3$$D		Analysis: Polydisperse	Residual: 0.435 %
Modifications: None			

Conc. = 0.0269 %Vol	Density = 1.000 g/cm^3	S.S.A.= 0.6346 m^2/g
Distribution: Volume	D[4, 3] = 57.46 um	D[3, 2] = 9.46 um
D(v, 0.1) = 6.09 um	D(v, 0.5) = 40.22 um	D(v, 0.9) = 134.57 um
Span = 3.194E+00	Uniformity = 9.823E-01	

Size (um)	Volume Under%	Size (um)	Volume Under%	Size (um)	Volume Under%	Size (um)	Volume Under%
0.05	0.00	0.67	1.31	9.00	14.22	120.67	87.43
0.06	0.00	0.78	1.64	10.48	16.31	140.58	90.95
0.07	0.00	0.91	2.02	12.21	18.67	163.77	93.87
0.08	0.00	1.06	2.43	14.22	21.34	190.80	96.23
0.09	0.00	1.24	2.87	16.57	24.35	222.28	98.02
0.11	0.00	1.44	3.33	19.31	27.75	258.95	99.25
0.13	0.00	1.68	3.80	22.49	31.57	301.68	99.91
0.15	0.01	1.95	4.28	26.20	35.84	351.46	100.00
0.17	0.02	2.28	4.78	30.53	40.55	409.45	100.00
0.20	0.05	2.65	5.31	35.56	45.65	477.01	100.00
0.23	0.10	3.09	5.89	41.43	51.07	555.71	100.00
0.27	0.17	3.60	6.55	48.27	56.69	647.41	100.00
0.31	0.27	4.19	7.33	56.23	62.37	754.23	100.00
0.36	0.40	4.88	8.27	65.51	68.01	878.67	100.00
0.42	0.56	5.69	9.41	76.32	73.53		
0.49	0.76	6.63	10.78	88.91	78.66		
0.58	1.01	7.72	12.38	103.58	83.32		

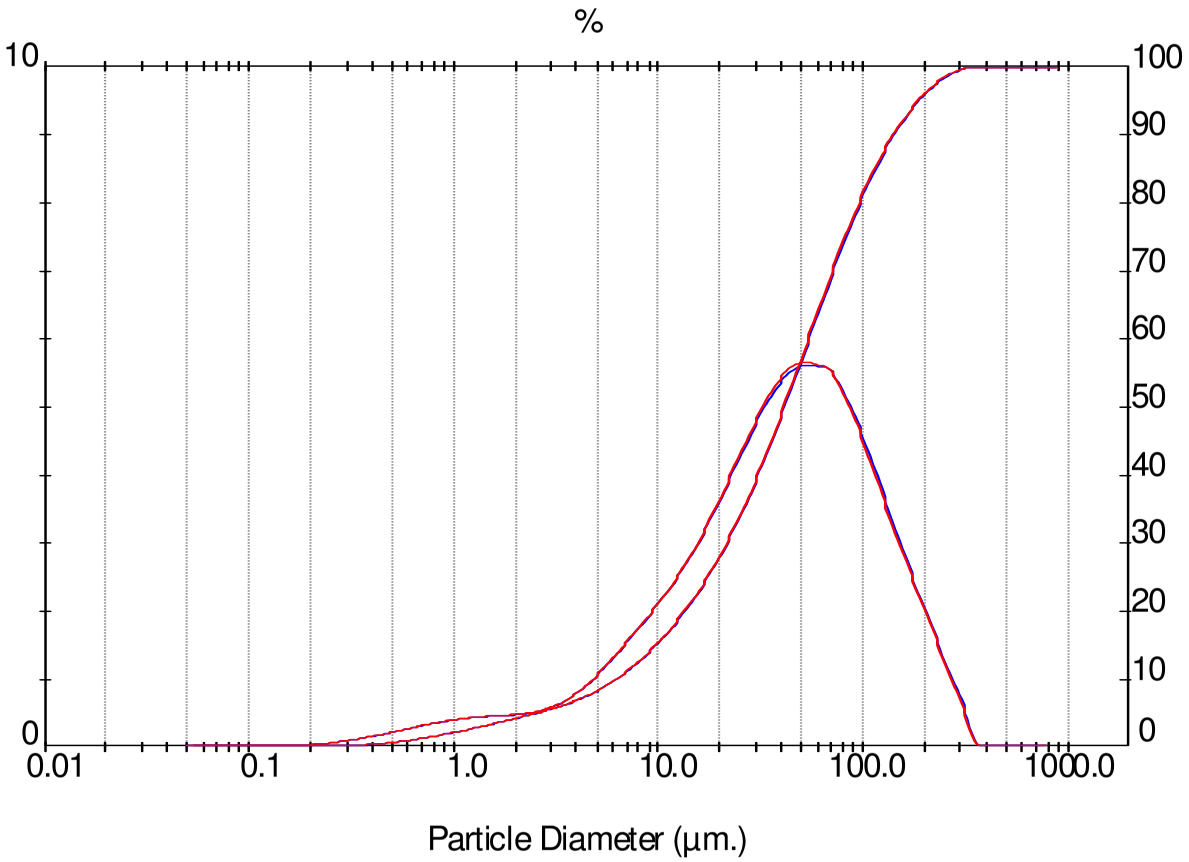


Figure D.1: Matimba Power Station Ash Particle Size

Table D.3: Lethabo and Matla Power Stations Ash Chemical Composition

LETHABO AND MATLA ASH ANALYSIS REPORT

Attention:	**Mr Richard Shandu**	**SPL Report No.**	**2/3081**
Company:	**Witwatersrand University**	**Date:**	**12/12/2002**
Order No:	**School of Mech. Eng.**		
Address:	**Private Bag 3**		
	Wits		
	2050		

SAMPLE NAME	Fe_2O_3 %	MnO %	Cr_2O_3 %	V_2O_5 %	TiO_2 %	CaO %	K_2O %	P_2O_5 %	SiO_2 %	AL_2O_3 %	MgO %	Na_2O %	CL %	S %	L.O.I %	S.G g/cm^3
LETHABO	3.67	0.03	0.03	0.02	1.61	5.01	0.73	0.35	55.2	30.8	1.4	0.2	0	0.2	0.63	0.936
MATLA	4.55	0.05	0.02	0.02	1.73	10.7	0.88	1.12	46.3	29.5	2.4	0.5	0	0.7	0.99	0.951

Dr CJ Rademeyer
(Managing Director)

Margaret Farrell
(Spectroscopist)

Table D.4: Lethabo Power Station Ash Analysis (Particle Size)

LIMS number:1021200759
Sample Lethabo Ash

Result: Analysis Table

ID: 1021200759	Run No: 6	Measured: 11/12/2002 15:42PM
File: 21200759	Rec. No: 2	Analysed: 11/12/2002 15:42PM
Path: C:\SIZERS\DATA\		Source: Analysed

Range: 300RF mm	Beam: 2.40 mm	Sampler: MS17	Obs': 18.7 %
Presentation: 3$$D	Analysis: Polydisperse		Residual: 0.422 %
Modifications: None			

Conc. = 0.0154 %Vol	Density = 1.000 g/cm^3	S.S.A.= 1.1180 m^2/g
Distribution: Volume	D[4, 3] = 53.40 um	D[3, 2] = 5.37 um
D(v, 0.1) = 1.98 um	D(v, 0.5) = 25.20 um	D(v, 0.9) = 148.34 um
Span = 5.808E+00	Uniformity = 1.775E+00	

Size (um)	Volume Under%	Size (um)	Volume Under%	Size (um)	Volume Under%	Size (um)	Volume Under%
0.05	0.00	0.67	2.30	9.00	29.76	120.67	86.20
0.06	0.00	0.78	3.06	10.48	32.57	140.58	89.06
0.07	0.00	0.91	3.95	12.21	35.45	163.77	91.64
0.08	0.00	1.06	4.95	14.22	38.39	190.80	93.93
0.09	0.00	1.24	6.05	16.57	41.38	222.28	95.92
0.11	0.00	1.44	7.25	19.31	44.44	258.95	97.56
0.13	0.00	1.68	8.53	22.49	47.59	301.68	98.81
0.15	0.00	1.95	9.88	26.20	50.84	351.46	99.63
0.17	0.00	2.28	11.30	30.53	54.22	409.45	100.00
0.20	0.00	2.65	12.79	35.56	57.73	477.01	100.00
0.23	0.02	3.09	14.37	41.43	61.35	555.71	100.00
0.27	0.10	3.60	16.07	48.27	65.06	647.41	100.00
0.31	0.23	4.19	17.91	56.23	68.81	754.23	100.00
0.36	0.45	4.88	19.92	65.51	72.54	878.67	100.00
0.42	0.75	5.69	22.12	76.32	76.23		
0.49	1.15	6.63	24.51	88.91	79.76		
0.58	1.67	7.72	27.07	103.58	83.09		

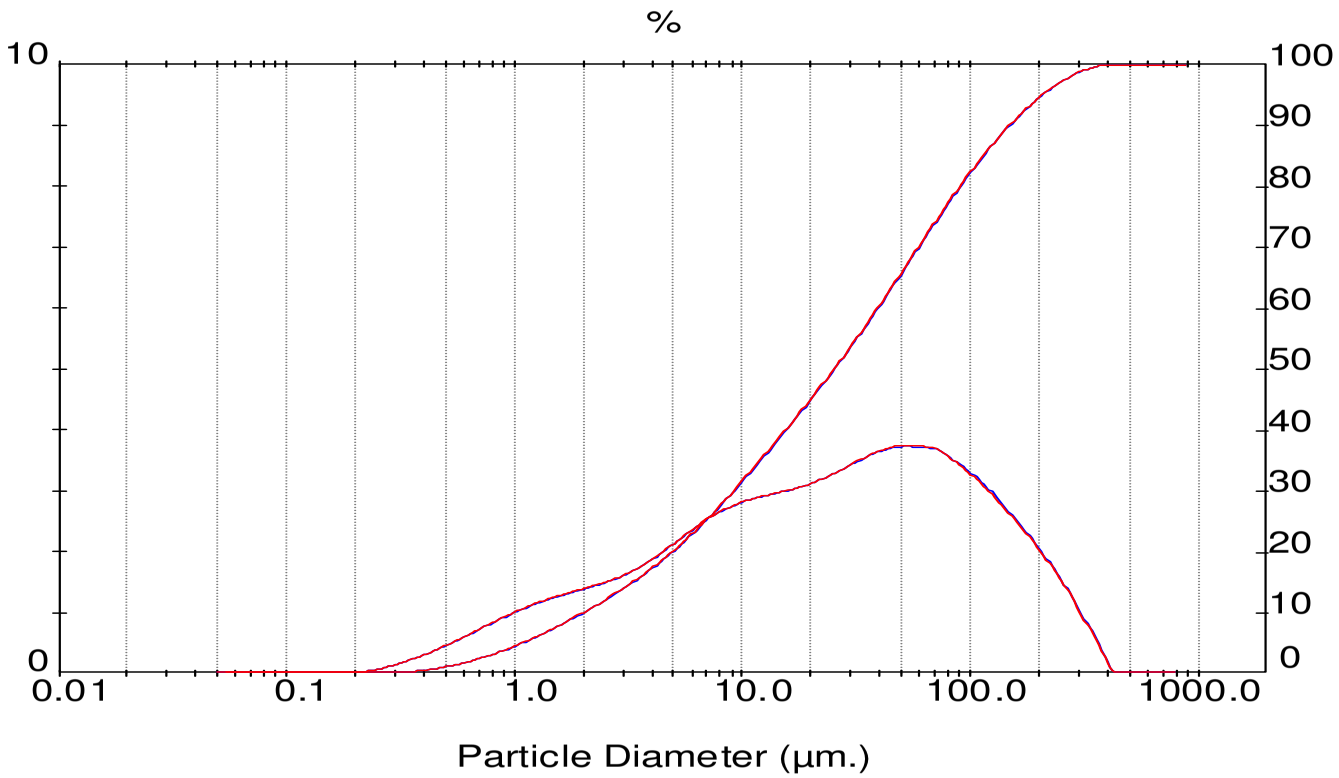


Figure D.2: Lethabo Power Station Ash Particle Size

Table D.5: Matla Power Station Ash Analysis (Particle Size)

LIMS number :1021200760
Sample Matla Ash

Result: Analysis Table

ID: 1021200760	Run No: 7	Measured: 11/12/2002 15:59PM
File: 21200760	Rec. No: 2	Analysed: 11/12/2002 15:59PM
Path: C:\SIZERS\DATA\		Source: Analysed

Range: 300RF mm	Beam: 2.40 mm	Sampler: MS17	Obs': 19.5 %
Presentation: 3$$D		Analysis: Polydisperse	Residual: 0.422 %
Modifications: None			

Conc. = 0.0160 %Vol	Density = 1.000 g/cm^3	S.S.A.= 1.1309 m^2/g
Distribution: Volume	D[4, 3] = 37.04 um	D[3, 2] = 5.31 um
D(v, 0.1) = 1.99 um	D(v, 0.5) = 22.41 um	D(v, 0.9) = 92.28 um
Span = 4.030E+00	Uniformity = 1.271E+00	

Size (um)	Volume Under%	Size (um)	Volume Under%	Size (um)	Volume Under%	Size (um)	Volume Under%
0.05	0.00	0.67	2.53	9.00	28.68	120.67	94.56
0.06	0.00	0.78	3.39	10.48	31.83	140.58	96.45
0.07	0.00	0.91	4.34	12.21	35.16	163.77	97.90
0.08	0.00	1.06	5.37	14.22	38.65	190.80	98.97
0.09	0.00	1.24	6.47	16.57	42.29	222.28	99.67
0.11	0.00	1.44	7.59	19.31	46.10	258.95	100.00
0.13	0.00	1.68	8.72	22.49	50.10	301.68	100.00
0.15	0.00	1.95	9.87	26.20	54.30	351.46	100.00
0.17	0.00	2.28	11.03	30.53	58.69	409.45	100.00
0.20	0.00	2.65	12.23	35.56	63.25	477.01	100.00
0.23	0.00	3.09	13.51	41.43	67.96	555.71	100.00
0.27	0.04	3.60	14.94	48.27	72.78	647.41	100.00
0.31	0.17	4.19	16.56	56.23	77.46	754.23	100.00
0.36	0.40	4.88	18.43	65.51	81.84	878.67	100.00
0.42	0.74	5.69	20.58	76.32	85.79		
0.49	1.21	6.63	23.02	88.91	89.24		
0.58	1.80	7.72	25.73	103.58	92.16		

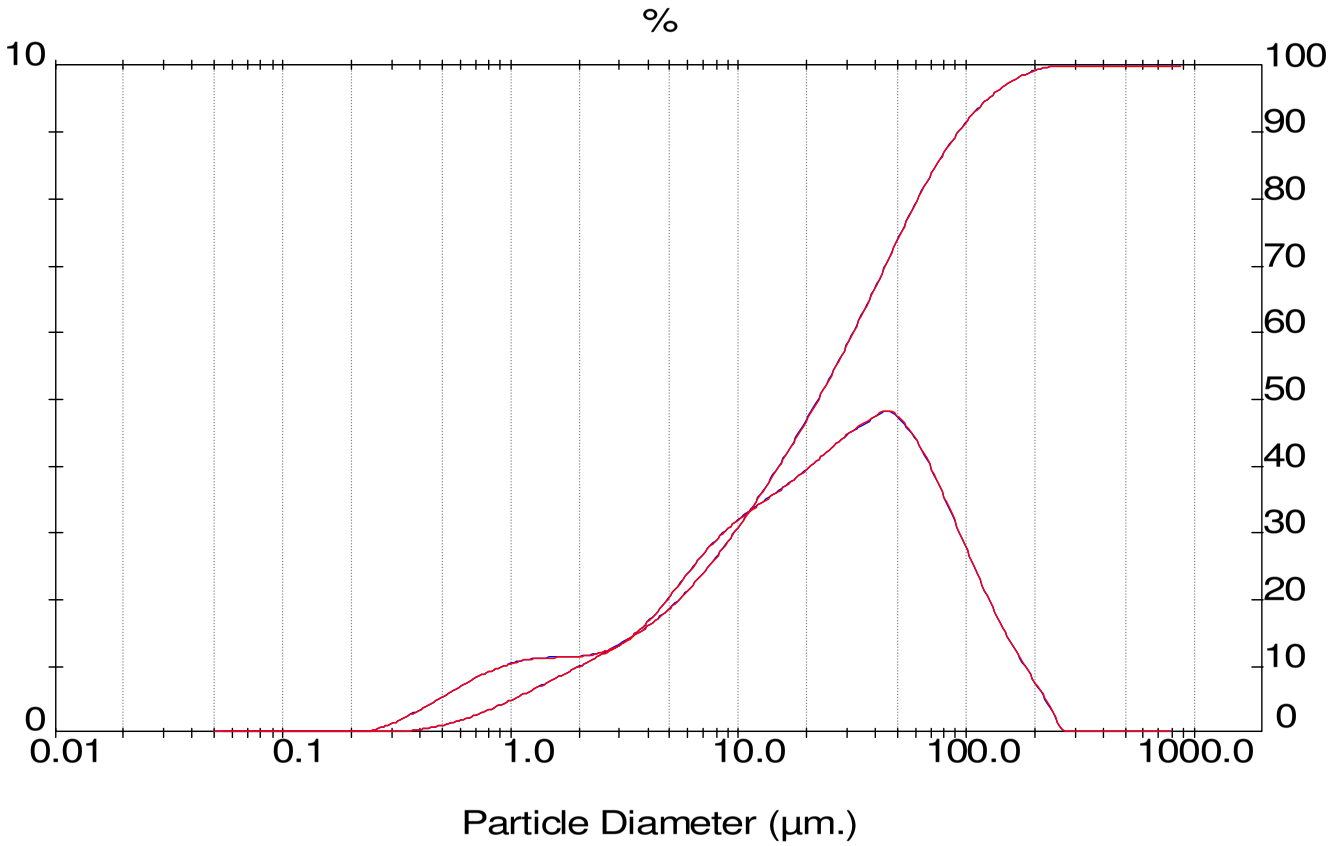


Figure D.3: Matla Power Station Ash Particle Size

APPENDIX E

MATIMBA DAILY COAL ANALYSIS

TABLE E.1: MATIMBA POWER STATION DAILY COAL ANALYSIS REPORT
KUMBER NUMBER: 4648

ANALYST: Pinky DATE SAMPLED: 17 June 2002 DATE ANALYSED: 18 June 2002

ANALYSIS: A SHIFT										
	MJ/Kg C.V.	% ASH	% VOL	% TOT MOIST	% INH MOIST	% SURF MOIST	H.G.I.	mg / Fe ABRAS	% SULPHUR	% FIX CARB
AS TESTED	19.95	34.43	25.16	8.70	2.49	6.21	47.00	362.00	1.10	
DRY ASH FREE			39.89							
AS RECEIVED	18.68	32.24	23.56						1.03	35.50
DRY	20.46	35.31	25.80						1.13	
ISCOR MINE	20.46	35.30	39.80	8.70	1.70	7.00	50.00	334.00	1.13	

ANALYSIS: B SHIFT										
	MJ/Kg C.V.	% ASH	% VOL	% TOT MOIST	% INH MOIST	% SURF MOIST	H.G.I.	mg / Fe ABRAS	% SULPHUR	% FIX CARB
AS TESTED	19.98	34.94	25.32	10.10	1.93	8.17	47.00		1.15	
DRY ASH FREE			40.10							
AS RECEIVED	18.32	32.03	23.21						1.05	34.66
DRY	20.38	35.63	25.81						1.17	
ISCOR MINE	20.38	35.40	40.10	10.10	1.70	8.40	50.00		1.17	

ANALYSIS: C SHIFT										
	MJ/Kg C.V.	% ASH	% VOL	% TOT MOIST	% INH MOIST	% SURF MOIST	H.G.I.	mg / Fe ABRAS	% SULPHUR	% FIX CARB
AS TESTED	20.06	34.69	25.20	10.10	2.08	8.02			0.91	
DRY ASH FREE			39.85							
AS RECEIVED	18.41	31.85	23.14						0.84	34.92
DRY	20.48	35.43	25.73						0.93	
ISCOR MINE	20.48	35.40	39.10	10.10	1.80	8.30			0.93	

COAL GRADING					
mm	37.50	25.00	10.50	6.70	4.75	< 4.75
PERCENT	2.03	6.72	34.51	11.53	5.43	39.77

TOTAL TONNAGE RECEIVED FROM ISCOR MINE PER SHIFT		
A SHIFT	B SHIFT	C SHIFT
19 561.00	17 965.65	19 852.25

TABLE E.2: MATIMBA POWER STATION DAILY COAL ANALYSIS REPORT
KUMBER NUMBER: 4649

ANALYST: Pinky DATE SAMPLED: 18 June 2002 DATE ANALYSED: 19 June 2002

ANALYSIS: A SHIFT										
	MJ/Kg C.V.	% ASH	% VOL	% TOT MOIST	% INH MOIST	% SURF MOIST	H.G.I.	mg / Fe ABRAS	% SULPHUR	% FIX CARB
AS TESTED	20.13	33.40	24.91	9.30	2.28	7.02	55.00	247.00	1.08	
DRY ASH FREE			38.73							
AS RECEIVED	18.69	31.00	23.12						1.01	36.58
DRY	20.60	34.18	25.49						1.11	
ISCOR MINE	20.60	34.20	37.80	9.30	2.00	7.30	50.00	296.00	1.11	

ANALYSIS: B SHIFT										
	MJ/Kg C.V.	% ASH	% VOL	% TOT MOIST	% INH MOIST	% SURF MOIST	H.G.I.	mg / Fe ABRAS	% SULPHUR	% FIX CARB
AS TESTED	20.18	24.55	25.74	10.00	1.79	8.21			1.13	
DRY ASH FREE			40.43							
AS RECEIVED	18.49	31.66	23.59						1.03	34.75
DRY	20.55	35.18	26.21						1.15	
ISCOR MINE	20.55	35.20	39.80	10.00	1.70	8.30			1.15	

ANALYSIS: C SHIFT										
	MJ/Kg C.V.	% ASH	% VOL	% TOT MOIST	% INH MOIST	% SURF MOIST	H.G.I.	mg / Fe ABRAS	% SULPHUR	% FIX CARB
AS TESTED	20.08	34.66	25.99	10.10	2.00	8.10			0.98	
DRY ASH FREE			41.03							
AS RECEIVED	18.42	31.79	23.84						0.90	34.27
DRY	20.49	35.36	26.52						1.00	
ISCOR MINE	20.49	35.30	40.40	10.10	1.80	8.30			1.00	

COAL GRADING					
mm	37.50	25.00	10.50	6.70	4.75	< 4.75
PERCENT	1.42	8.07	31.68	12.81	5.42	40.62

TOTAL TONNAGE RECEIVED FROM ISCOR MINE PER SHIFT		
A SHIFT	B SHIFT	C SHIFT
21 261.15	17 251.20	22 180.10

TABLE E.3: MATIMBA POWER STATION DAILY COAL ANALYSIS REPORT
KUMBER NUMBER: 4650

ANALYST: Pinky DATE SAMPLED: 19 June 2002 DATE ANALYSED: 20 June 2002

ANALYSIS: A SHIFT										
	MJ/Kg C.V.	% ASH	% VOL	% TOT MOIST	% INH MOIST	% SURF MOIST	H.G.I.	mg / Fe ABRAS	% SULPHUR	% FIX CARB
AS TESTED	20.50	32.93	25.78	9.00	2.19	6.81	52	298.00	1.22	
DRY ASH FREE			39.74							
AS RECEIVED	19.07	30.64	23.99						1.14	36.37
DRY	20.96	33.67	26.36						1.25	
ISCOR MINE	20.96	34.10	40.10	9.00	1.70	7.30	52	298.00	1.25	

ANALYSIS: B SHIFT										
	MJ/Kg C.V.	% ASH	% VOL	% TOT MOIST	% INH MOIST	% SURF MOIST	H.G.I.	mg / Fe ABRAS	% SULPHUR	% FIX CARB
AS TESTED										
DRY ASH FREE										
AS RECEIVED										
DRY										
ISCOR MINE										

ANALYSIS: C SHIFT										
	MJ/Kg C.V.	% ASH	% VOL	% TOT MOIST	% INH MOIST	% SURF MOIST	H.G.I.	mg / Fe ABRAS	% SULPHUR	% FIX CARB
AS TESTED	20.50	32.93	25.78	9.00	2.19	6.81			1.22	
DRY ASH FREE			39.74							
AS RECEIVED	19.07	30.64	23.99						1.14	36.37
DRY	20.96	33.67	26.36						1.24	
ISCOR MINE	20.96	34.10	40.10	9.00	1.70	7.30			1.25	

COAL GRADING					
mm	37.50	25.00	10.50	6.70	4.75	< 4.75
PERCENT	3.21	13.07	38.70	10.30	4.64	30.09

TOTAL TONNAGE RECEIVED FROM ISCOR MINE PER SHIFT		
A SHIFT	B SHIFT	C SHIFT
23 271.50		908.50

TABLE E.4: MATIMBA POWER STATION DAILY COAL ANALYSIS REPORT
KUMBER NUMBER: 4651

ANALYST: Pinky DATE SAMPLED: 20 June 2002 DATE ANALYSED: 21 June 2002

ANALYSIS: A SHIFT										
	MJ/Kg C.V.	% ASH	% VOL	% TOT MOIST	% INH MOIST	% SURF MOIST	H.G.I.	mg / Fe ABRAS	% SULPHUR	% FIX CARB
AS TESTED	20.77	32.82	26.27	9.10	2.30	6.80	55	336.00	1.24	
DRY ASH FREE			40.49							
AS RECEIVED	19.33	30.54	24.44						1.15	35.92
DRY	21.26	33.60	26.89						1.27	
ISCOR MINE	21.26	33.90	40.50	9.10	2.00	7.10	50	309.00	1.27	

ANALYSIS: B SHIFT										
	MJ/Kg C.V.	% ASH	% VOL	% TOT MOIST	% INH MOIST	% SURF MOIST	H.G.I.	mg / Fe ABRAS	% SULPHUR	% FIX CARB
AS TESTED	20.77	32.82	26.24	9.10	2.30	6.80			1.24	
DRY ASH FREE			40.25							
AS RECEIVED	19.33	30.54	24.42						1.15	35.94
DRY	21.26	33.60	26.86						1.27	
ISCOR MINE	21.26	33.90	40.50	9.10	2.00	7.10			1.27	

ANALYSIS: C SHIFT										
	MJ/Kg C.V.	% ASH	% VOL	% TOT MOIST	% INH MOIST	% SURF MOIST	H.G.I.	mg / Fe ABRAS	% SULPHUR	% FIX CARB
AS TESTED	20.31	33.74	25.79	9.60	2.45	7.15			0.90	
DRY ASH FREE			40.42							
AS RECEIVED	18.82	31.27	23.90						0.83	35.23
DRY	20.82	34.59	26.44						0.92	
ISCOR MINE	20.82	34.30	39.50	9.60	1.90	7.70			0.92	

COAL GRADING					
mm	37.50	25.00	10.50	6.70	4.75	< 4.75
PERCENT	1.33	6.05	35.18	12.90	5.81	38.74

TOTAL TONNAGE RECEIVED FROM ISCOR MINE PER SHIFT		
A SHIFT	B SHIFT	C SHIFT
20 696.10	2 022.00	16 921.55

TABLE E.5: MATIMBA POWER STATION DAILY COAL ANALYSIS REPORT
KUMBER NUMBER: 4652

ANALYST: Pinky DATE SAMPLED: 21 June 2002 DATE ANALYSED: 24 June 2002

ANALYSIS: A SHIFT										
	MJ/Kg C.V.	% ASH	% VOL	% TOT MOIST	% INH MOIST	% SURF MOIST	H.G.I.	mg / Fe ABRAS	% SULPHUR	% FIX CARB
AS TESTED	20.60	32.99	25.92	9.60	2.26	7.34	47.00	334.00	1.08	
DRY ASH FREE			40.04							
AS RECEIVED	19.05	30.52	23.98						0.99	35.91
DRY	21.08	33.76	26.53						1.10	
ISCOR MINE	21.08	33.50	39.20	9.60	2.00	7.60	50.00	323.00	1.10	

ANALYSIS: B SHIFT										
	MJ/Kg C.V.	% ASH	% VOL	% TOT MOIST	% INH MOIST	% SURF MOIST	H.G.I.	mg / Fe ABRAS	% SULPHUR	% FIX CARB
AS TESTED	20.17	34.43	26.45	9.40	2.11	7.29			1.13	
DRY ASH FREE			41.68							
AS RECEIVED	18.66	31.87	24.48						1.04	34.25
DRY	2060	35.18	27.02						1.15	
ISCOR MINE	20.60	35.30	41.30	9.40	2.10	7.30			1.15	

ANALYSIS: C SHIFT										
	MJ/Kg C.V.	% ASH	% VOL	% TOT MOIST	% INH MOIST	% SURF MOIST	H.G.I.	mg / Fe ABRAS	% SULPHUR	% FIX CARB
AS TESTED	20.02	34.55	24.72	8.80	2.01	6.79			1.18	
DRY ASH FREE			38.97							
AS RECEIVED	18.63	32.16	23.01						1.09	36.04
DRY	20.43	35.26	25.23						1.20	
ISCOR MINE	20.43	35.30	38.70	8.80	2.10	6.70			1.20	

COAL GRADING					
mm	37.50	25.00	10.50	6.70	4.75	< 4.75
PERCENT	3.38	9.14	34.16	11.13	4.96	37.23

TOTAL TONNAGE RECEIVED FROM ISCOR MINE PER SHIFT		
A SHIFT	B SHIFT	C SHIFT
20 814.15	18 902.05	25 521.40

TABLE E.6: MATIMBA POWER STATION DAILY COAL ANALYSIS REPORT
KUMBER NUMBER: 4653

ANALYST: Pinky DATE SAMPLED: 22 June 2002 DATE ANALYSED: 24 June 2002

ANALYSIS: A SHIFT										
	MJ/Kg C.V.	% ASH	% VOL	% TOT MOIST	% INH MOIST	% SURF MOIST	H.G.I.	mg / Fe ABRAS	% SULPHUR	% FIX CARB
AS TESTED	19.92	34.78	25.53	9.50	2.55	6.95	50	303.00	1.34	
DRY ASH FREE			40.74							
AS RECEIVED	18.50	32.30	23.71						1.24	34.49
DRY	20.44	35.69	26.20						1.37	
ISCOR MINE	20.44	35.50	40.60	9.50	2.20	7.30	51	288.00	1.37	

ANALYSIS: B SHIFT										
	MJ/Kg C.V.	% ASH	% VOL	% TOT MOIST	% INH MOIST	% SURF MOIST	H.G.I.	mg / Fe ABRAS	% SULPHUR	% FIX CARB
AS TESTED	20.52	33.28	26.45	9.10	2.21	6.89			0.93	
DRY ASH FREE			40.99							
AS RECEIVED	19.08	30.93	24.58						0.86	35.38
DRY	20.99	34.03	27.04						0.95	
ISCOR MINE	20.99	34.00	40.60	9.10	2.00	7.10			0.95	

ANALYSIS: C SHIFT										
	MJ/Kg C.V.	% ASH	% VOL	% TOT MOIST	% INH MOIST	% SURF MOIST	H.G.I.	mg / Fe ABRAS	% SULPHUR	% FIX CARB
AS TESTED	20.70	33.40	26.24	9.60	2.32	7.28			0.91	
DRY ASH FREE			40.83							
AS RECEIVED	19.16	30.91	24.29						0.84	35.20
DRY	21.19	34.19	26.87						0.93	
ISCOR MINE	21.19	33.80	40.60	9.60	2.10	7.50			0.93	

COAL GRADING					
mm	37.50	25.00	10.50	6.70	4.75	< 4.75
PERCENT	3.27	6.77	32.89	12.01	5.18	39.88

TOTAL TONNAGE RECEIVED FROM ISCOR MINE PER SHIFT		
A SHIFT	B SHIFT	C SHIFT
24 647.60	24 649.20	23 501.50

TABLE E.7: MATIMBA POWER STATION DAILY COAL ANALYSIS REPORT
KUMBER NUMBER: 4654

ANALYST: Pinky DATE SAMPLED: 23 June 2002 DATE ANALYSED: 24 June 2002

ANALYSIS: A SHIFT										
	MJ/Kg C.V.	% ASH	% VOL	% TOT MOIST	% INH MOIST	% SURF MOIST	H.G.I.	mg / Fe ABRAS	% SULPHUR	% FIX CARB
AS TESTED	21.22	31.80	26.84	9.50	2.33	7.17	50	288.00	0.84	
DRY ASH FREE			40.75							
AS RECEIVED	19.67	29.47	24.87						0.78	36.16
DRY	21.73	32.56	27.48						0.86	
ISCOR MINE	21.73	32.40	40.80	9.50	1.90	7.60	50	288.00	0.86	

ANALYSIS: B SHIFT										
	MJ/Kg C.V.	% ASH	% VOL	% TOT MOIST	% INH MOIST	% SURF MOIST	H.G.I.	mg / Fe ABRAS	% SULPHUR	% FIX CARB
AS TESTED										
DRY ASH FREE										
AS RECEIVED										
DRY										
ISCOR MINE										

ANALYSIS: C SHIFT										
	MJ/Kg C.V.	% ASH	% VOL	% TOT MOIST	% INH MOIST	% SURF MOIST	H.G.I.	mg / Fe ABRAS	% SULPHUR	% FIX CARB
AS TESTED										
DRY ASH FREE										
AS RECEIVED										
DRY										
ISCOR MINE										

COAL GRADING					
mm	37.50	25.00	10.50	6.70	4.75	< 4.75
PERCENT	3.00	2.75	30.59	12.54	4.64	45.54

TOTAL TONNAGE RECEIVED FROM ISCOR MINE PER SHIFT		
A SHIFT	B SHIFT	C SHIFT
19 875.30		

TABLE E.8: MATIMBA POWER STATION DAILY COAL ANALYSIS REPORT
KUMBER NUMBER: 4655

ANALYST: Pinky DATE SAMPLED: 24 June 2002 DATE ANALYSED: 25 June 2002

ANALYSIS: A SHIFT										
	MJ/Kg C.V.	% ASH	% VOL	% TOT MOIST	% INH MOIST	% SURF MOIST	H.G.I.	mg / Fe ABRAS	% SULPHUR	% FIX CARB
AS TESTED	20.61	33.22	25.94	8.60	2.12	6.48	47	341.00	1.20	
DRY ASH FREE			40.12							
AS RECEIVED	19.25	31.02	24.22						1.12	36.16
DRY	21.06	33.93	26.50						1.23	
ISCOR MINE	21.06	33.80	40.60	8.60	2.00	6.60	50	323.00	1.23	

ANALYSIS: B SHIFT										
	MJ/Kg C.V.	% ASH	% VOL	% TOT MOIST	% INH MOIST	% SURF MOIST	H.G.I.	mg / Fe ABRAS	% SULPHUR	% FIX CARB
AS TESTED	20.65	33.34	25.67	9.50	1.92	7.58			1.44	
DRY ASH FREE			39.65							
AS RECEIVED	19.05	30.77	23.69						1.33	36.5
DRY	21.05	34.00	26.17						1.47	
ISCOR MINE	21.05	33.90	39.70	9.50	1.70	7.80			1.47	

ANALYSIS: C SHIFT										
	MJ/Kg C.V.	% ASH	% VOL	% TOT MOIST	% INH MOIST	% SURF MOIST	H.G.I.	mg / Fe ABRAS	% SULPHUR	% FIX CARB
AS TESTED	20.39	33.76	25.85	8.80	1.94	6.86			1.18	
DRY ASH FREE			40.20							
AS RECEIVED	18.96	31.40	24.04						1.09	35.76
DRY	20.79	34.43	26.36						1.20	
ISCOR MINE	20.79	34.50	40.00	8.80	1.70	7.10			1.20	

COAL GRADING					
mm	37.50	25.00	10.50	6.70	4.75	< 4.75
PERCENT	1.88	7.00	32.76	13.04	7.06	38.27

TOTAL TONNAGE RECEIVED FROM ISCOR MINE PER SHIFT		
A SHIFT	B SHIFT	C SHIFT
21 658.75	19 664.10	21 872.70

Hi Richard

This is what I have for now, about density I'll have to find out from Performance and Testing or from the mine.

ASH ELEMENTAL %

	JAN 02	FEB 02	Mar 02
SILICON (AS SiO2)	58.1	48.7	59.3
ALUMINIUM (AS AL2O3)	27.5	28.4	25.5
IRON (AS Fe2O3)	5.8	3.3	5.7
TITANIUM (AS TiO2)	1.3	1.5	1.1
PHOSPHORUS (AS P2O5)	0.45	0.83	0.37
CALCIUM(ASCaO)	3.1	8.8	2.7
MAGNESIUM(AS MgO)	1.0	2.6	0.9
SODIUM(AS Na20)	0.0	0.5	0.3
POTASIUM(AS K2O)	0.6	0.5	0.7
SULPHUR (AS SO3)	1.5	3.4	1.9
MANGANESE (AS MnO)	0.06	0.04	0.06

I hope this will help some how.

Bye,

Pinky
Analyst
Matimba Power Station

APPENDIX F

TEST SPECIMEN ANALYSIS

Sent by the Award Winning Cheyenne Bitware

SCROOBY'S LABORATORY SERVICE cc

Spectrographic and Chemical Analysis of Materials

CK 1999/047204/23
21 O'Reilly Merry St
Rynfield Benoni 1501

TEL: (011) 425-1074
FAX: (011) 849-3571
CELL: 082-675-4536

P O Box 13401
Northmead
1511

University of the Witwatersrand

17 December 2002

ATTENTION: Mr Richard Shandu

O/N:

CERTIFICATE of ANALYSIS

REFERENCE No: **Student**

Element		Composition in Mass %
Carbon		≤ 0.01
Manganese		0.14
Sulphur		0.012
Phosphorus		0.011
Silicon		≤ 0.01
Chromium		≤ 0.01
Molybdenum		≤ 0.01
Nickel		≤ 0.01
Copper		≤ 0.01
Aluminium		0.040
Vanadium		≤ 0.005
Niobium		≤ 0.005
	MECHANICAL PROPERTIES	
Dimensions	mm	12.5 x 2.0
Cross Sectional Area	mm^2	25.0
Gauge Length	mm	50
Yield Stress	MPa	236.1
Ultimate Tensile Strength	MPa	354.2
Elongation	%	37.0

Description of Sample's

Steel plate ± 2.0mm thick

Laboratory Manager

All information in this document is given in good faith, but without warranty or guarantee of any kind whatsoever, whether implied or expressed.

Figure F.1: Test Specimen Analysis

APPENDIX G

UNCERTAINTY ANALYSIS

In the uncertainty analysis this is where the test results' degree of accuracy is determined. The experimental results' certainty is clarified in this section. This analysis starts by giving derivations of equations relevant to each parameter of the test results, for instance the determination of velocity derived from volumetric flow rate. The volumetric flow rate of air is given by the following equation:

$$Q = C_d \frac{\pi d_0^2}{4} \sqrt{\frac{2\Delta P}{\rho}} \qquad \text{(G.1)}$$

where; Q is the volumetric flow rate, C_d is the coefficient of discharge of the orifice, d_o is the orifice diameter, ρ is the density of air, ΔP is the pressure drop across the orifice. Particle velocity is assumed to be the same as the velocity of the free stream of air before mixture, thus the particle velocity is given by the following equation:

$$V = \frac{4Q}{\pi d^2} = C_d \left(\frac{d_0}{d} \right)^2 \sqrt{\frac{2\Delta P}{\rho}} \qquad \text{(G.2)}$$

where d is the diameter of the pipeline transporting the ash to the test section.

The uncertainty in the velocity is given by the following equation:

$$U^2(V) = C_{do}^2 U^2(d_o) + C_d^2 U^2(d) + C_{\Delta P}^2 (\Delta P) + C_\rho^2 U^2(\rho) \qquad \text{(G.3)}$$

where; U(V), $U(d_o)$, U(d), U(ΔP) and U(ρ) are the uncertainties in the measured values of the velocity, orifice diameter, diameter of the pipe at the inlet to the test section, pressure drop across the orifice and the density of air, respectively; $C_{do,}$ $C_{d,}$ $C_{\Delta P}$ and C_ρ are the sensitivity coefficients for the orifice diameter, diameter of the pipe at the inlet to the test section, pressure drop across the orifice and the density of air, respectively. The sensitivity coefficients are calculated by using the following equations:

$$C_{do} = \frac{\partial V}{\partial d_o} = 2C_d \frac{d_o}{d^2}\sqrt{\frac{2\Delta P}{\rho}} \quad \text{(G.4)}$$

$$C_d = \frac{\partial V}{\partial d} = -2C_d \frac{d_o^2}{d^3}\sqrt{\frac{2\Delta P}{\rho}} \quad \text{(G.5)}$$

$$C_{\Delta P} = \frac{\partial V}{\partial \Delta P} = \frac{1}{2} C_d \left(\frac{d_o}{d}\right)^2 \sqrt{\frac{2}{\rho \Delta P}} \quad \text{(G.6)}$$

$$C_\rho = \frac{\partial V}{\partial \rho} = -\frac{1}{2} C_d \left(\frac{d_o}{d}\right)^2 \sqrt{\frac{2\Delta P}{\rho^3}} \quad \text{(G.7)}$$

Table G.1 Parameters used in the experimental test

Parameter	Value
Orifice diameter, d_o	0.032m
Pipe diameter at the inlet to the test section, d	0.0224m
Coefficient of discharge, C_d	0.6
Density of air, ρ	1.17kg/m^3

These parameter values and experimental results were used in equations (G.1) – (G.7) above to get the sensitivity coefficients shown here below in Table G.4.

Table G.2 Sensitivity coefficients for Matimba Power Station ash

V (m/s)	ΔP (N/m^2)	$C_{\Delta P}$	C_{do}	C_d	C_ρ
19.41	146.99	0.07	1213.11	-1733.02	-8.29
21.86	186.44	0.06	1366.24	-1951.77	-9.34
24.70	238.03	0.05	1543.74	-2205.34	-10.56
25.55	254.70	0.05	1596.88	-2281.25	-10.92
26.59	275.86	0.05	1670.90	-2374.12	-11.36

Table G.3 Sensitivity coefficients for Lethabo Power Station ash

V (m/s)	ΔP (N/m^2)	$C_{\Delta P}$	C_{do}	C_d	C_ρ
18.49	133.39	0.07	1155.63	-1650.90	-7.90
21.14	174.36	0.06	1321.24	-1887.48	-9.03
23.49	215.28	0.06	1468.11	-2097.30	-10.04
24.62	236.49	0.05	1538.73	-2198.19	-10.52
26.66	277.31	0.05	1666.25	-2380.36	-11.39

Table G.4 Sensitivity coefficients for Matla Power Station ash

V (m/s)	ΔP (N/m^2)	$C_{\Delta P}$	C_{do}	C_d	C_ρ
18.28	130.38	0.07	1142.52	-1632.17	-7.81
20.29	160.62	0.06	1268.11	-1811.59	-8.67
23.15	209.10	0.06	1446.89	-2066.98	-9.89
24.54	234.96	0.05	1533.75	-2191.07	-10.49
27.66	298.50	0.05	1728.74	-2469.63	-11.82

Measuring tools that were used to measure ambient temperature, pressure drop across the orifice and pipeline diameters are thermometer, manometer and vernier callipers; respectively.

Table G.5 Uncertainties in the measured values of temperature, pressure drop and diameters

Measuring Tool	Uncertainty	Value
Thermometer	U(T)	± 1ºC
Manometer	U(ΔP)	± 1 N/m^2
Vernier callipers	U(d_o), U(d)	$\pm 10^{-4}$ m

Density of gas is given by the following equation:

$$\rho = \frac{P}{RT} \qquad \text{(G.8)}$$

where; P is the gas pressure, R is the Universal Gas Constant and T is the gas temperature. Sensitivity coefficients equations of these parameters were derived from the density equation thereby taking first order derivative of the equation with respect to each parameter. Since R is a constant its sensitivity coefficient is zero. Thus the uncertainty in the air density is given as follows:

$$U^2(\rho) = C_P^2(P) + C_T^2 U^2(T) \qquad \text{(G.9)}$$

where; U(ρ), U(P) and U(T) are uncertainties in the density of air, ambient pressure and temperature, respectively; C_P and C_T are sensitivity coefficients in the measured values of the ambient pressure and temperature, respectively. These sensitivity coefficients are given by the flowing equations:

$$C_p = \frac{\partial \rho}{\partial P} = \frac{1}{RT} \qquad \text{(G.10)}$$

$$C_T = \frac{\partial \rho}{\partial T} = -\frac{P}{RT^2} \qquad \text{(G.11)}$$

Table G.6 Parameters used to calculate uncertainty in the air density

Parameter	Value
Ambient temperature, T	293 K (20ºC)
Ambient pressure	98 500 N/m^2
Universal Gas Constant	287 J/kg.K

These parameters were used in equations (G.10) – (G.11) to calculate the sensitivity coefficients of the ambient pressure and temperature values. These values were then used to calculate the uncertainty in the air density. The calculated results are presented in Table G.7 here below.

Table G.7 Sensitivity coefficients and uncertainty in the air density

C_P	C_T	Density of air, ρ (kg/m^3)	Uncertainty, U(ρ) (kg/m^3)
-0.004	1.19 x 10^{-5}	1.17	±0.004

The overall uncertainties in the experimental results are tabulated in Tables G.8 – G.10.

Table G.8 Uncertainties in the Matimba Power Station velocity test results

Velocity, V (m/s)	Uncertainty, U (V) (m/s)
19.41	± 0.22
21.86	± 0.25
24.70	± 0.28
25.55	± 0.29
26.59	± 0.30

Table G.9 Uncertainties in the Lethabo Power Station velocity test results

Velocity, V (m/s)	Uncertainty, U (V) (m/s)
18.49	± 0.22
21.14	± 0.24
23.49	± 0.26
24.62	± 0.28
24.66	± 0.30

Table G.10 Uncertainties in the Matla Power Station velocity test results

Velocity, V (m/s)	Uncertainty, U (V) (m/s)
18.28	± 0.21
20.29	± 0.23
23.15	± 0.26
24.54	± 0.28
27.66	± 0.31

The experimental erosion rate was determined by two parameters, mass of the test specimen that was attacked by ash particles and the total mass of the ash that was used in that specific test. The erosion rate is equal to the difference between the mass of the test specimen before and after the test divided by the total mass of the ash used in the test. The quantity of the ash used in each test run was determined by the use of a load cell whereas the amount of eroded material in the test specimen was determined by weighing the test specimen in the electronic balance scale before and after the test. The calibration of these measuring tools gave uncertainties of ±1g for the load cell and ±0.001g for the electronic balance scale.

The erosion rate is given by the following equation:

$$E = \frac{M_m}{M_p} \qquad \text{(G.12)}$$

where; M_m is the difference between the initial and final mass of the test specimen, and M_p is the total mass of the ash that was used in the test to erode the test specimen material.
The uncertainty in the erosion rate is given by the following equation:

$$U^2(E) = C_{mm}^2 U^2(M_m) + C_{mp}^2 U^2(M_p) \qquad \text{(G.13)}$$

where C_{mm} and C_{mp} are sensitivity coefficients for the amount of eroded material and total mass of the ash used in the test run, respectively; U (M_m) and U (M_p) are the uncertainties for the amount of eroded material and total mass of the ash used in the test run, respectively.
The sensitivity equations are derived from the erosion rate equation by taking the first derivative of the erosion rate with respect to each parameter. The result of the derivative gives the following sensitivity equations:

$$C_{mm} = \frac{\partial E}{\partial M_m} = \frac{1}{M_p} \quad \text{(G.14)}$$

$$C_{mp} = \frac{\partial E}{\partial M_p} = -\frac{M_m}{M_p^2} = -\frac{E}{M_p} \quad \text{(G.15)}$$

Table G.11 Uncertainties in the measured values

Measuring Tool	Uncertainty	Value
Electronic Balance Scale	U (M_m)	±1mg
Load Cell	U (M_p)	±0.001kg

The uncertainties in the measured values shown in Table G.11 were used to determine the overall uncertainties in the erosion rates and the sensitivity coefficients. These results are presented in Tables G12 – G14 here below.

Table G.12 Sensitivity coefficients and uncertainties in Matimba Power Station test results

V (m/s)	M_p (kg)	C_{mm}	C_{mp} (x10^{-6})	E (mg/kg)	U (E) (mg/kg)
19.41	70.78	0.01	-0.05	3.53	±0.01
21.86	70.15	0.01	-0.08	5.41	±0.01
24.70	76.83	0.01	-0.10	7.59	±0.01
25.55	79.85	0.01	-0.11	8.49	±0.01
26.59	81.37	0.01	-0.12	9.37	±0.01

Table G.13 Sensitivity coefficients and uncertainties in Lethabo Power Station test results

V (m/s)	M_p (kg)	C_{mm}	C_{mp} (x10^{-6})	E (mg/kg)	U (E) (mg/kg)
18.49	93.95	0.01	-0.02	2.18	±0.01
21.14	102.27	0.01	-0.03	3.38	±0.01
23.49	114.28	0.01	-0.04	4.38	±0.01
24.62	124.32	0.01	-0.04	4.39	±0.01
26.66	143.92	0.01	-0.04	5.40	±0.01

Table G.14 Sensitivity coefficients and uncertainties in Matla Power Station test results

V (m/s)	M_p (kg)	C_{mm}	C_{mp} (x10^{-6})	E (mg/kg)	U (E) (mg/kg)
18.28	79.61	0.01	-0.01	0.60	±0.01
20.29	87.74	0.01	-0.01	1.09	±0.01
23.15	96.72	0.01	-0.02	1.81	±0.01
24.54	71.15	0.01	-0.03	1.84	±0.01
27.66	106.40	0.01	-0.03	2.88	±0.01

APPENDIX H

PUBLISHED TECHNICAL PAPER